OULUN YLIOPISTO
UNIVERSITY of OULU

FACULTY OF TECHNOLOGY

PETROLOGY AND MINERAL CHEMISTRY OF THE YLIVIESKA GABBRO-PERIDOTITE INTRUSION: CONSTRAINTS ON THE PETROGENESIS AND Ni SULFIDE ORE POTENTIAL

Lotta Kiuttu

Master's thesis
Oulu Mining School
University of Oulu
2020

ABSTRACT FOR THESIS

University of Oulu Faculty of Technology

Degree Programme (Bachelor's Thesis, Master's Thesis)	Major Subject (Licentiate Thesis)
Degree Programme in Geology and Mineralogy, specialization in economic geology	
Author	**Thesis Supervisor**
Kiuttu, Lotta Karoliina	Yang, S., Hanski, E., Halkoaho, T.

Title of Thesis

Petrology and mineral chemistry of the Ylivieska gabbro-peridotite intrusion: constraints on the petrogenesis and Ni sulfide ore potential

Major Subject	Type of Thesis	Submission Date	Number of Pages
Geosciences	Master's Thesis	February 2020	90 p., 4 App.

Abstract

The 1.90 Ga Ylivieska gabbro-peridotite intrusion is located in the Nivala gneiss complex in the Central Ostrobothnia. The bedrock of the Ylivieska area consists of Svecofennian Paleoproterozoic supracrustal and plutonic rocks including schists, ultramafic rocks, gabbros, diorites, granites, granitic veins, and diabases. In terms of the mineralization type, the intrusion is classified as an intermediate intrusion of the Kotalahti Nickel Belt. The intrusion consists mostly of layered gabbro, but also contains a circular peridotite unit and other mafic-ultramafic rocks.

In this thesis, the mineralized units on the eastern part of the intrusion are studied in order to increase our knowledge of the mineralogy and petrography of the mineralized parts of the intrusion. In addition, electron microprobe analyses are used to constrain the petrogenesis of the intrusion, and comparison to other analogous intrusions in the Kotalahti Nickel Belt is made. The potential for Ni-Cu sulfide minerlization is also evaluated. A total of 25 thin sections were prepared for transmitted and reflected light microscopy and 137 EPMA analyses were made to determine olivine, pyroxene and plagioclase compositions.

The studied intrusion shows similarities to other known Ni-Cu mineralized Kotalahti-type intrusion with respect to the cumulate and ore mineral assemblages, mineral chemistry and the presence of disseminated sulfides in the gabbroic rocks. The occurrence of the massive and matrix sulfides in the pyroxenitic units differs from the majority of the intrusions of the Kotalahti Belt, in which sulfides mainly occur in olivine-rich cumulates.

The study area comprises olivine-pyroxene orthocumulates, pyroxene orthocumulates, plagioclase-pyroxene and pyroxene-plagioclase adcumulates, plagioclase-pyroxene mesocumulates as well as plagioclase-pyroxene-olivine meso- and adcumulates. Magmatic interstitial amphibole, phlogopite and plagioclase are common. Orthopyroxene is dominant over clinopyroxene in all rock units of the study area except in lherzolites and gabbros. Abundant orthopyroxene could be explained by reactions between olivine and residual melt or by assimilation of silica. The latter may increase the ore potential of the inrusion, but requires further studies.

The most common ore minerals in the intrusion are pyrrhotite, chalcopyrite, and pentlandite. Sulfides are most abundant in websterites, forming matrix ore. Sulfides are also present as dissemination in lherzolites, hornblende pyroxenites, gabbros, gabbronorites, olivine gabbronorites, and olivine norites. On the basis of the petrography, websterites seem to be the most potential for Ni-Cu mineralization. Sulfide saturation has probably occurred early during the evolution of the magma, as indicated by the ore mineral textures and the wide compositional range of olivine and pyroxene, indicating a high ore potential of the intrusion.

Additional Information

Keywords: Svecofennian, mafic-ultramafic intrusions, magmatic Ni-Cu sulfide deposits, convergent setting, petrogenesis, mineral chemistry, ore potential

TIIVISTELMÄ
OPINNÄYTETYÖSTÄ Oulun yliopisto Teknillinen tiedekunta

Koulutusohjelma (kandidaatintyö, diplomityö) Geologian ja mineralogian koulutusohjelma		Pääaineopintojen ala (lisensiaatintyö)	
Tekijä Kiuttu, Lotta Karoliina		Työn ohjaaja yliopistolla Yang, S., Hanski, E., Halkoaho, T.	
Työn nimi Ylivieskan gabro-peridotiitti intruusion petrologia ja mineraalikemia: rajoitteet petrogenetiikalle sekä Ni malmipotentiaalille			
Opintosuunta Geotieteet	Työn laji Pro gradu	Aika Helmikuu 2020	Sivumäärä 90 s., 4 liitettä

Tiivistelmä

1900 miljoonan vuoden ikäinen Ylivieskan gabro-peridotiitti-intruusio sijaitsee Nivalan gneissikompleksissa Keski-Pohjanmaalla. Ylivieskan alueen kallioperä koostuu erilaisista paleoproterotsooisista svekofennisistä pinta- ja syväkivistä pitäen sisällään liuskeita, gabroja, dioriitteja, graniitteja, graniittisia juonia sekä diabaaseja. Intruusio koostuu pääosin kerroksellisesta gabrosta, mutta pitää sisällään myös kuppimaisen peridotiitti-osan sekä muita mafis-ultramafisia kivilajeja. Mineralisaatiotyypin perusteella intruusio voidaan luokitella Kotalahden nikkelivyöhykkeen keskitason intruusioihin.

Tämän pro gradu -tutkielman tarkoitus on kasvattaa tietämystä intruusion mineralisoituneiden kivilajiyksiköiden mineralogiasta ja petrologiasta, malmipotentiaalista ja petrogenetiikasta tutkimalla intruusion itäisen osan mineralisoituneita yksiköitä. Lisäsi tutkielmassa tarkastellaan intruusion synnyttäneen magman mahdollista köyhtymistä metalleista sekä suoritetaan vertailu muihin vastaaviin Kotalahti-tyypin intruusioihin. Työtä varten valmistettiin 25 ohuthiettä, joista tehtiin mikroskooppisten tutkimusten lisäksi 137 elektronimikroanalyysiä oliviinin, pyrokseenien ja plagioklaasin koostumusten selvittämiseksi.

Tutkimusalue koostuu oliviini-pyrokseeniortokumulaateista, pyrokseeniortokumulaateista, plagioklaasi-pyrokseeni- ja pyrokseeni-plagioklaasiadkumulaateista, plagioklaasi-pyrokseenimesokumulaateista sekä plagioklaasi-pyrokseeni-oliviinimeso- ja adkumulaateista. Magmaattinen amfiboli, flogopiitti sekä plagioklaasi ovat yleisiä mineraaleja kivien interkumulustilassa. Pyrokseenit ovat tutkituissa kivissä pääosin ortopyrokseenia, mikä voi johtua oliviinin ja residuaalisulan peritektisestä reaktioista tai magman kontaminoitumisesta kiillegneissillä. Mahdollinen kontaminoituminen kasvattaisi intruusion malmipotentiaalia. Asian varmistaminen vaatii kuitenkin lisätutkimuksia.

Malmimineraaleista yleisimmät ovat magneettikiisu, pentlandiitti ja kuparikiisu. Sulfideja esiintyy eniten websteriiteissa, joissa ne esiintyvät verkkomaisena tekstuurina. Sulfideja esiintyy myös piroitteena lherzoliiteissa, sarvivälkepyrokseniiteissa, gabroissa, gabronoriiteissa, oliviinigabronoriiteissa ja oliviininoriiteissa. Petrografian perusteella websteriiteilla näyttäisi olevan suurin malmipotentiaali. Oliviinin sekä pyrokseenien laaja koostumuksellinen vaihtelu sekä malmimineraalien tekstuurit antavat viitteitä sille, että magman kyllästyminen sulfideilla on mahdollisesti tapahtunut jo intruusion kehittymisen aikaisessa vaiheessa nostaen näin intruusion malmipotentiaalia.

Ylivieskan intruusio vastaa petrografian, mineraalikemian ja esiintyvien malmimineraalien osalta tyypillisiä Kotalahden-intruusioita. Massiivisen ja verkkomaisen malmin esiintymisen osalta intruusio kuitenkin eroaa valtaosasta Kotalahti-tyypin intruusioista, sillä verkkomaiset sulfidit ovat pyrokseniiteissa harvinaisia.

Muita tietoja

Asiasanat: Svekofenninen, mafis-ultramafiset intruusiot, magmaattiset Ni-Cu sulfidi esiintymät, petrogenetiikka, mineraalikemia, malmipotentiaali

CONTENTS

APPENDICES

1. INTRODUCTION

The magmatic Ni-Cu-PGE sulfide deposits hosted by mafic and ultramafic intrusions of the synorogenic ca. 1.88 Ga Svecofennian magmatism have been a significant source of nickel in Finland since 1941 (Peltonen 2005; Puustinen et al. 1995). These intrusions are mostly located in the Kotalahti and Vammala Nickel Belts and they can be classified into barren, intermediate and mineralized categories on the basis of the amount and composition of sulfides (Makkonen et al. 2008). Rasilainen et al. (2012) and Makkonen et al. (2017) estimate that there is 50% probability that a similar amount of nickel that is currently known can be found in deposits at a level between 0 and 1000 m below the surface.

This study deals with the Ylivieska gabbro-peridotite intrusion situated five kilometers SW of the Ylivieska village in central Finland. In terms of the mineralization type, it is classified as an intermediate intrusion of the Kotalahti Nickel Belt (Kontoniemi and Mäkinen, 2001; Makkonen et al., 2008). The previous studies of the intrusion by Sipilä (1976, 1984) were mostly focused on describing structures and lithological units of the intrusion, contributing to the knowledge of the ore potential of the peridotitic and pyroxenitic parts of the intrusion. Kontoniemi and Mäkinen (2001) refined the previous lithological classificitation applying petrological and geochemical studies.

Chemical data on olivine from the intrusion reveal a high spread in Ni at a given forsterite content, with a large number of samples showing a strong depletion in Ni (Makkonen et al., 2008). This indicates that separation of sulfide melt has occurred in the intrusion, increasing the ore potential of the intrusion. According to Kontoniemi and Mäkinen (2001), potentially contaminated pyroxenites and more primitive peridotites in the western part of the intrusion seem to be most prospective for the follow-up studies. However, more evidence is required for the hypothetical contamination event during the formation of the pyroxenites, and mineralization types related to the different rock units need to be identified in order to discriminate between potentially ore-bearing and barren rock units. This study is aimed to increase our knowledge of the mineralogy and petrography of the mineralized parts of the intrusion and to investigate the metal depletion

of the magma that produced the intrusion. Possible relations between different lithological units are also interpreted and comparison is made to other analogous intrusions in the Kotalahti Nickel Belt.

2. LAYERED MAFIC ULTRAMAFIC INTRUSIONS AND RELATED Ni-Cu SULFIDE DEPOSITS

2.1. Layered intrusions

Ashwal (1993) defines layered intrusions as differentiated igneous bodies that display layering and have emplaced into the continental crust. They are commonly found in an extensional tectonic setting, such as rifted continental margins and intracratonic flood basalt provinces (Naldrett, 1989). These intrusions can be related to a mantle plume event, but they can also occur in orogenic belts (Ashwal, 1993; Naldrett, 1989). According to Scoates and Wall (2015), layered intrusions have formed throughout the Earth's history and therefore are not restricted to any particular geological time period.

Parental magmas of layered intrusions form a continuous series, developing progressively from partial melting of the mantle to differentiation in the crust (Cawthorn et al., 2005). Rocks in layered intrusions usually consist of gabbroic, noritic or troctolitic rocks and various ultramafic rocks. The ultramafic varieties tend to be more dominant in the lower parts of the intrusions and in their feeder channels.

The chemical composition of the parental magma varies depending on the mantle source composition, P-T conditions and degree of partial melting (e.g., Grove, 2000). During their transfer to higher crustal levels, magmas may assimilate crustal material and undergo fractional crystallization, which changes the chemical composition of the magma. When the chemical composition of the magma is completely regulated by the degree of melting and mineralogical and chemical composition of the source rock, involving no differentiation processes, the magma is referred to as ”primary” (Winter, 2001).

Rocks of layered intrusions become increasingly more evolved in composition inwards and upwards in the magmatic body due to fractional crystallization (Latypov, 2015), forming a thick layered series. However, nearly all layered intrusions show basal reversals tens to hundreds of meters in thickness, in which minerals and rocks become compositionally more primitive upwards. The basal reversals can be divided into two different types depending on the relationship with the overlying layered series. The more common type is a fully-developed reversal, which gradually passes into the overlying layered series through a crossover horizon with the most primitive compositions, with the layered series becoming progressively more evolved above the crossover horizon. This reversal type is like a mirror image of the overlying layered series. Fully developed reversals are formed during a continous evolution and therefore show gradational change. Aborted reversals are separated from layered series by a sharp textural and compositional break. They are formed when the evolution is interrupted by a pulse of primitive magma that resets the crystallization history in the chamber.

Cumulates are common constituents of layered intrusions (Morse, 1986). They are rocks that start to form on the floor, wall and roof of a magma chamber as a framework of touching minerals (Wager and Brown, 1967; Irvine, 1982; Scoates and Wall, 2015). The minerals are called cumulus crystals and the pore spaces between them are filled with intercumulus melt. Initial high porosity and permeability in the framework allow exchange of melt between the crystal mush and the main magma body by compositional convection and diffusion (Morse, 1986; Jerram et al., 2003). When the crystal mush consolidates, the porosity is eliminated. Consolidation may involve various processes, including mechanical compaction, continued crystallization and growth of cumulus crystals from interstitial melt, crystallization of new minerals from evolved interstitial melt as poikilitic or subpoikilitic crystals and crystallization of remaining melt as zoned overgrowths or as mono-mineralic rims on cumulus crystals (Wager and Brown, 1967; Irvine, 1982; Hunter, 1996).

Wager and Brown (1967) defines layering as an overall structure of cumulates, which develops through the combination of individual layers. Each layer forms a sheet-like unit that differs from other units by varying mineral modes and textural features or by having its own stratigraphically uniform assemblage (Irvine, 1982; Namur et al., 2015; Naslund and McBirney, 1996). The layering might vary widely within a single intrusion and from one intrusion to another: fluctuating from a prominent layering to poorly defined, from

planar to other structures as well as from continuous to discontinuous (Namur et al., 2015).

There are numerous different mechanisms that might form layering in mafic-ultramafic intrusions (Scoates and Wall, 2015). The mechanisms act from the liquidus temperature down to subsolidus conditions and can be classified either into dynamic or non-dynamic layer-forming processes (Boudreay and McBirney, 1997; McBirney and Nicolas, 1997; Irvine, 1982). Dynamic processes act during crystallization and filling of the magma chamber and are usually most efficient near the margins of the magma chamber (Namur et al., 2015). These processes include differential settling or flotation of crystals with different densities and grain sizes, flow segregation of crystal-rich magma and crystal segregation during convective liquid movement into the magma chamber. Double diffusive convection can produce layering by developing a stratified liquid column in the magma chamber. Other dynamic processes include injection of new magma into the chamber, which mixes or stratificates the magmas, crystal mush contraction and silicate liquid immiscibility, though the latter two have commonly been considered an insignificant layer-forming mechanism in the literature.

Non-dynamic layer-forming processes include the following mechanisms: variation in nucleation rates, mineral reorganization in a crystal mush through grain rotation as well as dissolution-precipitation due to initial heterogeneity (Namur et al., 2015). These processes occur during crystallization and are related to quick changes in crystallization conditions or self-organization of minerals in a crystal mush.

2.2. Magmatic Ni-Cu sulfide deposits

Mafic and ultramafic magmas typically form in the astenospheric or lithospheric mantle (Barnes and Lightfoot, 2005). Olivine is the main phase in the mantle that controls the nickel content of the magma. Therefore, partial melting of the mantle has to be very high for the magma to reach its maximum nickel content and release nickel from olivine. The abundance of copper in the mantle melts is primarily controlled by the presence of

sulfides in the mantle residue, with the copper content being highest just after all sulfides have been melted.

Barnes and Lightfoot (2005) present that, to form an economical Ni-Cu sulfide deposit, the magma has to ascent efficiently from the mantle to the crust with a minimum degree of olivine fractionation because crystallization of olivine decreases the nickel content of the melt. There are several factors that control the solubility of sulfur in silicate melt, including pressure, temperature, $FeO+TiO_2$ content of the melt, oxidation state of the melt as well as proportions of mafic and felsic components in the melt (Mavrogenes and O'Neill, 1999; Naldrett, 2004; Barnes and Lightfoot, 2005).

After the magma has emplaced into the crust, it must become saturated in a base metal sulfide liquid in order to form a Ni-Cu sulfide deposit (Barnes and Lightfoot, 2005). If the magma is saturated in sulfide when leaving the mantle, segregation of sulfides can be achieved by the above-mentioned factors. However, the most significant Ni-Cu sulfide deposits have formed from magmas that were sulfur undersaturated when they left the mantle or ascended into the crust. In sulfur-undersaturated magmas, assimilation of crustal rocks may lead to sulfur saturation due to a decrease in temperature and increase in the sulfur content. Ripley and Li (2013) propose that in most of the deposits, sulfur saturation of the magma is achieved by assimilation of sulfur-bearing country rocks. This view is supported by the frequent occurrence of sulfur-bearing crustal rocks in association with Ni-Cu sulfide deposits and by the S isotope compositions of the ores indicating that S was mostly derived from country rocks.

Saturation in sulfur leads to the formation of sulfide droplets within the silicate magma (Barnes and Lightfoot, 2005). The droplets are able to collect chalcophile metals from the silicate magma and can be transported by further flow of the magma. The effective silicate melt/sulfide melt mass ratio is called "R-factor" (Campbell and Naldrett, 1979; Barnes and Lightfoot, 2005), whereas the total mass of sulfide to the total mass of silicate magma is called the "N" factor (Naldrett, 2004; Barnes and Lightfoot, 2005). The partition coefficient of Ni between sulfide and silicate liquids ranges from 100 for komatiitic magmas to 300 for basaltic magmas. Therefore, an R or N factor of 1000 is needed in komatiites to achieve maximum Ni enrichment, whereas in basaltic systems , an R or N factor of 3000 is required for the maximum enrichment. Interaction of the sulfide liquid

with a very large volume of silicate magma is prerequisite for the formation of PGE-rich sulfide ore. The maximum PGE enrichment is achieved at an R factor of >10 000.

A process that gathers sulfide droplets together and concentrates them is required to form a sulfide deposit with a reasonable concentration of chalcophile element-bearing sulfides. Massive and matrix sulfides are commonly located towards the base of a lava flow or an intrusion. They can also be located as an offset deposit in veins within the adjacent footwall. A large intrusion that contains disseminated sulfides may form when accumulation of the sulfide droplets is restricted, but the grade may not be sufficient for an economical deposit.

Massive ores are typically found in footwall embayments (Barnes and Lightfoot, 2005). This type of location may be explained by a model where a silicate magma, which transports sulfide droplets, rises on the downstream side of the embayment and then slows down in its flow rate, resulting in a decrease in the magma's capacity to to carry the sulfide droplets with it and the droplets start to accumulate on the lee side of the embayment. Another common location for massive ore is a place where a feeder conduit enters an intrusion. Upon entering the chamber through a narrow feeder zone, the magma decreases in flow rate, spreading into the chamber and loosing its capable to carry heavy sulfide droplets. Accumulation of sulfide liquid can also occur in other places when the flowing silicate magma reaches a structural trap and slows down, concentrating sulfide droplets at the base of a flow or an intrusion.

According to Barnes and Lightfoot (2005), disseminated sulfides often reach higher metal tenors than massive sulfides. This phenomenon can be explained by longer interaction of the sulfide droplets with the silicate magma, as they did not settle out of the magma. Besides the metal abundance, the metal ratios also vary with the sulfide type. Massive sulfide ores usually have lower Pd/Ir ratios than disseminated sulfides. The range in the Ni/Cu and Pd/Ir ratios is also wider in massive and matrix sulfides than in disseminated sulfides. This can be explained by the segregation of iron-rich monosulfide solution (mss) from the sulfide liquid during cooling. Mss is a high-temperature equivalent of pyrrhotite (Naldrett, 2004) and is the first phase to crystallize from base metal sulfide liquid at temperatures of ~1200 °C (Kullerud et al., 1969). The sulfide liquid contains variable amounts of oxygen, which is manifested by the presence of primary magnetite in sulfide

ores (Naldrett, 2011). Osmium, Ir, Ru and Rh are highly compatible with the mss at temperatures greater than 1150 °C whereas Ni, Cu, Pd and Pt are incompatible (Barnes and Lightfoot, 2005). Below 1000 °C, Ni is moderately compatible with mss and starts to become enriched in the mss. During fractional crystallization, the remaining liquid becomes progressively depleted in Fe and enriched in Cu, as Cu is strongly incompatible with mss (Naldrett, 2004). At ~850 °C, intermediate solid solution (iss), rich in Cu, starts to crystallize from a residual liquid enriched in Pt, Pd and Au (Barnes et al., 1997; Barnes and Lightfoot, 2005; Li et al., 1992; Dare et al., 2014). Iss solidifies much later than mss at temperatures <900 °C. Pentlandite, the most important Ni-bearing mineral in Ni-Cu deposits, forms only at temperatures <850 °C. The higher the sulfur content of the deposit is, the lower will be the temperature at which pentlandite exsolves (Naldrett, 2011). Once the sulfide-oxide liquid has crystallized, the minerals continue to re-equilibrate together with decreasing temperature.

On the basis of the parental magma composition, magmatic Ni-Cu sulfide deposits can be divided into seven sub-types (Naldrett, 2010):

1. Komatiitic magmatism related
2. Flood basaltic magmatism related
3. Ferropicritic magmatism related
4. Anorthosite-granite-troctolite complexes
5. MgO-rich basaltic magmatism related
6. Extraterrestial impact related deposits
7. Ural-Alaskan type ultramafic complexes

2.3. Ni-Cu deposits in convergent settings

Many magmatic Ni-Cu sulfide deposits are hosted by intrusions occurring in within plate settings, e.g., Archean komatiite-related deposits in Australia and deposits in LIP-related mafic-ultramafic layered intrusions, such as Noril'sk in Siberia (Naldrett, 2010). However, there are also important Ni-Cu resources in convergent margin environments (Manor et al., 2016). Because of the synorogenic timing of the mafic magmatism, the

intrusions commonly have a complicated tectonomagmatic history that makes them distinctive compared to anorogenic Ni-Cu sulfide-bearing intrusions, such as Kambalda in Australia (Naldrett, 2010) or Norilsk in Russia (Makkonen, 2015).

The synorogenic mafic and ultramafic intrusions can be further classified into 1) those that emplaced during active and compressive orogeny and 2) zoned Alaskan-type intrusions (Irvine, 1974) that were emplaced during epi-orogenic readjustments (Naldrett, 1997). The former are hosts to relatively small Ni-Cu mineralization, including ultramafic and mafic intrusions of the Kotalahti and Vammala Nickel Belts in Finland (Cox and Signer, 1986) and the Moxie pluton in Maine (Thompson and Naldrett, 1984). So far, Alaskan-type intrusions have not been considered as significant hosts of Ni-Cu ores (Naldrett, 1997) though some of them are known to contain sulfide rich horizons, including the Duke Island Complex (Thakurta et al., 2008).

According to Maier (2015), the mineralized igneous bodies in convergent settings are generally relatively small and irregular in shape. They consist of lava channels, dikes, sills and chonoliths. All of them are usually interpreted as magma feeder conduits for intrusions (Naldrett, 1997). The typical ore mineral assemblage in sulfide ores is pyrrhotite-pentlandite-chalcopyrite, and PGE contents are frequently low (Papunen, 1986, 1989; Makkonen and Halkoaho, 2007; Makkonen, 2015). Nickel ores are usually within the stratigraphically lowermost part of the intrusion (Makkonen et al., 2017). Ore bodies are often zoned, with the most massive ore being situated at the basal contact. Massive ore can be up to a few meters thick and it often forms breccias with the wall rock. Disseminated ores are the most common ore type observed in the deposit. In these ores, Ni/Co of the sulfides and Ni tenors increase towards the stratigraphic base. Disseminated ores grade into net-textured ore when the amount of sulfides increase. In net-textured ore, sulfides form an interconnected network enclosing silicate minerals. In addition to the above-mentioned ore types, the deposits often contain massive to semi-massive off-set ores hosted by the wall rocks. They occur usually in the stratigraphic floor of the intrusive bodies, being located 50-200 meters away from the main intrusion.

The Svecofennian Ni-Cu sulfide deposits in Finland were formed in a convergent setting during the peak deformation and metamorphism of the Svecofennian orogeny at ca. 1.88 Ga (Makkonen, 2015; Peltonen, 2005). They occur in two separate belts, known as the

Kotalahti and Vammala Nickel Belts. The geochemical characteristics of the Svecofennian intrusions suggest a craton margin or marginal basin environment, for example, a back-arc setting (Makkonen, 1996; Makkonen and Huhma, 2007).

Deposits that resemble the Finnish ones in terms of their tectonic setting occur in the Nagssugtoqidian Mobile Belt in Greenland (Lebrun et al., 2018), the Lappvattnet nickel belt in Sweden (Weihed et al., 1992), the Sveconorwegian belt in Norway and the Grenville belt in Canada (Boyd and Mathieson, 1979; Boyd et al., 1988; Lamberg, 2005), the Variscan orogeny of Spain (Pina et al., 2010), the circum-superior belt of Canada (Hulbert et al., 2005), the Fox River belt (Heaman et al., 1986), the Lynn Lake belt (Turek et al., 2000), and the Halls Creek orogen in Australia (Hoatson and Blake, 2000). The metamorphic grade of these belts varies typically from amphibolite facies to granulite fasies (Makkonen, 2015). Due to the emplacement during the peak deformation and metamorphism, intrusions occur in highly variable settings and in many cases they are dismembered.

Two hypotheses have been proposed for the genesis of the Svecofennian Ni-Cu mineralization. Peltonen (1995a) suggests that the intrusions were emplaced above an active subduction zone during progressive regional metamorphism and deformation. Some of the intruding magma penetrated sulfidic black schist layers while ascending to higher crustal levels. Assimilation of external sulfur provoked segregation of an immiscible sulfide melt and formed the nickel deposits at the stratigraphic base of the intrusions. The residual barren magmas ascended to higher crustal levels forming unmineralized intrusions.

Papunen (2003) proposes a somewhat different scheme by which the magma was contaminated already at an early stage. Fractionation and segregation of sulfide melt occurred after contamination in a lower crustal chambers. The final emplacement to the present position of the intrusions took place in the form of distinct magma pulses. Sulfides were injected into low-stress areas as a consequence of tectonic filter pressing, forming high-grade ores in mafic-ultramafic intrusions and high-grade offset ores. To explain the formation of the intrusions that only contain ultramafic cumulates, Papunen (2003) suggest that the residual mafic magma escaped from the magma chamber to the surface.

Figure 1 displays a simplified model for the formation of the Svecofennian Ni-Cu sulfide ores after Makkonen (2015). He suggests that tholeiitic magmas with MgO of around 15 wt% ascended from the mantle along different pathways, undergoing varying amounts of crustal assimilation and olivine fractionation. Consequently, the parental magma compositions of the intrusion differ somewhat from each other. After its ascent, the magma intruded into sulfur-rich sediments at a crustal depth of 15-20 km. According to Makkonen (2015), sulfide segregation occurred in the magma conduits and in larger chambers. Sulfur saturation was mostly caused by assimilation of sulfur-rich sedimentary material. Contamination was most effective in comparatively large intrusions. The crustal level where assimilation took place varied. In cases where sulfur saturation was reached after significant olivine fractionation, the intrusions may contain Cu ± PGE-rich mineralization. The R factor varied mostly between 200 and 1300 and therefore a wide range in nickel tenor can be recognized. The average nickel grade in disseminated ore types is ≤1 wt%. Massive ores can contain up to 7 wt% Ni.

Some magmas reached the surface remaining uncontaminated. This is supported by their initial ε_{Nd}(1880 Ma) values of around +4 and by insignificant chalcophile element depletion (Ni, PGE) (Barnes et al., 2009). Distinctively, most of the Svecofennian intrusions are strongly depleted in PGE. These intrusions show a wide range of the initial ε_{Nd}(1880Ma) values from −2.4 to +3.1 ±0.4 depending on the amount and type of the assimilated material (Makkonen 1996; Makkonen and Huhma 2007).

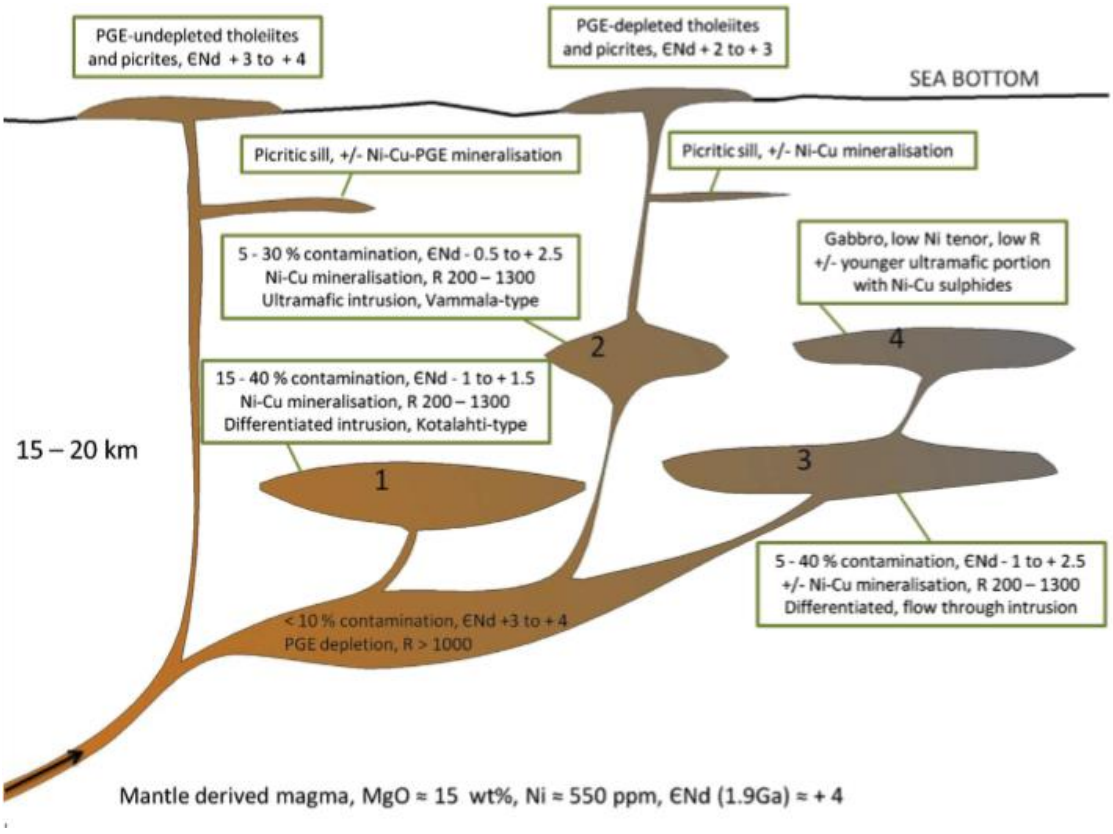

Figure 1: Simplified model for the Svecofennian mafic-ultramafic magmatism and related Ni-Cu deposits (Makkonen, 2015). The εNd values are lower when the intrusion is near the Archean rocks. Numbers 1-4 refer to (1) the Kotalahti-type intrusions, which are differentiated and layered ultramafic to gabbroic rocks; (2) Vammala-type intrusions, which represent ultramafic and weakly differentiated magma conduits; (3) ultramafic cumulate bodies from which the residual melt has been dynamically expelled upwards; (4) gabbroic intrusions, with or without peridotite, which were formed as a result of later pulses of olivine-bearing melt from the lower magma chamber. Published with permission from Elsevier.

Svecofennian intrusions frequently contain a gabbroic and ultramafic portion that are separated by a sharp contact (Makkonen, 2015). The ultramafic part is usually intrusive in relationship to the gabbroic portion. The relationship can be illustrated by the following model. The ascending magma fractionates in a staging chamber below the final emplacement location. The differentiated magma at the top of the staging chamber ascends further first. Olivine-rich slurries, with 15-20 wt% MgO, follow the same route and intrude the gabbroic body. Flow differentiation can lead to further concentration of olivine and sulfide, forming sulfide-rich peridotites.

3. GEOLOGICAL OVERVIEW

3.1. Svecofennian domain and its geotectonic evolution

The study area is located in the Western Finland Subprovince of the Svecofennian domain (SD) (Nironen, 2017). The SD covers an area of 800 x 800 km in Finland and Sweden (Kähkönen, 2005). In the east and northeast, it is bordered by the Archean basement with its Karelian sedimentary-volcanic rock cover (Lundqvist and Autio, 2000). In the west, the domain is bounded by the Caledonides and in the southwest by the Southwest Scandinavian domain.

The supracrustal rocks in the SD are mostly turbiditic metasedimentary rocks, though graphite-bearing schists, black schists, and carbonate beds are also abundant (Weihed and Mäki, 1997). The plutonic rocks in the SD comprise dioritic to granitic intrusions and mafic-ultramafic intrusions (Simonen, 1980). Volcanic rocks crop out as a narrow discontinuous belts among metasedimentary rocks and intrusive complexes (Weihed and Mäki, 1997).

Luukas et al. (2017) divide the Svecofennian domain into two areas: the Southern Finland Subprovince and the Western Finland Subprovince (Fig. 2). The Ylivieska gabbro belongs to the latter. The Western Finland subprovince is mostly occupied by the Central Finland granitoid complex (CFGC) and it was formed by the Svecofennian orogeny and related magmatism at around 1.92-1.89 Ga. The event was accompanied by the accretion of the Southern Finland Subprovince to the Karelian craton.

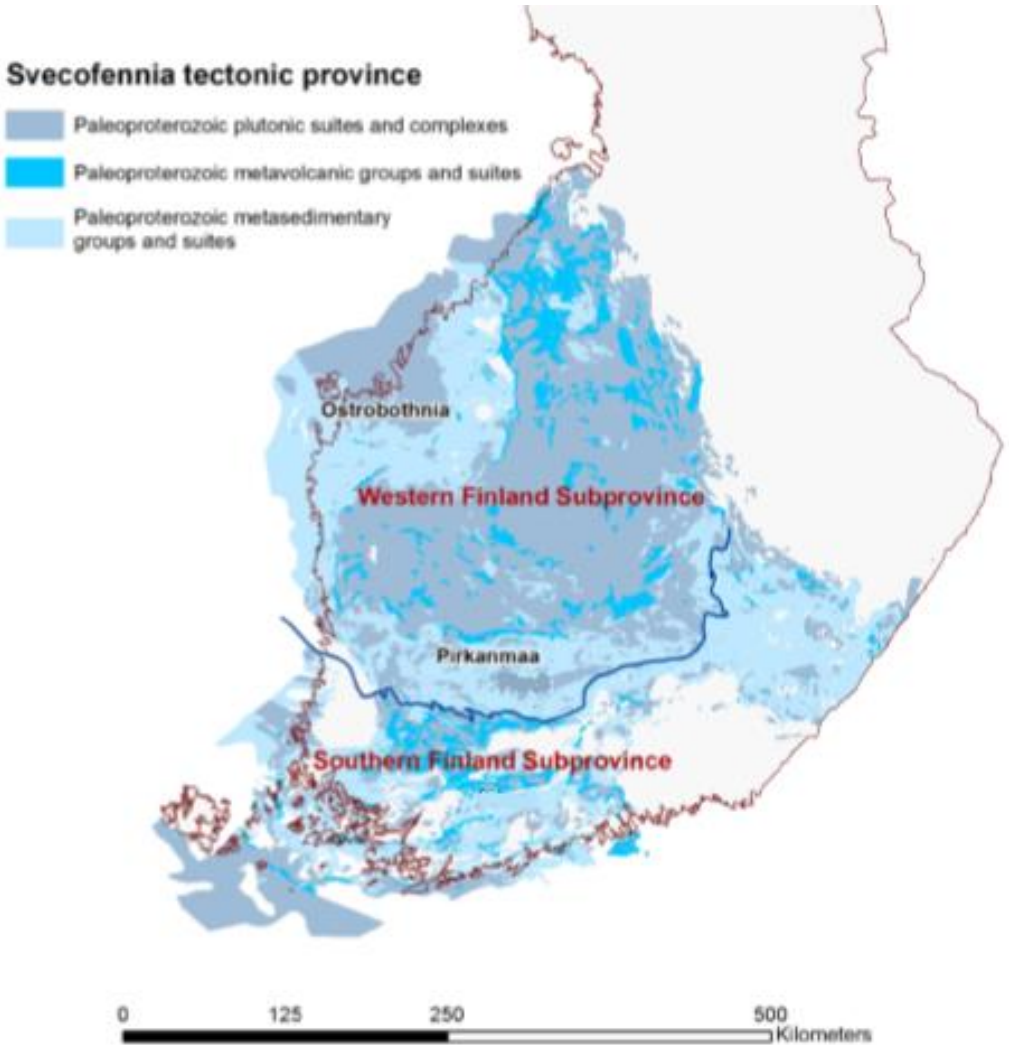

Figure 2. Location of the Western Finland and Southern Finland Subprovinces within the Svecofennian domain (Luukas et al., 2017). Published with permission of GTK.

Nironen (2017) describes the Svecofennian orogeny as a complex set of tectonic events including continental extension, multiple collisional events, accretion of several microcontinents and finally an orogenic collapse before the crust stabilized. The geological evolution of the Svecofennian orogeny is summarized in Table 1.

Table 1. Svecofennian orogeny and related geotectonical events (Nironen, 2017).

Age (Ga)	*Event*
1.92	Initiatiation of the Svecofennian orogeny by collision of the continental blocks of Karelia and Norrbotten. A volcanic Knaften arc attached to the Norbotten block before the collision.
1.92-1.91	Deposition of foreland sediments of the Karelia-Norrbotten collision with contemporary accretion of Keitele microcontinent and its attached volcanic arc to the Karelia continental margin.
1.91-1.90	Change in the plate movement direction occurs (Kalliomäki et al, 2014; Nironen, 1997; Lahtinen et al. 2005).
1.90-1.89	Bothnia microcontinent advances towards the already accreted complex from the south and transform fault develops between the two microcontinental blocks.
1.89-1.88	Bergslagen microcontinent approaches from the south.
1.88-1.87	Orthogonal collision of the Keitele and Bergslagen microcontinents.
	Peak of early Svecofennian deformation, metamorfism and felsic-mafic magmatism occurs. Keitele microcontinent starts to rotate dextrally contemporally with magmatism (Pajunen et al., 2008).
1.87	Amalgamation of all previously mentioned continental and microcontinental blocks, remnants of oceanic crusts as well as intervening arcs and passive margin sequences forming the protocontinent Fennoscandia.

Change in deformation from contractional into transtensional excluding southern Finland where contractional deformation prevailed.

Emplacement of A-type granitoids along transtensional shear zones (Nironen, 2005).

1.84-1.83 Crustal extension accompanied by the mafic-felsic magmatism (Nironen, 2005; Pajunen et al., 2008).

1.82-1.81 Amalgamation of protocontinents Fennoscandia and Volgo-Sarmatia.

Luukas et al. (2017) divide the rocks of the Western Finland Subprovince into two supergroups, of which the older (>1.9 Ga) is called the Northern Ostrobothnia supergroup and the younger (<1.9 Ga) the Central Ostrobothnia supergroup. The Northern Ostrobothnia supergroup includes the metavolcanic rocks of the lower Pyhäsalmi group and the metavolcanic rocks of the upper Vihanti group as well as the related lithodemic units: the tonalitic Venepalo plutonic suite and the Kokkoneva intrusive suite (Mäki et al., 2015; Laine et al., 2015, Luukas et al., 2017). All the above-mentioned units represent the same magmatic event that occured at 1.93-1.91 Ga. The Central Ostrobothnia supergroup consists of the Tampere group in Pirkanmaa and the Ylivieska group in Ostrobothnia (Luukas et al, 2017). These groups surround the Central Finland Granitoid Complex (Kähkönen, 2005).

3.2. Central Ostrobothnia

Central Ostrobothnia is a region in Central Finland located by the Gulf of Bothnia. The bedrock of Central Ostrobothnia is bordered by the Archean Basement Complex in the east, by the Central Finland Granitoid Complex in the south and by the Bothnian belt in the southwest (Weihed and Mäki, 1997). The supracrustal rocks of Central Ostrobothnia can be divided geographically into three different areas that are separated from each other by shear zones, thrust and intrusions. The block formed by the south-westernmost part of Central Ostrobothnia consists predominantly of greywackes and pelites that have been metamorphosed to biotite-plagioclase schists and gneisses. They both occur within elongated formations of intermediate to mafic metavolcanic rocks (Vaarma and Kähkönen, 1994). Well-preserved primary sedimentary and volcanic structures suggest a turbiditic origin for the schists and a subaqueous depositional environment for the metavolcanic rocks (Weihed and Mäki, 1997). The metamorphic grade increases towards the Bothnian Bay.

The study area belongs to the second area: the 1.90–2.00 Ga Nivala gneiss complex (Isohanni et al., 1985). The complex is situated between a N-trending belt of granitoid batholiths (Toholampi-Rautio-Kalajoki) and the SE-trending Ruhanperä Fault Zone (Weihed and Mäki, 1997). The majority of the rocks are mica gneisses that locally have amphibole-, graphite- and sulfide-bearing intercalations (Isohanni et al., 1985). The migmatites are host rocks to the Ni-bearing ultramafic intrusions in the Nivala area (Weihed and Mäki, 1997). The complex is surrounded by several formations of metavolcanic rocks, such as the Kuusaa, Kangas, Sievi and Antinneva Formations. The metavolcanic formations are separated from each other by volcaniclastic rocks, such as polymict conglomerates, siltstones and sandstones. The Ylivieska gabbro-peridotite intrusion is located on the western side of the Nivala gneiss complex between the Kangas and Sievi Formations.

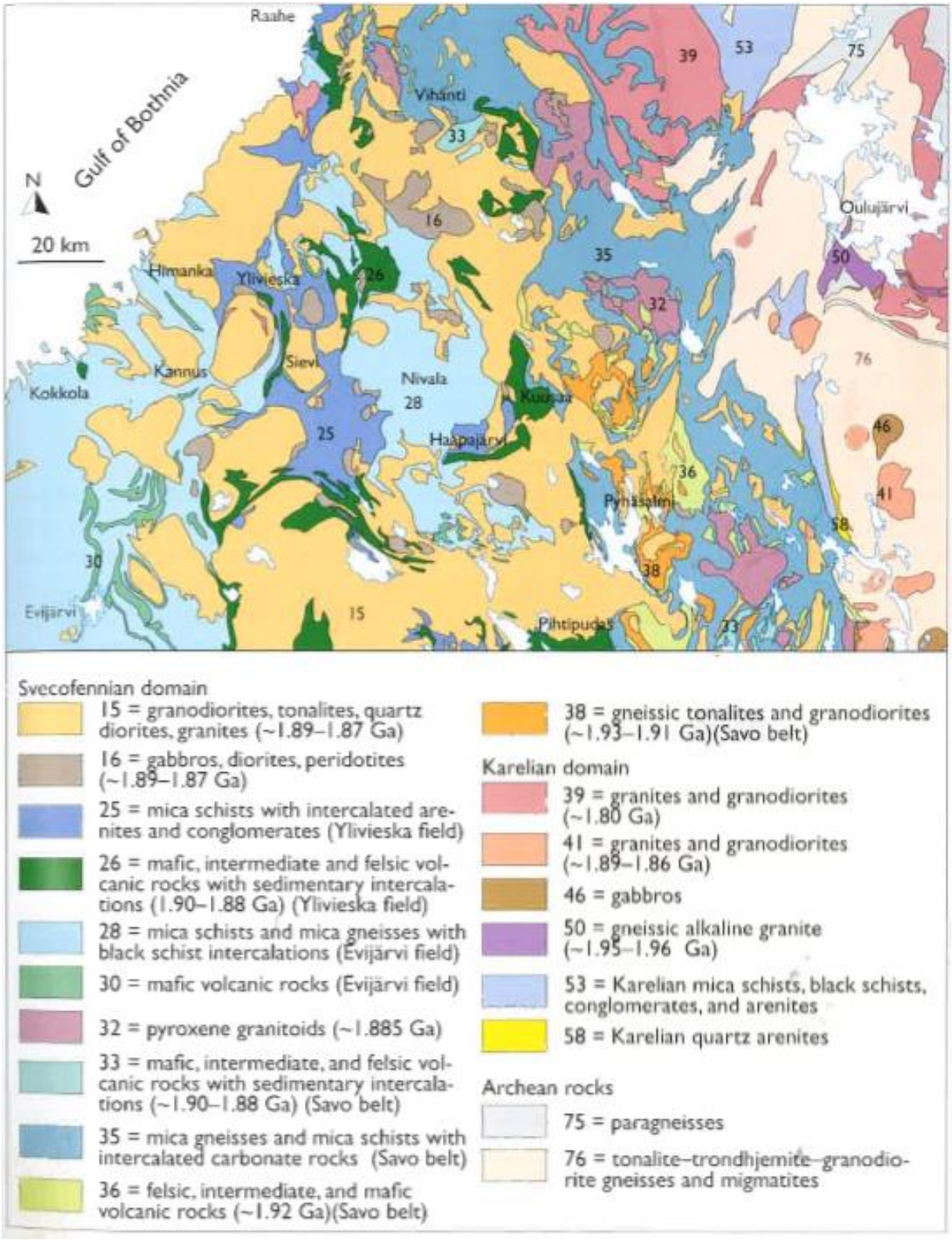

Figure 3. Simplified geologic map of Central Ostrobothnia (Kähkönen, 2005). Published with permission of Elsevier.

The Vihanti-Pyhäsalmi ore belt represents the third major area in Central Ostrobothnia (Weihed and Mäki, 1997). The block constitutes the north-western part of the Savo Belt. It is bordered by the Ruhaperä Fault Zone and the Haapavesi igneous complex in the south-west and by the Revonneva Shear Zone and the Archaean Basement Complex in the north and east. The area is notably metamorphosed and incorporates predominantly migmatitic mica gneisses., which are intercalated with quartz feldspar gneisses, black schists, skarn rock beds, and some volcanic amphibolites.

3.3. Kotalahti Nickel Belt

The majority of orogenic mafic-ultramafic intrusions that host nickel mineralization in Finland are located within the Kotalahti and Vammala Nickel Belts in the Western Finland Subprovince (Makkonen et al. 2017). The Kotalahti belt is situated close to the margin of the Archean craton between the Keitele microcontinent and the Archean craton whereas the Vammala belt is located along the southern margin of the Keitele microcontinent against the Bergslagen microcontinent. The Vammala belt continues to the Skellefteå area in Sweden, being a 1000-km-long rift/passive margin to accretionary wedge zone. Lebrun et al. (2018) recently proposed that the the Ammassalik Intrusive Complex and the south-east Greenland region in Greenland are direct continuities of the Kotalahti belt.

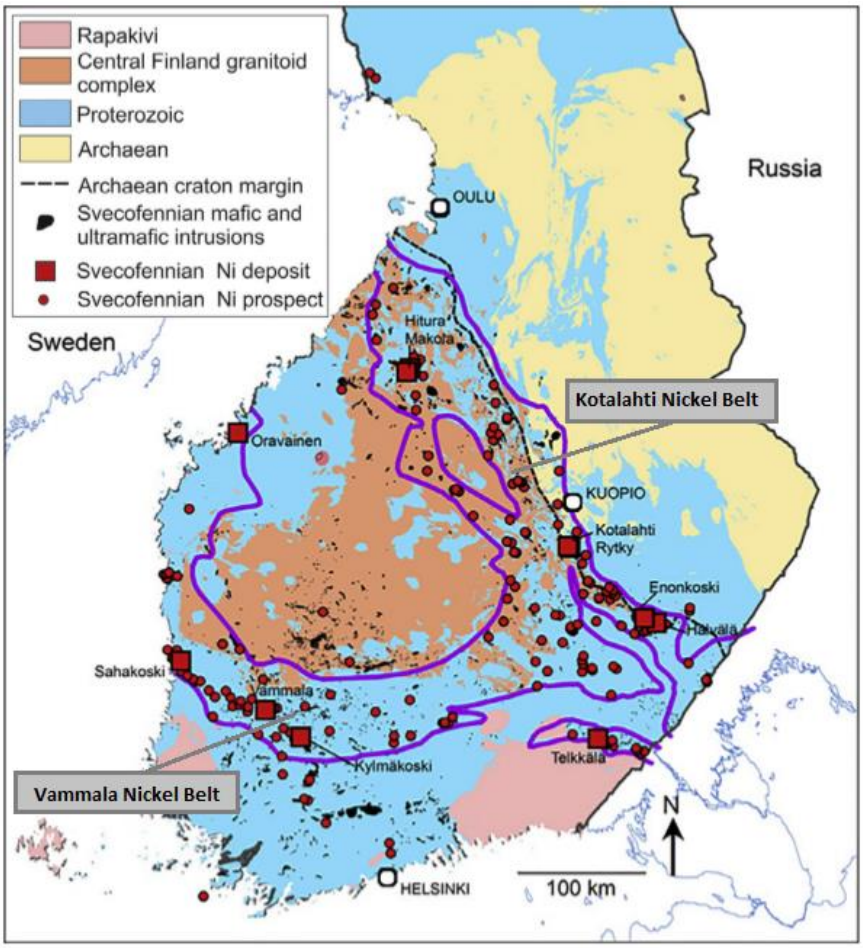

Figure 4. Distribution of the mafic and ultramafic intrusions and related nickel deposits in the Kotalahti and Vammala Nickel Belts (Makkonen et al., 2017). Published with permission from Elsevier.

Intrusions of the Kotalahti belt were emplaced along transtensional shear zones during the collision of the Keitele microcontinent to the Archean craton (Peltonen, 2005; Nironen, 2017). Therefore, the intrusions are generally strongly deformed and located in areas of relatively high metamorphic grade. Mineralized intrusions are usually found within migmatitic mica gneisses, which often contain graphite-rich layers. Some intrusions occur within Archean gneisses or within rock of the craton margin sequence, including Paleoproterozoic quartzites, limestones, calc-silicate rocks, black schists and diopside-bearing amphibolites.

The majority of the intrusions are relatively small, being usually up to several kilometers long and a few hundred meters wide at the surface (Makkonen, 2015). The maximum thickness is commonly less than 2 km. Intrusions of the Kotalahti Nickel Belt are strongly

differentiated, consisting of olivine cumulates, pyroxene cumulates, and plagioclase-bearing cumulates (Mäkinen, 1987; Makkonen, 1996; Makkonen, 2015). Intrusions that only contain ultramafic rocks are rare. Magmatic layering can be observed in some intrusions even though the initial layers are often confused by polyphase deformation. The largest intrusions within the belt includes the mafic and ultramafic bodies of Ylivieska, Alpua in the Vihanti area and Saarela in the Pielavesi area. None of them is known to host economically important Ni-Cu mineralization. The Vammala-type intrusions present magma conduits and are less differentiated compared to the Kotalahti-type intrusions. They are mostly composed of olivine cumulates and other ultramafic rocks.

Makkonen et al. (2008) classifies 11 mafic and ultramafic intrusions of the Kotalahti Nickel Belt into barren, intermediate and mineralized categories on the basis of the amount and composition of sulfides. The mineralized group includes the Naistenrako, Niinimäki, Rytky and Törmälä intrusions. The Heimonvuori, Kerkonkoski and Ylivieska intrusions belong to the intermediate class, whereas the Majasaari, Luikujärvi, Luusniemi and Kylmälahti bodies are classified as barren intrusions. The locations of the intrusions are presented in Fig. 5.

Figure 5. Distribution of mafic and ultramafic intrusions and related nickel deposits in the Kotalahti Nickel Belt on a geological map. Intrusions shown by the numbers: 1 = Ylivieska, 2 = Majasaari,
3=Kerkonkoski,4=Törmälä,5=Naistenrako,6=Luusniemi,7=Rytky,8=Heimonvuori,9=Kylmälahti,10=Luikujärvi,11=Niinimäki (Makkonen et al., 2008). Published with permission from Elsevier.

The Ylivieska gabbro-peridotite intrusion is located in the Nivala area (Isohanni et al., 1985), which contains several Ni-bearing ultramafic and mafic bodies including the nickel deposits of Hitura and Makola (Weihed and Mäki, 1997). Fine-grained disseminated sulfide is common in the peridotitic parts of the Ylivieska intrusion (Makkonen et al., 2008). The best intersections are: 1.5 m at 0.51 wt% Ni and 0.29 wt% Cu in plagioclase-bearing lherzolite and 8 m at 0.72 wt% Ni and 0.30 wt% Cu in metapyroxenite. A more detailed description of the intrusion is presented in Chapter 4.

The ultramafic bodies of the Hitura and Makola areas are analogous to the Vammala-type intrusions, even though they are located geographically in the Kotalahti Nickel Belt. The Hitura ultramafic complex consists of three small and closely spaced mineralized serpentinite bodies, which are located in an area of 0.3 x 1.5 km (Isohanni et al., 1985; Weihed and Mäki, 1997). Geophysical surveys indicate that the complex continues to a depth of at least 1000 m. Sulfides are present throughout the northern part of the complex. The ore is divided into three textural types: scattered fine-grained sulfide dissemination in the serpentinite core, medium- to coarse-gained and moderate dissemination in the marginal serpentine-amphibole rock, and high-grade interstitial sulfide disseminations and massive accumulations in the amphibole rock of the contact zone.

The Makola deposit is located 3.5km south-west from Hitura, occurring in a deep funnel-shaped ultramafic intrusion (Isohanni et al., 1985). The ultramafic body is 120 x 20-40 m^2 wide at the surface and reaches a depth of 200 m. It is composed of metadunites, metaperidotites and metapyroxenites. Almost the whole body is mineralized. In metadunites, sulfides occur as homogenous and abundant interstitial dissemination, whereas in metaperidotites and metapyroxenites, they are more randomly distributed and also the textures of the sulfides are more variable.

According to Makkonen et al. (2008), the Majasaari intrusion is located in the Viitasaari area as a 1-km-wide, roundish body. The central part of the intrusion is mostly composed of norite. Gabbronorite and olivine gabbronorite are present locally. Olivine gabbronorite transfers gradationally into plagioclase-bearing lherzolite at the SE margin of the intrusion. Plagioclase has a distinct cumulus form in the gabbroic rocks, whereas in the lherzolites, it occurs as an intercumulus mineral. Sulfides are present only locally, including pyrrhotite, pentlandite, and chalcopyrite.

The Törmälä and Kerkonkoski intrusions are situated in the Rautalampi area (Makkonen et al., 2008). The former is 50 x 150 m wide at the surface and extends to a depth of 40 m. The intrusion is mainly composed of olivine gabbronorite and plagioclase-bearing lherzolite. Coarse-grained pyroxenite and gabbronorite are present along the intrusion margins. Pyrrhotite, pentlandite, and chalcopyrite occur throughout the intrusion in varying amounts as coarse-grained dissemination and breccias. The estimated mineral resources of the Törmälä intrusion are 0.12 Mt at 0.6 wt% Ni, 0.3 wt% Cu and 6.0 wt% S.

According to Makkonen et al. (2008), the Kerkonkoski intrusion is exposed as three separate blocks, which are located in a 1.5 km wide area. The intrusion is 50 m thick and displays no compositional variation. It is mostly composed of serpentinized peridotitic rocks that have olivine and clinoamphibole as the main minerals. Pyrrhotite, pentlandite, and chalcopyrite are present locally. The average Ni content in the mineralized areas is 0.2-0.3 wt%.

The Heimonvuori, Kylmälahti, Luusniemi, Naistenrako and Rytky intrusions are located in the Kotalahti area (Makkonen et al., 2008). The Luusniemi intrusion is composed of serpentinized lherzolites, olivine websterites, websterites, and gabbroic rocks. The intrusion is up to 5 km in width at surface, and the ultramafic part occurs as a 1-km-wide cone. Sulfides are very rare in the intrusion.

The Naistenrako intrusion is small (150 x 150 m) layered body, with its composition changing from metagabbro and olivine gabbronorite into plagioclase-bearing lherzolite (Makkonen et al., 2008). Disseminated sulfides are common in the gabbroic rocks and lherzolite, including pyrrhotite, pentlandite, and chalcopyrite. Breccia ore is present in metagabbro in the southern margin of the intrusion.

The Heimonvuori forms a small (70 x 70 m), funnel-shaped body (Makkonen et al., 2008). The central part of the intrusion consists of plagioclase-bearing lherzolites, which gradationally change upwards into olivine-bearing websterites and gabbros. Weak magmatic lamination is present in the lherzolite. Pyrrhotite, pentlandite and chalcopyrite occur locally. The best intersection is 1 m long and contains 0.37 wt% Ni, 0.16 wt% Cu, and 2.9 wt% S.

According to Makkonen et al. (2008), the Rytky intrusion is composed of two blocks, which have a surface section of 0.5 x 1 km. The main rock types include lherzolites,

websterites, melagabbros, gabbros, and gabbronorites. Sulfides are most abundant in coarse-grained lherzolites, websterites and melagabbros, in which they are present as matrix ore. Medium-grained lherzolites and websterites contain sulfides as dissemination. Narrow massive ore layers occur locally. The mineral resources of the intrusion are around 1 Mt at 08 wt% Ni, 0.3 wt% Cu and 4.4 wt% S.

The Kylmälahti intrusion is a 50-m-wide, N-S-trending, vertical body. It is composed of homogenous wehrlitic peridotite, which is strongly sheared and altered. Metapyroxenite and hornblendite are found locally along the intrusion margins. Disseminated sulfides are common, even though the Ni and Cu concentrations are less than 0.2 wt%.

The Juva area hosts the Niinimäki and Luikujärvi intrusions (Makkonen et al., 2008). The former is mainly composed of gabbroic rocks. Harzburgite occurs as 50- to 150-m-thick layers within the gabbro. At the surface, the intrusion is only 1 km^2 in size, but at the 100-m level below the surface, it is 1 x 2 km wide. The total thickness of the body is 300 meters. Altered gabbros contain 0.22 Mt disseminated, net-textured and massive sulfides with 0.9 wt% Ni, 0.3 wt% Cu and 8.3 wt% S. Harzburgites host 2 to 3 Mt disseminated sulfides with 0.3 to 0.4 wt% Ni. The Luikujärvi intrusion is 0.5 x 1 km wide at the surface. It consists of gabbros, hornblende gabbros, hornblendites, and strongly serpentinized lherzolites. The overall sulfide content of the intrusion is very low.

Whole-rock compositions of the mineralized, intermediate and barren intrusions differ notably (Makkonen et al., 2008). The mineralized intrusions commonly have elevated Al_2O_3/CaO ratios and Zr, P_2O_5, Th and LREE contents in peridotites, indicating country rock contamination. They are also orthopyroxene-rich and have plagioclase as an intercumulus mineral at an early stage of the magma crystallization. Barren intrusions are typically clinopyroxene-rich. Chemical data on olivine from the mineralized intrusion show nickel depletion. In barren intrusions, olivine is undepleted or only shows relatively low Fo and Ni values. According to Makkonen (2015), the most prospective intrusions are those that contain high-Fo (>80 mol%) and high-Ni (>1500 ppm) samples toward low-Ni samples (≈500 ppm), implying that sulfide segregation has taken place in the intrusion. If the intrusion contains only nickel-depleted olivine, it indicates that olivine fractionation took place prior to the final emplacement of the intrusion. The geochemical differences between the intrusions can be mostly explained by contamination with country rock material.

Figure 6 shows a Ni versus Fo plot for olivines analyzed from 11 mafic-ultramafic intrusions of the Kotalahti Nickel Belt (Makkonen et al., 2008). Most of the samples plot in the sulfur-saturated field. Some samples from Ylivieska, Luikujärvi and Majasaari as well as a significant number of samples from Rytky and Niinimäki plot in the sulfide-undersaturated field.

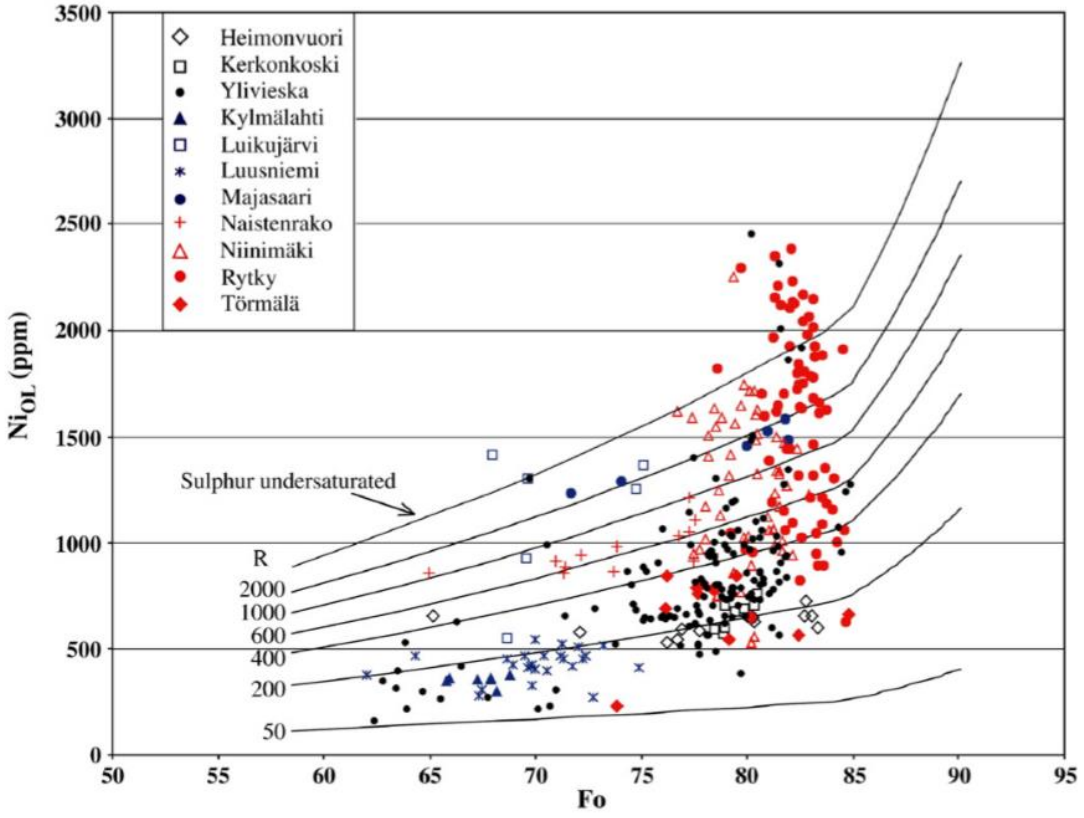

Figure 6. Nickel versus Fo plot for olivines from selected intrusions of the Kotalahti Nickel Belt. Red symbol = mineralized intrusion, black symbol = intermediate intrusion, blue symbol = barren intrusion (Makkonen et al., 2008). Published with permission from Elsevier.

Chemical data on olivine displays distinctly the mineralized character of the Rytky and Niinimäki intrusions and the barren nature of the Kylmälahti, Luikujärvi, Luusniemi and Majasaari intrusions (Makkonen et al., 2008). The Törmälä intrusion shows nickel depletion but no signs of in-situ ore formation. The mineralized character of the Naistenrako intrusion requires further confirmation. From the intermediate intrusions, Heimonvuori and Kerkonkoski show an intermediate ore potential on the basis of their olivine compositions, whereas the Ylivieska intrusion displays a higher ore potential.

4. GENERAL GEOLOGY AND PREVIOUS STUDIES OF THE YLIVIESKA GABBRO-PERIDOTITE INTRUSION

The 1.90 Ga Ylivieska gabbro-peridotite intrusion is situated five kilometers southwest of the Ylivieska village (Pesonen and Stigzelius, 1972). It can be recognized from aeromagnetic maps as an area of an expectionally strong positive anomaly (Sipilä, 1976). The intrusion is approximately 30 km^2 in size and several km thick (Kontoniemi and Mäkinen, 2001). The ultramafic part of the intrusion extends to a depth of approximately 1 kilometer. The intrusion is encircled by intermediate tuffaceous sandstones and conglomerates in the north, south and west (Salli, 1955; Sipilä, 1984; Luukas et al., 2017). In the east, the intrusion is bounded by a narrow zone of felsic volcanic rocks (Fig. 7).

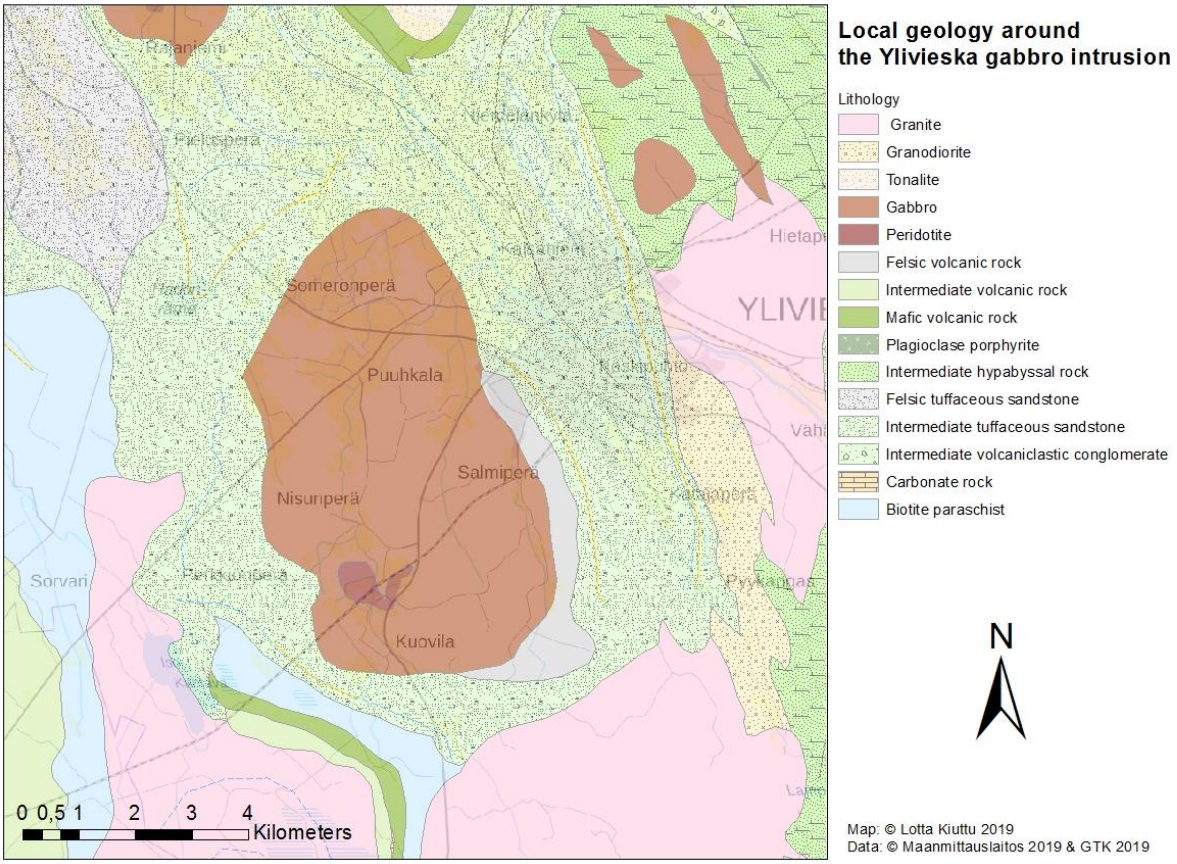

Figure 7. Local geological map around the Ylivieska gabbro-peridotite intrusion. (Modified after Bedrock of Finland – DigiKP)

The bedrock of the Ylivieska area consists of Svecofennian Paleoproterozoic supracrustal and plutonic rocks including the following rock types (from oldest to youngest): schists, ultramafic rocks, gabbros, diorites, granites, granitic veins and diabases (Kontoniemi and Mäkinen, 2001; Salli, 1955; Sipilä, 1984). The supracrustal rocks belong to the Younger Svecofennian group of Korsman et al. (1997) and are intruded by the syn- and late orogenic gabbros and granitoids.

The first geologial map sheet of the Ylivieska area was produced by Salli (1955), covering the Ylivieska gabbro intrusion and its surrounding rocks. The area was further studied in the 1960's when exploration for nickel started around the Ylivieska gabbro intrusion by the Malminetsijät AB and the Geological Survey of Finland (GTK) (Kontoniemi and Mäkinen, 2001). The exploration work included geological mapping, boulder search, moraine studies, geophysical surveys, and drilling. After these campaigns, the studies ceased for a while.

In the 1970's, GTK continued exploration work in the area covering the whole intrusion by geophysical surveys, carrying out some geochemical studies and doing more precise lithological mapping as well as more drilling (Sipilä, 1976). During these studies, the layered nature of the intrusion was discovered as well as the occurrence of a pipe-shaped ultramafic part at Perkkiönperä. During the geological mapping, T. Mutanen and E. Sipilä revised the geological map of the Ylivieska gabbro intrusion in 1973 (Sipilä, 1976). They divide the rocks of the intrusion into five classes:

1. Harrisites
2. Troctolites
3. Olivine gabbros
4. Pyroxene gabbros
5. Pegmatitic pyroxenites

The name "harrisite" is used to describe a dark peridotite unit with intercumulus plagioclase (Kontoniemi and Mäkinen, 2001). As shown by the map in Fig. 8, harrisites occur in the Perkkiö area as a wavy, circle-like pattern and, in the eastern part of the intrusion, as a stratiform unit. Sipilä (1976) suggest that the harrisite unit might be intrusive in character as it contains fragments of gabbro. Troctolite has been observed in

the eastern part of the intrusion in association with the harrisite unit (Kontoniemi and Mäkinen, 2001). Pyroxene gabbros seem to transfer gradationally from hornblende gabbros to diorites. The name pegmatitic pyroxenite is used in the map to display coarse-grained and non-magnetic pyroxenites as well as plagioclase pyroxenites (Kontoniemi and Mäkinen, 2001).

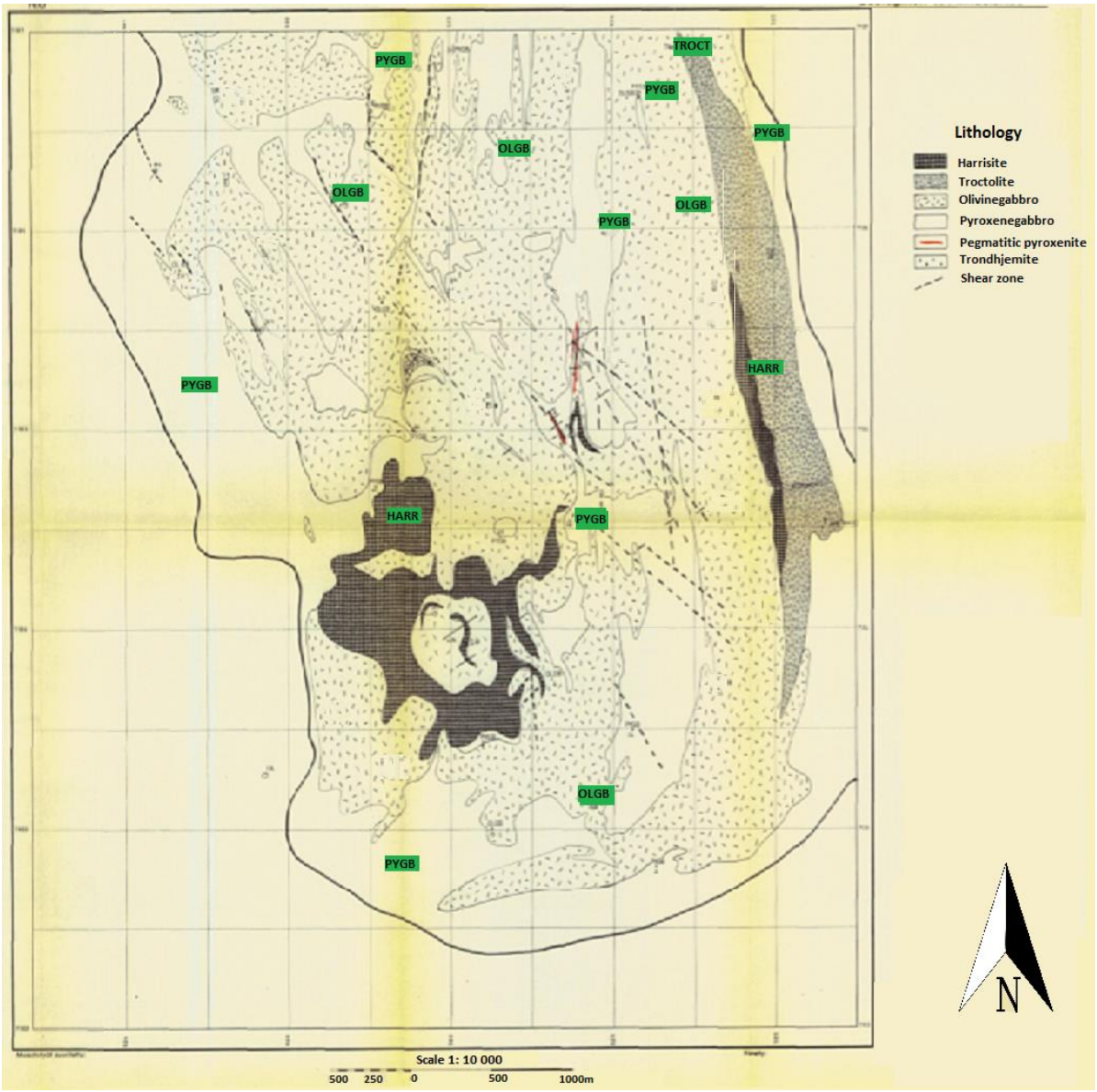

Figure 8. Lithological map of the southern part of the Ylivieska gabbro-peridotite intrusion. HARR = Harrisite, PYGB = Pyroxene gabbro, OLGB = Olivine gabbro and TROCT = Troctolite. Modified after Sipilä (1976). Published with permission of GTK.

Sipilä (1976) presents that the contacts between different rock units are sharp and the gabbroic part is clearly layered. He classifies the gabbroic rocks of the layered series as olivine gabbros and pyroxenite gabbros, but if the classification scheme of Streckeisen (1974) is used, the unit is mostly composed of olivine gabbronorites, gabbronorites, and norites. The harrisite unit displays some poorly defined layering by changing from fine-grained, dark serpentinite to plagioclase-rich harrisite and partly even to troctolite. The magmatic layering is developed most prominently in the Sydänneva area (Kontoniemi and Mäkinen, 2001). In the eastern part of the intrusion, the layering dips 40-50° to the west, but in the southern part, it dips with the same angle to the northeast.

In the 1980's, the GTK continued exploration work in the area (Sipilä, 1984). The aim of this study was to examine large and deep structures of the intrusion using geophysical methods and to increase the knowledge of the ore potential of the peridotitic and pyroxenitic parts of the intrusion. The results were confirmed with deep drilling. The study revealed that the gabbroic part extends to a depth of several kilometers and the ultramafic part at least to a depth of one kilometer. It was also observed that the harrisite-serpentinite unit occurs as a pipe-shaped formation. In addition, some large and narrow zones of disseminated sulfides were found that contain around 0.36 wt% Ni and 0.14 wt% Cu.

Kontoniemi and Mäkinen (2001) restarted exploration activities on the Ylivieska gabbro intrusion in the 1990's. The studies comprised boulder search, moraine and peat studies, geological mapping, lithological sampling, heavy and light diamond drilling, geophysical surveys, chemical analyses, and mineralogical studies. In the end, the overall results were compiled and the rocks of the intrusion were classified petrologically and geochemically. This produced new information about the parental magma and differentiation processes during the formation of the intrusion. Also more precise information about different rock types was obtained.

According to Kontoniemi and Mäkinen (2001), the intrusion is mostly composed of layered gabbro, which comprises olivine gabbros, pyroxenite gabbros, and troctolites. In the southeastern part of the intrusion, in the Perkkiö area, there is a cup-shaped heterogeneous peridotite unit, which extends to a depth of 400 m. It represents the only peridotite outcrop that has been detected so far. However, there are several peridotite units

observed in the drill holes in the eastern and western parts of the intrusion. In the west, the peridotite unit is very heterogeneous whereas in the east, there are 3-4 separate peridotite plates dipping gently to the west. The thickness of these plates varies from 10 to 100 m. Altered gabbros occur between the plates. The peridotite units are mostly serpentinite and plagioclase peridotite. In the east, it is likely that plagioclase peridotite transfers gradationally to melagabbro or troctolite with intercumulus plagioclase. Peridotites are frequently associated with greenish and coarse-grained pyroxenites. Especially in the westestern part, pyroxenites are abundant. Pyroxenites occur between the peridotite and layered gabbro units.

The relationship between the peridotite unit and the layered gabbro has not yet been fully resolved (Kontoniemi and Mäkinen, 2001). According to Sipilä (1984), the peridotitic magma might have intruded into layered gabbro in a late stage. The unclear positions of the peridotite units with respect of layering and the presence of pyroxenites supports this theory.

For the geochemical classification, the data were divided into the western and eastern groups (Kontoniemi and Mäkinen, 2001). In the west, a pyroxenite-peridotite associaton is typical whereas in the east, a plagioclase peridotite-melagabbro association is common. In addition to these groups, the samples from the Sydänneva area were treated separately.

Kontoniemi and Mäkinen (2001) classify the rocks of the intrusion into serpentinites, peridotites, melagabbros, layered gabbros, and pyroxenites. Serpentinites and peridotites are present in the ultramafic part of the intrusion. When plagioclase appears as an intercumulus mineral in the beginning of the differentiation, the rock is named as plagioclase peridotite. When a peridotitic rock contains orthopyroxene oikocrysts, an additional suffix mottled (kirjava) is given.

The composition of the peridotites in the western part differs distinctively from that of the peridotites in the eastern part (Kontoniemi and Mäkinen, 2001). Presumably, there has been two different magma types that have produced the peridotites: more primitive in the west and less primitive in the east. According to Kontoniemi and Mäkinen (2001), the overall REE contents of peridotites are low, which indicates that there has not been any significant contamination by wall-rock interaction. Kontoniemi and Mäkinen (2001)

reports that there are more sulfides in the peridotites that contain plagioclase compared to the other serpentinite-peridotite type of rocks in both parts. The estimation is based on his calculations of the ratios of copper, nickel and sulfur in the ultramafic rocks using the equation: Cu*Ni*S/ 1000000, ppm*ppm*%.

In the peridotites of the western part, the amount of Cr_2O_3 is much higher and the REE contents are lower compared to the eastern part (Kontoniemi and Mäkinen, 2001). There is also a greater variation in the composition of olivine in the western part, indicating that sulfide saturation took place in situ. The highest Ni and fosterite contents of olivine are detected from the western part. In the eastern part, the concentrations of incompatible elements, such as Zr and TiO_2, are higher.

According to Kontoniemi and Mäkinen (2001), the melagabbros are predominantly located in the eastern part of the Perkkiö area and in the Sydänneva area. They are characterized by gradational contacts to the plagioclase peridotites and by the occurrence of intercumulus plagioclase. In some parts of the intrusion, melagabbros seem to transfer into layered gabbros. In these cases, the contacts are usually sharp. The melagabbros are divided into three classes according to their chromium content: LOW_CR, MEDIUM_CR and HIGH_CR.

The HIGH_CR melagabbros contain high amounts of Cr_2O_3 (2-3.5 wt%) and usually have higher TiO_2 and V_2O_5 contents than LOW_CR (<0.5 wt% Cr_2O_3) and MEDIUM_CR (~1 wt% Cr_2O_3) (Kontoniemi and Mäkinen, 2001). Most of the HIGH_CR melagabbros are located in the Sydänneva area while the majority of the LOW_CR melagabbros occur as a massive unit in a deep horizon of the eastern part. MEDIUM_CR and HIGH_CR melagabbros are usually associated with plagioclase peridotites, and it is assumed that they form together a magmatic differentiation series. The LOW_CR melagabbros are suggested to be differentiates of other, more primitive, magma types.

Kontoniemi and Mäkinen (2001) observe that the Ni content of olivine at a given fosterite content is very high in the LOW_CR melagabbros in the eastern part and that the Ni content of olivine increases with increasing depth. A similar phenomenon prevails in the other gabbroic rocks and peridotites in the same area. Therefore, it seems that the ore potential increases with depth in the eastern part of the intrusion, even though peridotites

with higher than 1300 ppm of Ni in olivine have not been detected by drilling in deep horizons of the eastern part.

The layered gabbros are characterized by magmatic layering and the presence of autolithic fragments and cumulus plagioclase (Kontoniemi and Mäkinen, 2001). Based on their REE signature, they have not experienced any significant degree of contamination by wall-rock interaction. The layered gabbros can be divided geochemically into two main categories: GB1 and GB2. Group GB12 is compositionally between the two main categories. Layered gabbros of the GB1 type are located on the eastern side of the peridotite unit in the Perkkiö area, in deep horizons of the eastern part, presumably forming a consistent unit under the Perkkiö peridotite. According to Kontoniemi and Mäkinen (2001), it is possible that there were two slightly different types of gabbroic magma, of which one differentiated from a more primitive ultramafic magma and the other from a less primitive ultramafic magma.

In general, pyroxenites (PYR) occur as a sharply bounded units in the contact zone between layered gabbros and plagioclase peridotites (Kontoniemi and Mäkinen, 2001). They are usually greenish and coarse grained, but also darker, olivine-rich pyroxenites exist. Their major element composition differs notably from that of the other rock types of the intrusion. It is apparent that they were not formed from the parental ultramafic magma via normal magmatic differentiation. Olivine grains in pyroxenites show anomalously high Ni contents of up to 6730 ppm.

Kontoniemi and Mäkinen (2001) suggest that selective contamination of the ultramafic magma has presumably taken place during the formation of the the pyroxenites, because the pyroxenites contain considerable amounts of Cu, Zn, Rb and K_2O. On the other hand, the REE characteristics of the pyroxenites are similar to those of the peridotites and gabbros of the intrusion indicating that there has not been any significant contamination by wall-rock interaction.

Kontoniemi and Mäkinen (2001) suggest that both magma types that produced the peridotites were differentiated into melagabbros and after that into layered gabbros. The differencies in the parental magma and its primitivity can be recognized throughout the rock series by differencies in their whole-rock geochemistry. The more differentiated rock

series is located in the eastern part of the intrusion in the uppermost horizons of the Perkkiö area. The composition of the differentiates of the more primitive magma type varies more. The location of the less differentiated series is also more dispersed. According to Kontoniemi and Mäkinen (2001), it has been hard to determine how the different magma types intersect each other and also to solve what is their age relation. Therefore, it is also possible that the peridotitic magma intruded into layered gabbro afterwards.

According to Kontoniemi and Mäkinen (2001), significant fractionation of the sulfide phase did not take place during the crystallization of the intrusion. The magma became saturated in sulfide in its late stage of crystallization, which enabled the formation of disseminated sulfides only. Excluding the pyroxenites, there are no signs of contamination by wall-rock intercation in the rocks of the intrusion. This means that external sulfur needed for significant sulfide ore formation were not available.

5. SAMPLING AND METHODS

5.1. Sampling

Twenty-five representative samples from five different drill cores (M52-2431-95-426, YLIVIESKA-3, YLIVIESKA-4, YLIVIESKA-12 and YLIVIESKA-19) were collected by Timo Mäki from the Pyhäsalmi Mine Oy. A drill core log was available only for M52-2431-95-426. The drill holes used in this work were drilled by Malminetsijät AB and the Geological Survey of Finland (GTK) in the time period between 1973 and 1995. All of the studied drill holes are located in the Sydänneva area in the southern part of the intrusion (Fig. 9). The surface rock in drill hole M52-2431-95-426 is metagabbro (Digimap, GTK). The drill hole dip is 60° and the length 65.8 m. The location of the samples in the drill core is presented in Fig. 10. The dip of drill hole YLIVIESKA-3 is 45° and the hole lenght is 163.88 m. YLIVIESKA-4 extends to a depth of 200.03 m with a dip of 70°, whereas YLIVIESKA-12 dips with an angle of 45° to a depth of 133.03 m. The dip of drill hole YLIVIESKA-19 is 45° and the hole length 136 m.

The sampling was targeted to mineralized drill core intervals. Sample depths, rock types, thin section codes and coordinate information are presented in Table 2.

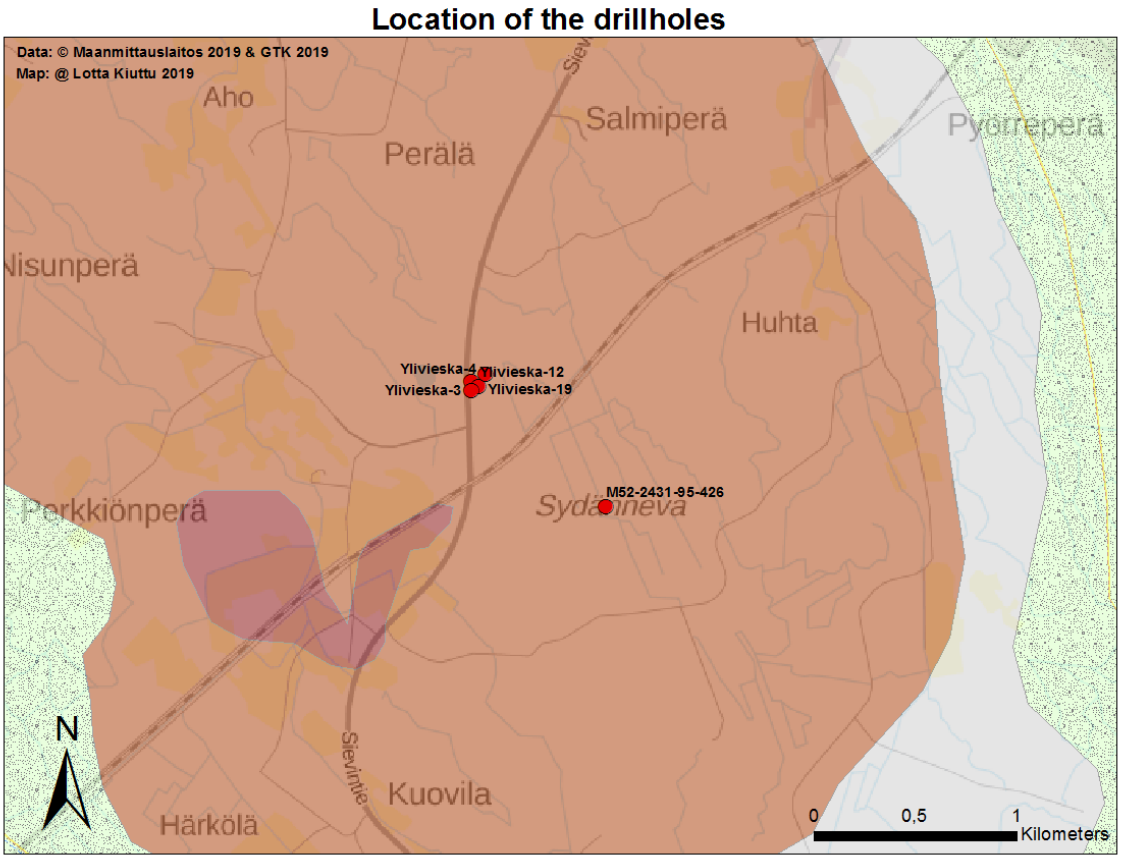

Figure 9. Location of the drill holes used in this work. Rock types shown by colours: reddish brown = peridotite, brown = gabbro, grey = felsic volcanit rock, green = intermediate tuffaceous sandstones and conglomerates (modified after Bedrock of Finland – DigiKP).

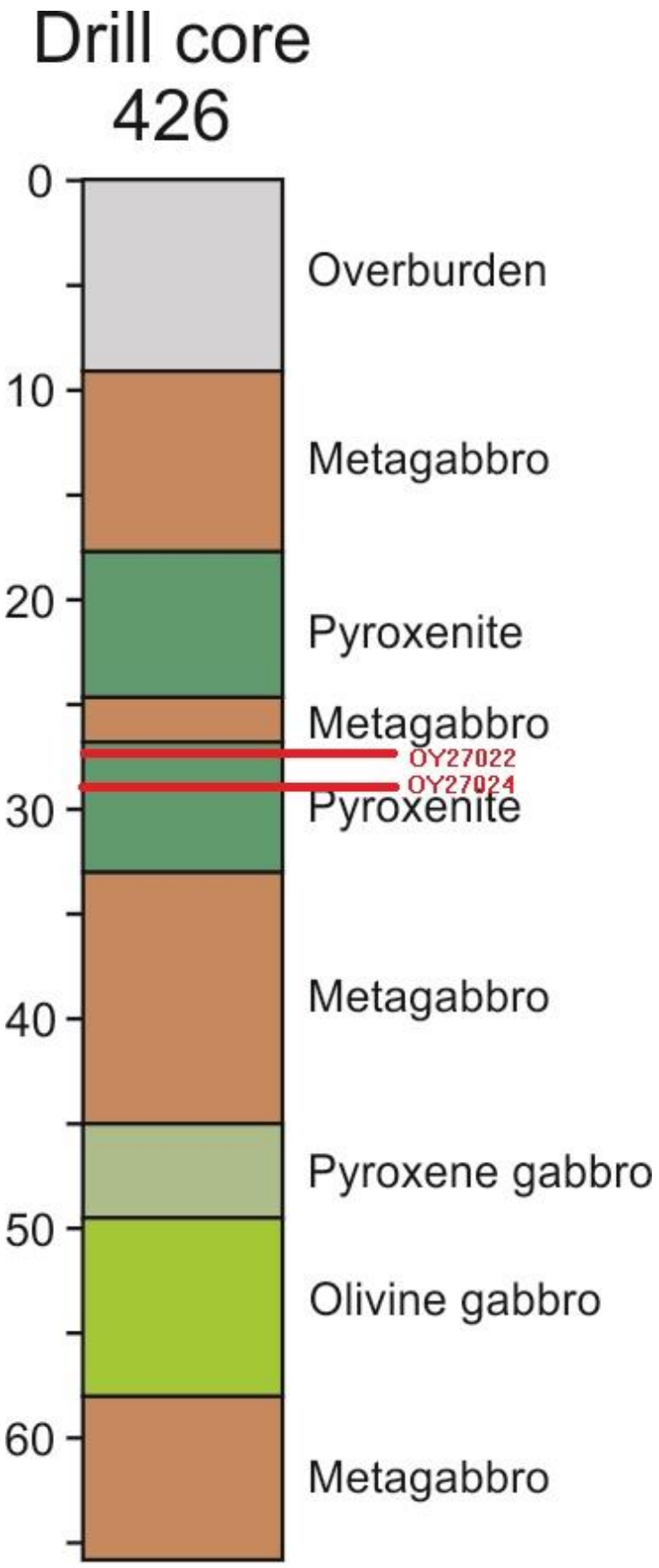

Figure 10. Location of the samples in the drill hole M52-2431-95-426.

Table 2. List of samples used in this study with spatial and lithological information.

Rock type	Thin section ID	Hole ID	Depth	E_TM35	N_TM35
Websterite	OY27022	M52-2431-95-426	27	377604	7103750
Websterite	OY27024	M52-2431-95-426	28.6	377605	7103750
Gabbro	OY27040	YLIVIESKA-3	117.2	376995	7104365
Websterite	OY27041	YLIVIESKA-3	123.4	376999	7104367
Websterite	0Y27042	YLIVIESKA-3	126.25	377000	7104368
Gabbro	OY27043	YLIVIESKA-3	131	377003	7104370
Websterite	OY27044	YLIVIESKA-3	132.3	377004	7104370
Websterite	OY27045	YLIVIESKA-3	133.7	377005	7104371
Gabbronorite	OY27046	YLIVIESKA-3	137.5	377008	7104372
Websterite	OY27047	YLIVIESKA-4	66.7	376951	7104387
Websterite	OY27048	YLIVIESKA-4	71.2	376948	7104386,585
Websterite	OY27049	YLIVIESKA-4	73	376947	7104386
Olivine gabbronorite	OY27027	YLIVIESKA-12	23	376934	7104380
Gabbro	OY27028	YLIVIESKA-12	37.1	376943	7104384
Gabbronorite	OY27029	YLIVIESKA-12	41.1	376946	7104385
Websterite	OY27030	YLIVIESKA-12	50.5	376952	7104388
Gabbronorite	OY27031	YLIVIESKA-12	53.5	376954	7104389
Lherzolite	OY27038	YLIVIESKA-19	7.5	376961	7104349
Hornblende pyroxenite	OYXXXX	YLIVIESKA-19	19.7	376968	7104353
Websterite	OY27035	YLIVIESKA-19	29.5	376975	7104356
Hornblende pyroxenite	OY27036	YLIVIESKA-19	33	376977	7104357
Olivine gabbronorite	OY27037	YLIVIESKA-19	47.7	376986	7104361

Olivine norite	OY27039	YLIVIESKA-19	75	377004	7104370
Olivine gabbronorite	OYXXXX1	YLIVIESKA-19	100.9	377020	7104378
Gabbronorite	OY27033	YLIVIESKA-19	115.8	377030	7104383

5.2. Thin section research

A total of 25 polished thin sections were prepared at the thin section laboratory of Oulu Mining School for transmitted and reflected light microscopy. They were studied with an Olympus BX60 transmitted- and reflected-light microscope. Photographs were taken using a Zeiss Axioplan 2 transmitted- and reflected-light microscope equipped with an Axiocam 105 color camera and Zen 2 core computer program. Polished thin sections were investigated for their main and accessory mineral assemblages, alteration and textural characteristics by transmitted light microscopy. The reflected light microscope was used to determine opaque minerals. The rock types in the thin sections were classified after Streckeisen (1974) using the relative abundances of rock-forming minerals, including orthopyroxene, clinopyroxene, olivine, plagioclase and hornblende. Information on the rock type of each thin sections is presented in Table 2 and more detailed petrographical observation sheets are available in Appendix 1.

5.3. Electron probe microanalysis

Nine thin sections (OY27031, OY27036, OY27038, OY27040, OY27041, OY27042, OY27044, OY27048, R19-100.9) were selected for plagioclase, pyroxene and olivine analyses with electron probe microanalyzer. Analyses were done with a JEOLJXA-8200 microprobe at the Center for Material Analysis, University of the Oulu.

In total, compositions of 42 plagioclase grains, 65 pyroxene grains and 30 olivine grains were measured, mostly from grain centers. The compositions were measured from the center of the grains. The operating conditions were an accelerating voltage of 15kV, an electron beam current 15 nA and a beam diameter of 10 μm. The following components were quantified: SiO_2, TiO_2, Al_2O_3, FeO, CaO, Na_2O, K_2O, MgO, MnO, Cr_2O_3, BaO and NiO. The results of microprobe analyses are listed in Appendices 2, 3 and 4.

The primary aim of the olivine analyses was to compare the nickel and fosterite contents of different lithological units in the intrusion. Plagioclase and pyroxene grains were studied to investigate their compositional variation in the different lithological units.

6. PETROGRAPHY

Websterites are the most abundant rocks in the study area (Table 2). They are present in all drill holes and contain the highest amount of sulfides. In addition to websterites, the study area incorporates hornblende pyroxenites, gabbronorites, olivine gabbronorites, gabbros and lherzolites. The observed rock types are described shortly below.

6.1. Peridotites

Peridotites occur predominantly in the Perkkiö area as a wavy, circle-like formation and, in the eastern part of the intrusion, as a stratiform unit (Chapter 4). One sample (OY27038) from drill hole YLIVIESKA-19 was classified as lherzolite based on its mineralogical features. The rock is olivine-pyroxene orthocumulate (Fig. 11). Subhedral cumulus olivine is the most abundant mineral in this sample, constituting 70% of the minerals. The diameter of olivine grains varies from 3 to 9 mm. All grains have been partially altered to serpentine minerals (Fig. 12). In addition to olivine, cumulus phases also comprise orthopyroxene and augite. Alteration of pyroxene minerals to actinolite is common. Pyroxenes locally form subpoikilitic crystals enclosing olivine grains. The intercumulus material is mostly composed of hornblende, but interstitial ore minerals are also present in small amounts. Serpentine minerals, chlorite, talc and titanite occur locally as accessory minerals.

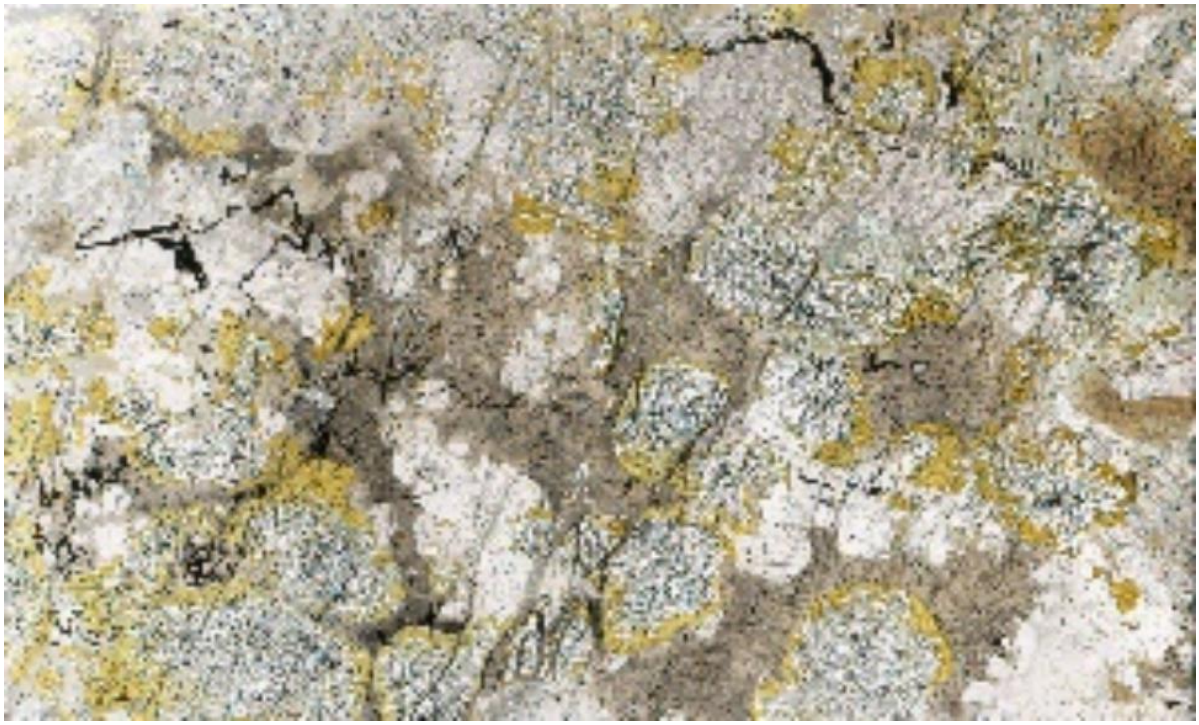

Figure 11. Scanned thin section image of olivine pyroxene orthocumulate. Thin section 0Y27038. Figure height of 2 cm. (Plane-polarized light = PPL hereafter).

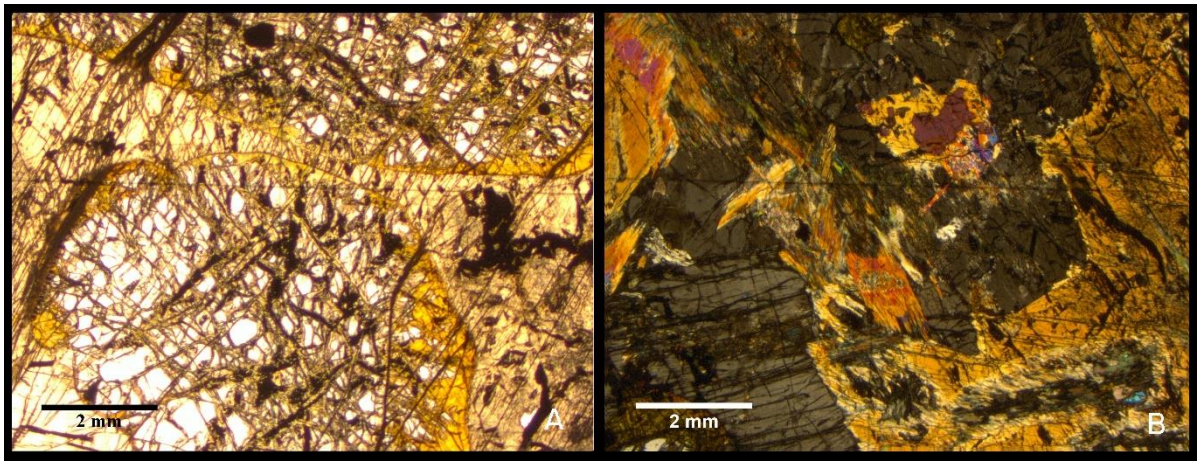

Figure 12. Photomicrographs of altered lherzolite. Thin section 0Y27038. A.) Serpentine minerals replacing coarse-grained olivine grains. Hornblende is present as and intercumulus phase. (PPL). B.) Alteration of pyroxene grains to actinolite. (crossed polarized light = XPL hereafter).

The ore minerals are generally present as fillings in the interstitial space between cumulus silicates, but also as rounded blebs within olivine and pyroxene grains and as interstitial disseminated blebs. However, in some grains, there is a small sulfide-filled embayment

at the grain margin (Fig. 13), so it is also possible that the appearance of sulfides as inclusions might result from a section through such an embayment. The ore minerals constitute 0.25 vol% of the minerals and include pyrrhotite, bornite, chalcopyrite, pentlandite, and digenite. Alteration of chalcopyrite to bornite or digenite is common.

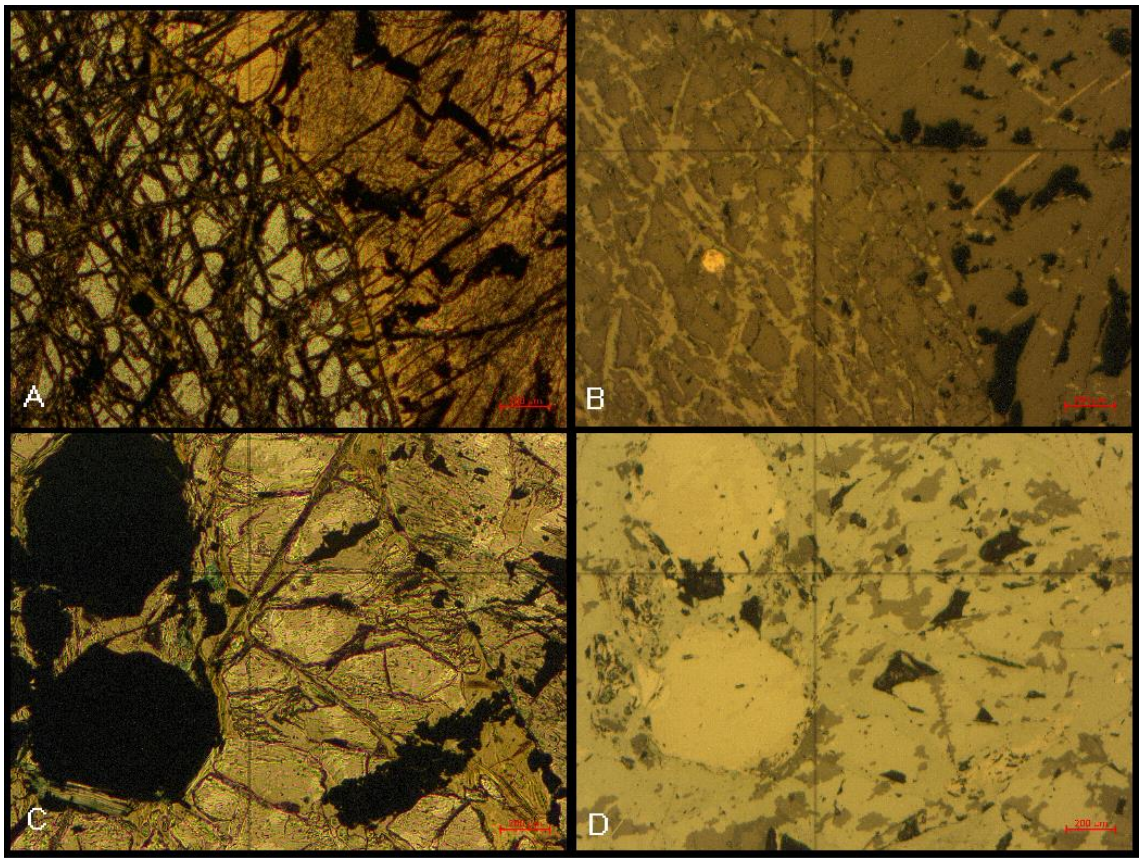

Figure 13. Photomicrographs of sulfide inclusions in lherzolite. Thin section 0Y27038. A.) Sulfide inclusion in olivine grain. (PPL). B.) Sulfide inclusion in olivine grain. (XPL). C.) Sulfide inclusions in olivine grain with embayment at the grain margin (PPL). C.) Sulfide inclusions in olivine grain with embayment at the grain margin (XPL).

6.2. Pyroxenites

Pyroxenites generally occur as sharply bounded units in contact of the layered gabbro and plagioclase peridotite units (Chapter 2.4). They are usually greenish and coarse-grained, but also darker and olivine-rich pyroxenites exist. In total, 13 samples from the study area were classified as pyroxenites. The samples in this class were further divided into websterites and hornblende pyroxenites based on their mineralogical features. The websterite group contains 11 samples and the hornblende pyroxenite group two samples.

6.2.1. Websterites

Websterites are present in all drill holes at depths varying from 27 to 133.7m. The rocks are pyroxene orthocumulates composed mainly of cumulus orthopyroxene and augite (Fig. 14). The diameter of the subhedral pyroxene grains varies greatly from 0.25 to 9 mm, being mostly between 0.4 and 5 mm. Cumulus phases also comprise a minor amount of chromite and olivine in some thin sections. The intercumulus material is mostly composed of ore minerals that are present as a net-textured and patchy net-textured framework. Interstitial hornblende, plagioclase, biotite/phologopite and titanite are present in smaller amounts in some of the thin sections. Plagioclase is mostly fresh, but some altered grains occur locally in some of the thin sections. The alteration styles include amphibolization and serpentinization.

Figure 14. Scanned thin section image of sulfide-bearing pyroxene orthocumulate. Thin section 0Y27024. Figure height 2 cm. (PPL).

Accessory and alteration minerals in websterites include actinolite, titanite, hornblende, chlorite, biotite, plagioclase, talc, phlogopite, apatite, tremolite, calcite, and serpentine minerals. In a few samples, talc, serpentine and titanite form narrow veins in the intercumulus space. Pyroxene grains are frequently altered to secondary amphiboles and serpentine minerals (Fig. 15). Secondary amphiboles are actinolite and tremolite. Alteration products usually occur in the intercumulus space as well as in cracks of the pyroxene grains and as rims at the edges of pyroxene grains. Occasionally, the rims can be composed of talc. The degree of alteration varies from very weak to moderate. Chlorite, talc, and biotite are common in the altered parts. In thin section OY27030, a vein composed of secondary amphibole intersects the thin section altering all the minerals around it.

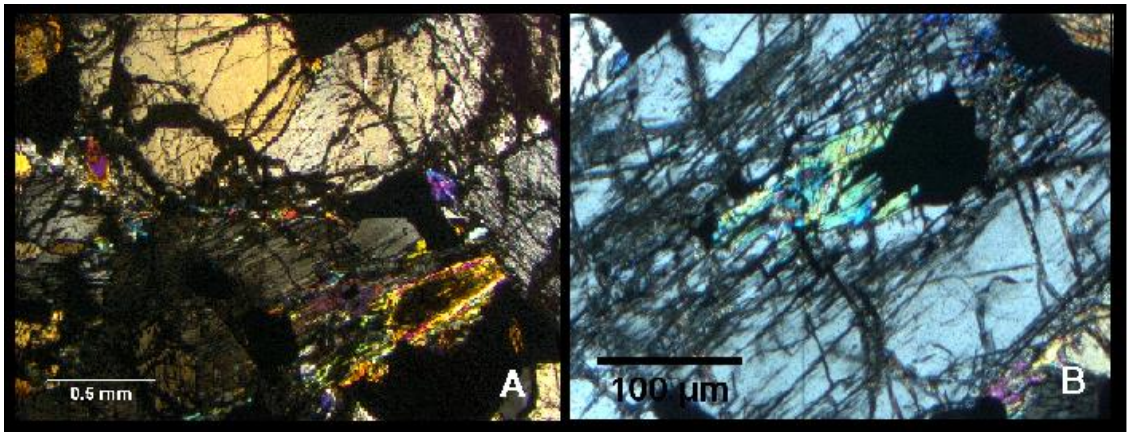

Figure 15. Photomicrographs of pyroxene grains that have altered to secondary amphiboles. A) Thin section OY27041 (XPL). B) Thin section OY27024 (XPL).

Ore minerals include pyrrhotite, chalcopyrite, pentlandite, ilmenite, magnetite, chromite, cubanite, digenite, and bornite, with the first three being most abundant. They are present as a net-textured or patchy net-textured framework in most of the websterites, making up to 15-45 vol% of the minerals (Fig. 16). Occasionally, the pyroxene grains contain small blebs of ore minerals. However, in some grains, there is a small sulfide-filled embayment at the grain margin (Fig. 17), so it is also possible that the appearance of sulfides as inclusions might result from a section through such an embayment. In moderately altered rocks, the ore minerals are mostly located in the non-altered parts. In thin sections OY27048 and OY27049, plagioclase fills the intercumulus space together with opaque

minerals. The ore minerals are located as dissemination in the parts where plagioclase is not present in the intercumulus space.

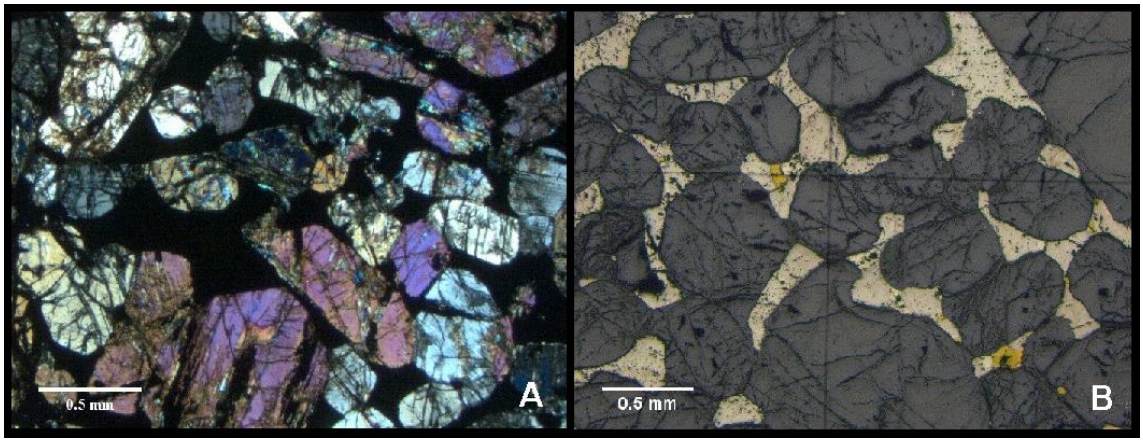

Figure 16. Photomicrographs of pyroxene orthocumulate. A) Subhedral pyroxene cumulus grains. Thin section OY27022 (taken with XPL). B) Interstitial pyrrhotite, chalcopyrite and pentlandite. Thin section OY27035 (taken with reflected light).

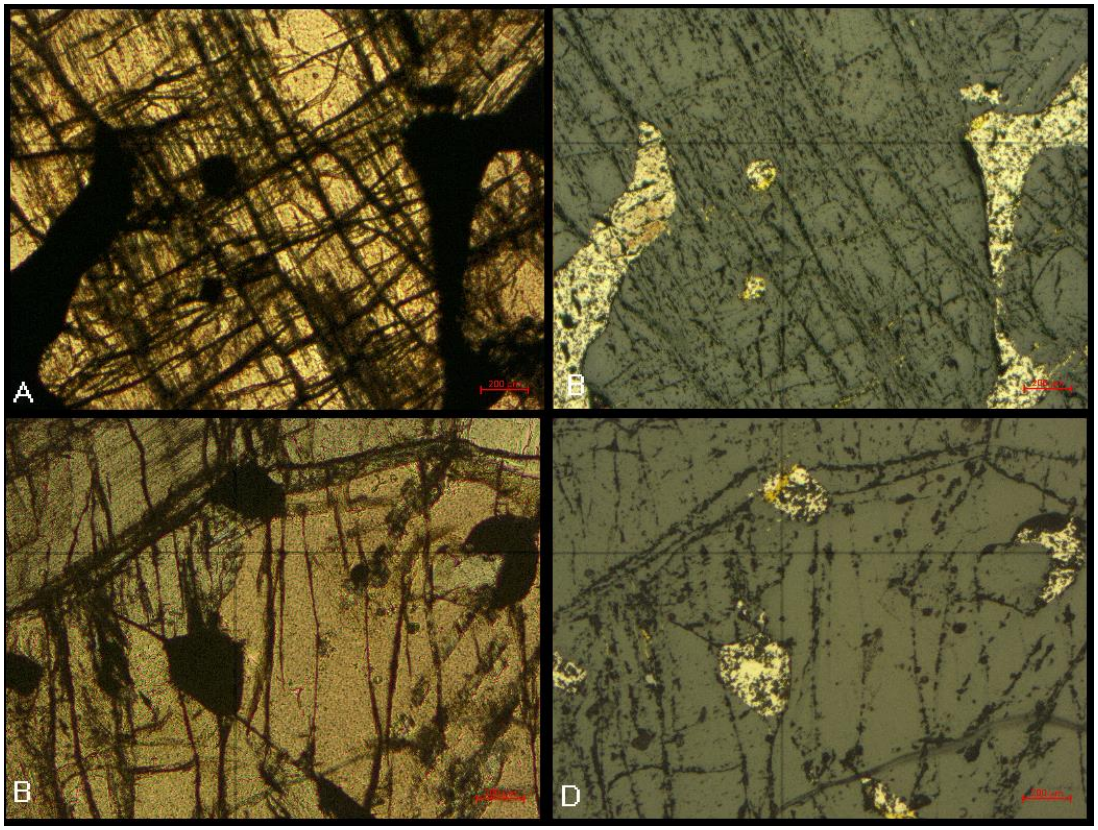

Figure 17. Photomicrographs of sulfide inclusions in websterite Thin section 0Y27024. A.) Sulfide inclusions in pyroxene grain. (PPL). B.) Sulfide inclusions in pyroxene grain. (XPL). C.) Sulfide inclusions in pyroxene grain with embayment at the grain margin (PPL). C.) Sulfide inclusions in pyroxene grain with embayment at the grain margin (XPL).

Pentlandite occurs within pyrrhotite grains as granular veinlets, separate grains and as flame-like grains and exsolution lamellae. Chalcopyrite often forms granular veins within pyrrhotite but is also present as separate grains (Fig. 18). Chalcopyrite grains may locally incorporate cubanite lamellae and can be replaced by bornite and digenite. Violarite is present in a few thin sections as an alteration product after pentlandite and pyrrhotite. In some websterite samples, the ore minerals are altered to a high degree and there are many replacement textures (e.g., in thin section OY27041). Ilmenite, magnetite, and chromite appear locally within pyrrhotite and as inclusions in pyroxene grains.

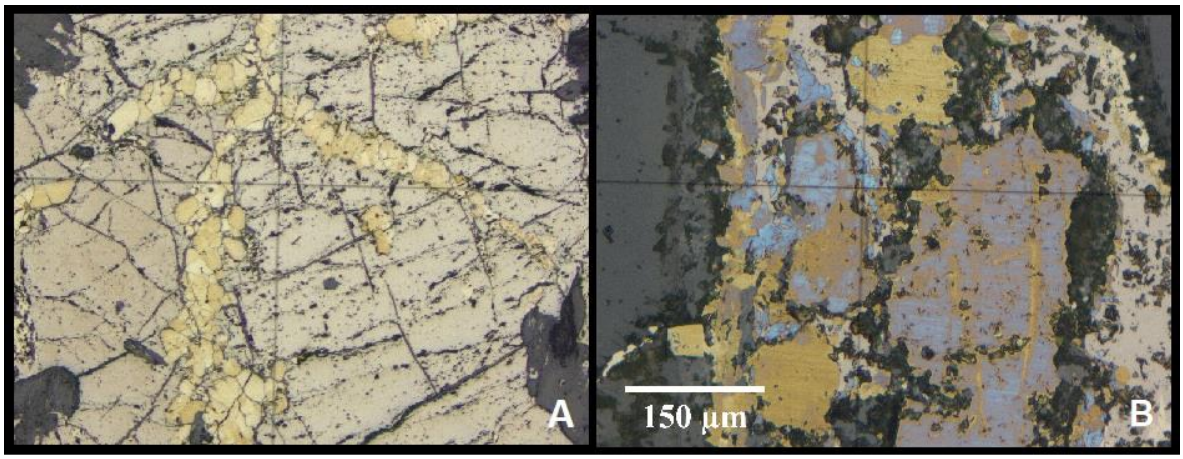

Figure 18. Photomicrographs of ore mineral textures. A) Pentlandite and chalcopyrite as granular veinlets within pyrrhotite. Thin section OY27030 (reflected light). B) Alteration of chalcopyrite to bornite and digenite. Thin section OY27045 (reflected light).

6.2.2. Hornblende pyroxenites

Hornblende pyroxenites are present in drill hole YLIVIESKA-19 at depths of 19.7 and 33 m. They are pyroxene orthocumulates consisting mainly of magmatic hornblende, orthopyroxene, and augite (Fig. 19). The cumulus phases comprise mostly of orthopyroxene and augite, but a minor amount of cumulus chromite is present locally. In thin section OYXXXX, the pyroxenes grains are mostly augite, whereas in thin section OY27036, orthopyroxene is more abundant. The diameter of pyroxene crystals varies greatly, being from 0.3 to 12 mm. Brown hornblende makes up to 30 vol% of the minerals, occurring as anhedral grains in the intercumulus space (Fig. 20). Interstitial plagioclase, phlogopite, and ore minerals are present as minor phases. Accessory and

alteration minerals also include varying amounts of tremolite, serpentine, calcite, chlorite and talc.

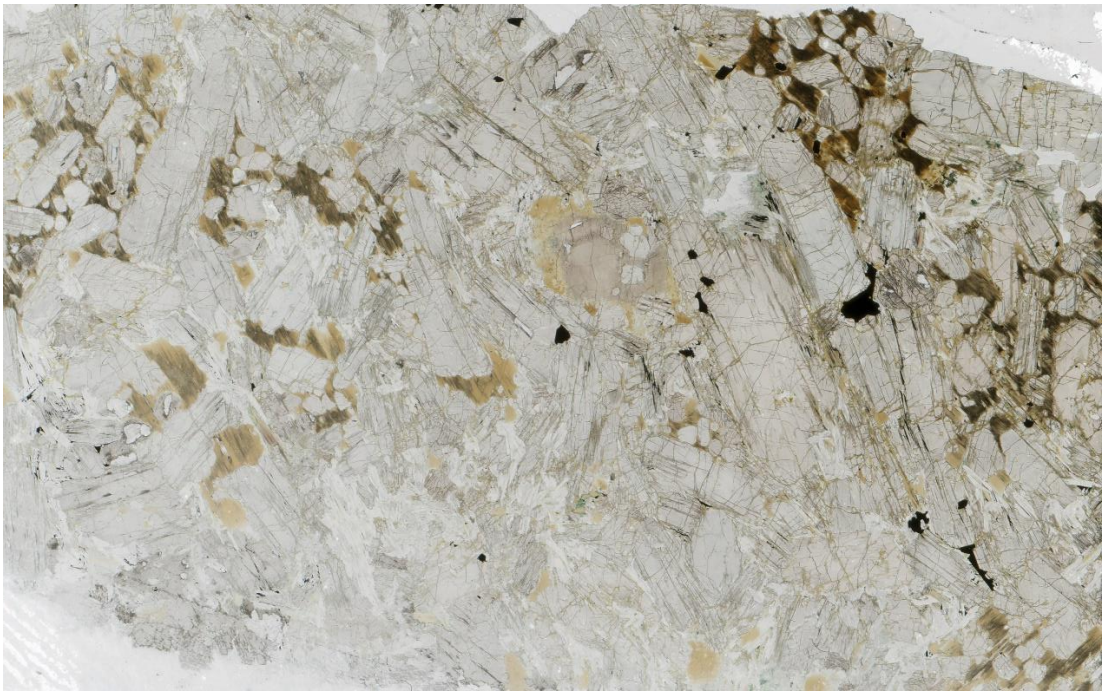

Figure 19. Scanned thin section image of pyroxene orthocumulate. Thin section 0Y27036. Figure height 2 cm. (PPL).

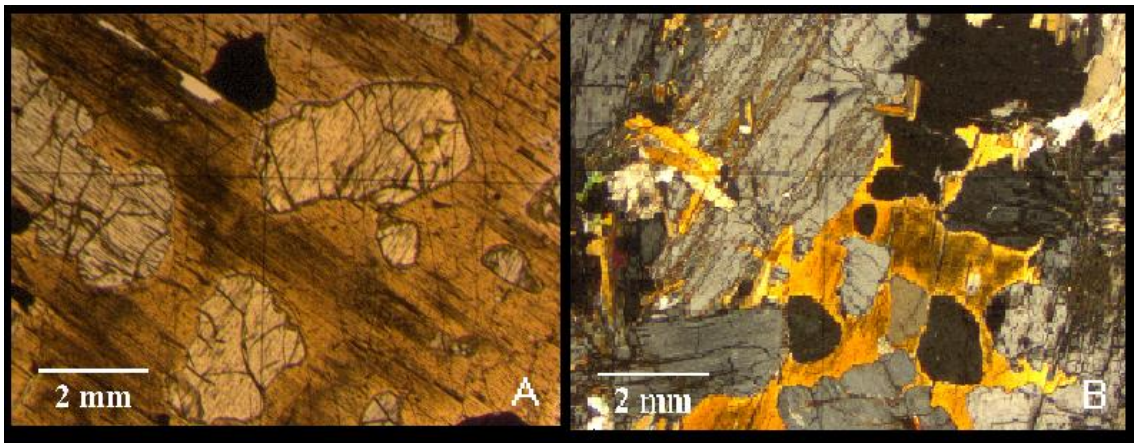

Figure 20. Photomicrographs of pyroxene orthocumulates. A) Anhedral cumulus pyroxene grains enclosed in intercumulus hornblende. Thin section OYXXXX (PPL). B) Orthopyroxene grain in the left partially replaced by tremolite. Thin section OY27036 (XPL)**.**

The hornblende pyroxenites are strongly altered and fresh grains appear only locally. The alteration styles comprise amphibolization and serpentinization. Partial replacement of

pyroxene grains by tremolite is very common (Fig. 21). Serpentine minerals occur locally as alteration rims around pyroxene grains. In thin section OYXXXX, a wide vein composed of tremolite, serpentine and carbonate minerals crosses the thin section altering the minerals around it.

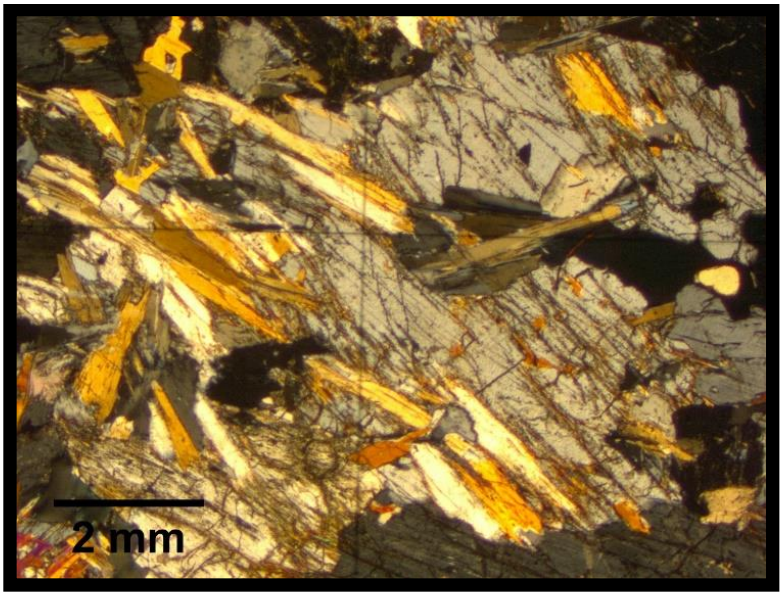

Figure 21. Photomicrograph of secondary amphibole replacing a pyroxene grain. Thin section OY27036 (XPL).

Ore minerals in hornblende pyroxenites include pyrrhotite, chalcopyrite, pentlandite, chromite, ilmenite, bornite, and digenite, of which pyrrhotite, pentlandite, and chalcopyrite are most abundant. They are present in small amounts as irregular dissemination in the intercumulus space and as small blebs in the pyroxene grains. However, in some grains, there is a small sulfide-filled embayment at the grain margin, so it is also possible that the appearance of sulfides as inclusions might result from a section through such an embayment. Pentlandite occurs as exsolution lamellae and granular veinlets in pyrrhotite. Replacement of chalcopyrite by bornite and digenite takes place locally.

6.3. Gabbros

Gabbroic rocks are present all around the Ylivieska gabbro-peridotite intrusion and they consist of melagabbros and layered gabbros (Chapter 2.4). Melagabbros are predominantly located in the eastern part of the Perkkiö area and in the Sydänneva area. They are characterized by their gradational contact to the plagioclase peridotites and by the occurrence of intercumulus plagioclase. In some parts of the intrusion, melagabbros seem to grade into layered gabbros with a sharp contact. The layered gabbros are mostly composed of olivine gabbronorites, gabbronorites, and norites. They are characterized by magmatic layering, the occurrence of autolithic fragments, and cumulus plagioclase. The magmatic layering has developed most prominently in the Sydänneva area. In total, 11 samples from drill cores YLIVIESKA-3, YLIVIESKA-12 and YLIVIESKA-19 were classified as gabbros. The samples in the class were further divided into gabbros, gabbronorites, olivine gabbronorites, and olivine norites on the basis of the modal compositions.

6.3.1. Gabbros

Gabbros are present in drill core YLIVIESKA-3 at depths of 117.2 and 131 m. In addition, there is one gabbro sample in drill core YLIVIESKA-12 at a depth of 37.1 m. The rocks are all plagioclase-pyroxene adcumulates (Fig. 22). The grain size of varies from fine to medium. The alteration styles include very weak to weak amphibolization and serpentinization.The gabbros consist mainly of cumulus plagioclase, augite, and orthopyroxene. Cumulus chromite is present in very small amounts. The diameter of pyroxene grains ranges from 0.15 to 7 mm. The pyroxenes grains are mostly clinopyroxene, even though orthopyroxene is also present in small amounts. In thin section OY27029 and OY27048, pyroxene grains form locally subpoikilitc to poikilitic crystals enclosing plagioclase grains. Partial replacement of pyroxenes by secondary amphiboles and serpentine mineral has frequently taken place.

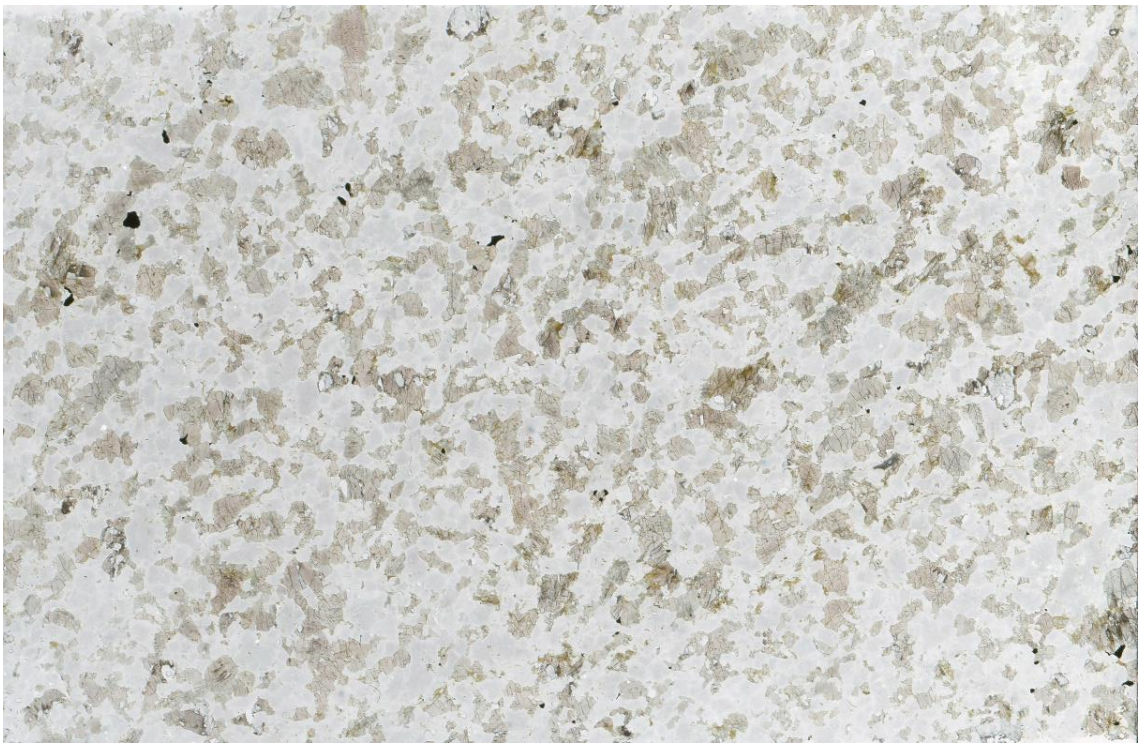

Figure 22. Scanned thin section image of plagioclase-pyroxene adcumulate. Thin section 0Y27040. Figure height 2 cm. (PPL).

Plagioclase occurs as subhedral grains and are bytownite in composition. Their diameter fluctuates from 0.2 to 4.3 mm. Plagioclase grains are mostly fresh, but altered grains are present locally in small amounts. The plagioclase grains in thin sections OY27043 and OY27028 are locally partially or completely enclosed by poikilitic pyroxene grains (Fig. 23).

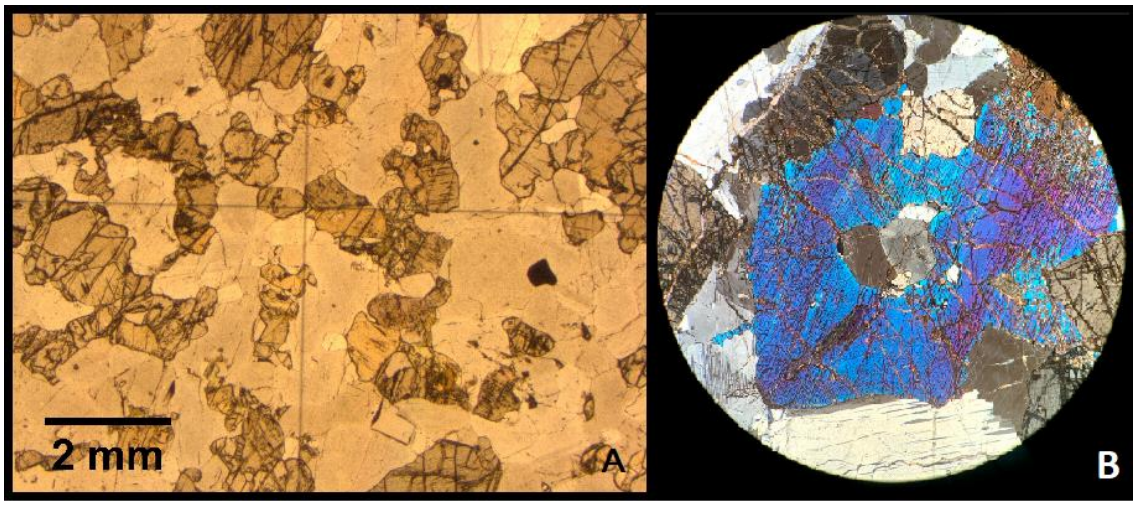

Figure 23. Photomicrographs of typical textures of gabbros. A) Plagioclase-pyroxene adcumulate. Thin section OY27040 (PPL). B) Poikilitic clinopyroxene crystal enclosing several plagioclase grains. Thin section OY27028 (XPL).

Interstitial ore minerals, hornblende, and biotite are present as minor phases. Additional accessory and alteration minerals include apatite, serpentine, actinolite-tremolite, titanite, talc, and chlorite. Narrow serpentine and talc veins intersect thin sections OY27043 and OY27028. The ore minerals occur as blebs at the edges of pyroxene grains and as interstitial disseminated blebs among the plagioclase grains. They make up to 1-2.5 vol% of the minerals and consist of pyrrhotite, pentlandite, chalcopyrite, bornite, magnetite, chromite, ilmenite, cubanite, and digenite, of which pyrrhotite, pentlandite, bornite, and chalcopyrite are most abundant. Replacement of chalcopyrite by bornite and digenite is common.

6.3.2. Gabbronorites

Gabbronorites are present in drill holes YLIVIESKA-3, YLIVIESKA-12 and YLIVIESKA-19 at depths varying from 41.1 to 137.5 m. The rock class contains four samples in total, comprising plagioclase-pyroxene adcumulates, pyroxene-plagioclase adcumulates (Fig. 24), and plagioclase-pyroxene mesocumulates. The alteration styles include serpentinization and amphibolization.

Cumulus phases in gabbronorites are plagioclase, augite, orthopyroxene, olivine, and chromite. The grain size of the subhedral plagioclase and pyroxene crystals varies from fine to medium, fluctuating from 0.1 to 7 mm. The plagioclase grains are labradorite in composition. They are mostly fresh, but some altered grains are present locally. In thin sections OY27031 and OY27033, clinopyroxene locally forms poikilitic crystals enclosing plagioclase grains. Pyroxene grains have been partially replaced by serpentine minerals. Some small-scale replacement of pyroxenes by secondary amphibole and magnetite has also taken place. Reaction rims between pyroxene and plagioclase grains are present in thin section OY27033 locally. Some roundish and serpentinized olivine grains exist in small amounts in thin section OY27033.

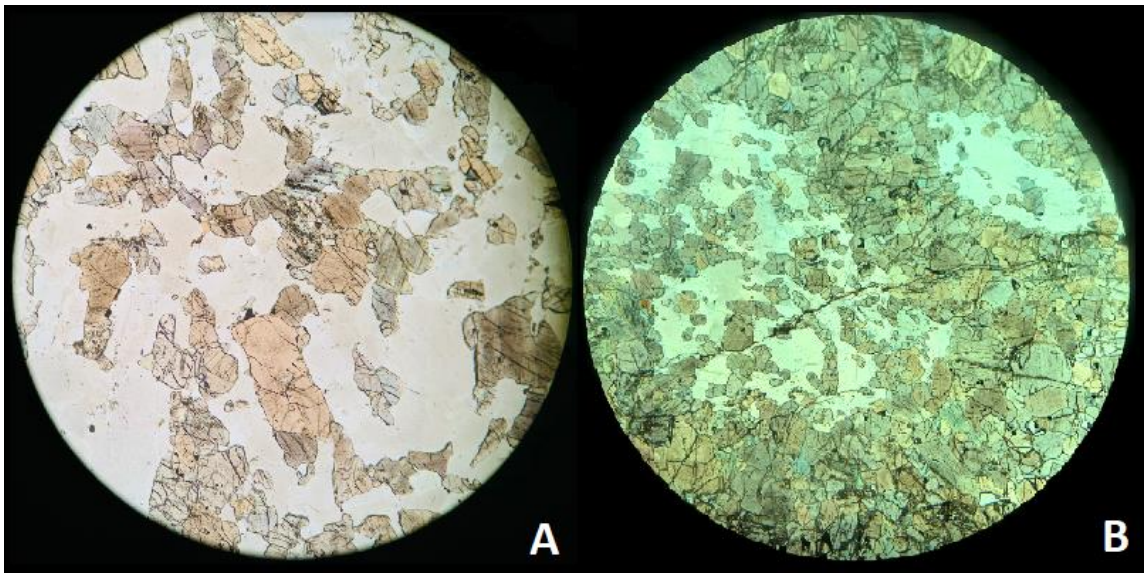

Figure 24. Photomicrographs of textural features of gabbronorites. A) Subhedral plagioclase, orthopyroxene, and augite cumulus grains. Thin section OY27046 (PPL). B) Pyroxene-plagioclase adcumulate, thin section OY27029 (PPL).

Intercumulus phases comprise ore minerals, hornblende, and biotite. Additional accessory and alteration minerals are present in variable amounts, including serpentine, titanite, actinolite, apatite, chlorite, and talc. The ore minerals make up to 2-6 vol% of the minerals, comprising pyrrhotite, pentlandite, chalcopyrite, magnetite, ilmenite, bornite, digenite, and chromite. The majority of them occur as irregular dissemination at the edges of pyroxene grains and as blebs in the pyroxene grains as well as interstitial disseminated

blebs among plagioclase grains. However, in some grains, there is a small sulfide-filled embayment at the grain margin, so it is also possible that the appearance of sulfides as inclusions might result from a section through such an embayment. In the parts where the pyroxene is abundant in thin section OY27029, the ore minerals form a net-textured matrix between pyroxene grains.

Pyrrhotite, pentlandite, and chalcopyrite are the most abundant opaque minerals. Pentlandite is mostly present as exsolution lamellae and flames within pyrrhotite grains (Fig. 25). Chalcopyrite is typically located at the edges of pyrrhotite grains. Alteration of chalcopyrite to bornite and digenite has taken place locally. In thin section OY27031, almost all chalcopyrite has been replaced. Magnetite grains may occasionally contain ilmenite exsolution lamellae.

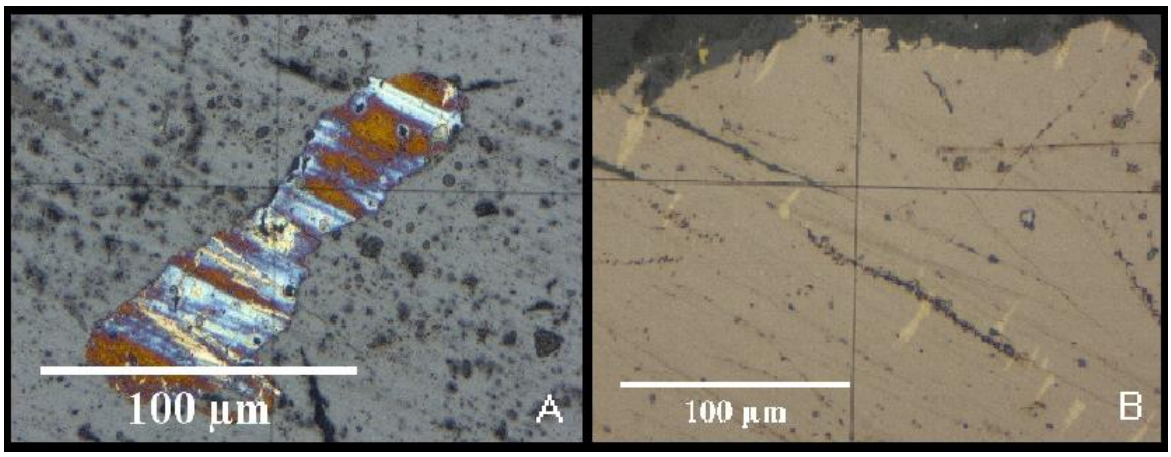

Figure 25. Photomicrographs of ore mineral textures in gabbronorite. A) Bornite and digenite replacing a chalcopyrite grain. Thin section OY27031 (reflective light). B) Pentlandite exsolution lamellae in pyrrhotite. Thin section OY27033 (reflective light).

6.3.3 Olivine gabbronorites

Olivine gabbronorites are present in drill hole YLIVIESKA-19 at depths of 47.7 and 100.9 m. In addition, there is one olivine gabbronorite sample in drill hole YLIVIESKA-12 at a depth of 23 m. The rocks consist mainly of cumulus plagioclase, augite, orthopyroxene, and olivine, being plagioclase-pyroxene-olivine adcumulates and plagioclase-pyroxene-olivine mesocumulates (Fig. 26). Cumulus chromite is present in very small amounts. The alteration styles comprise serpentinization and uralitization.

Plagioclase grains is bytownite in composition. It occurs as subhedral crystals, with grain size varying from 0.2 to 2 mm. Almost all olivine grains are roundish, medium grained and moderately to highly serpentinized. Therefore, thick alteration rims composed of serpentine minerals are common around the olivine grains. Pyroxene grains are predominantly clinopyroxene and their diameter ranges from 0.4 to 4 mm. Clinopyroxene grains form locally poikilitic crystals, enclosing plagioclase grains.

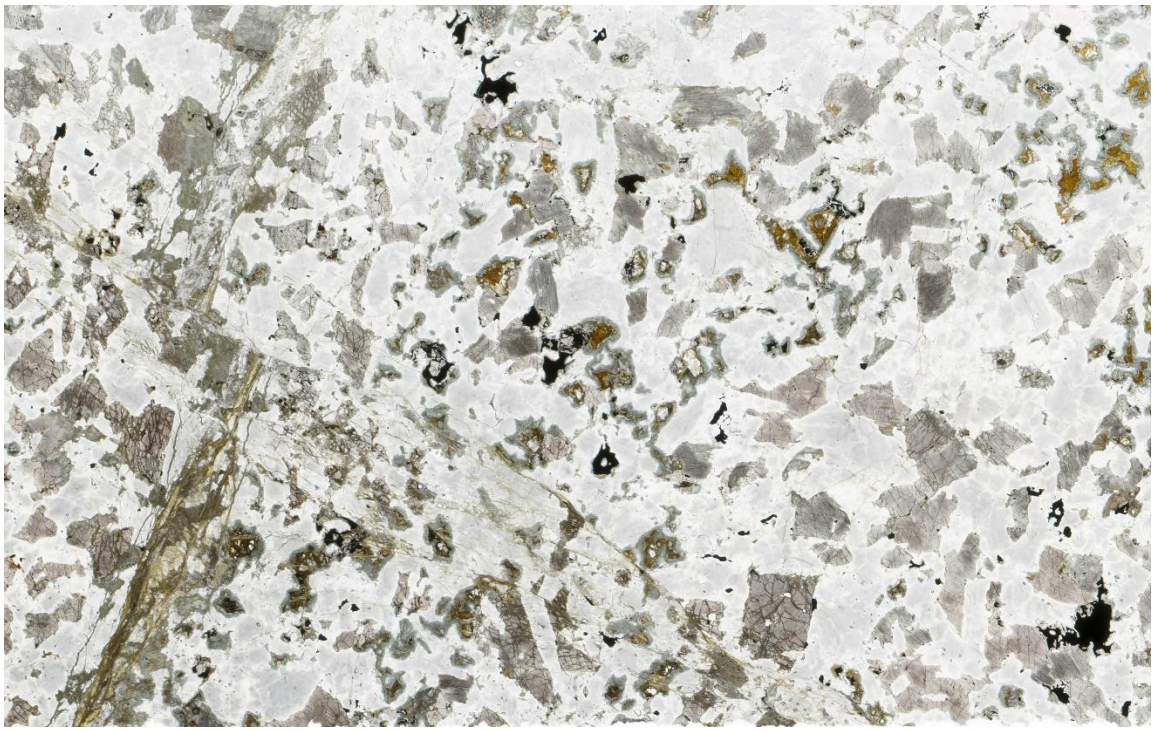

Figure 26. Scanned thin section image of plagioclase-pyroxene-olivine mesocumulate. Thin section 0Y27027. Figure height 2 cm. (PPL).

Interstitial phlogopite, hornblende, and ore minerals are present as minor phases. Additional accessory and alteration minerals include serpentine minerals, chlorite, talc and actinolite. Actinolite and serpentine minerals are present in olivine gabbronorites as veins and alteration products of olivine and pyroxene (Fig. 27). The alteration of pyroxene and olivine grains is more intensive in the areas where serpentine and amphibole veins are present.

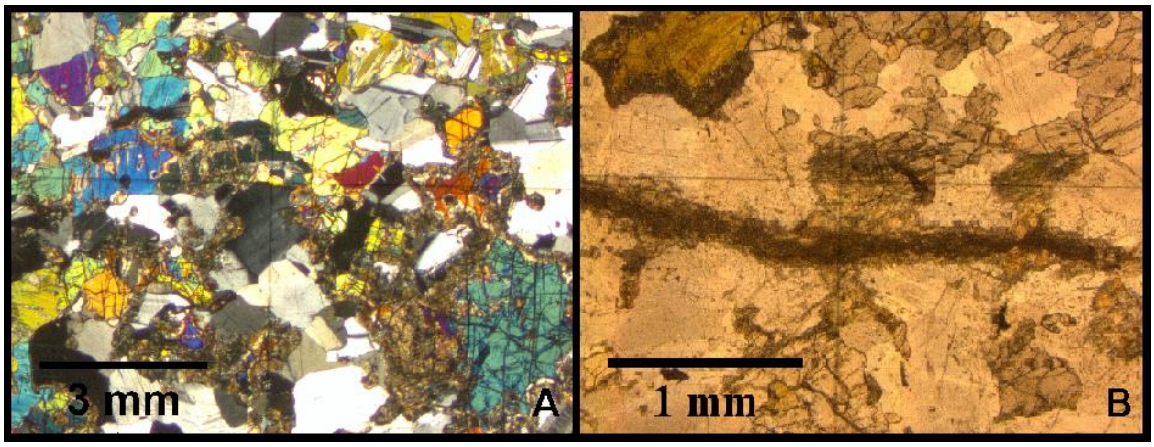

Figure 27. Photomicrographs of serpentinized and uralitized olivine gabbronorites. A) Roundish olivine grains partly replaced by serpentine minerals. Thin section OY27037 (XPL). B) Thick serpentine-actinolite vein cross-cutting olivine gabbronorite. Thin section OYXXXX1 (PPL).

The majority of the ore minerals occur as interstitial disseminated blebs in the serpentinized areas. In addition to intercumulus space, the ore minerals are also present as blebs in the pyroxene and olivine grains. However, in some grains, there is a small sulfide-filled embayment at the grain margin, so it is also possible that the appearance of sulfides as inclusions might result from a section through such an embayment. They constitute 0.5-5 vol% of the minerals, consisting of pyrrhotite, chalcopyrite, pentlandite, ilmenite, magnetite, chromite, digenite, and bornite, of which pentlandite, pyrrhotite, and chalcopyrite are the most abundant. Olivine grains are frequently partially replaced by magnetite. Locally the grains have been replaced completely. Alteration of chalcopyrite to bornite and digenite takes place occassionally.

6.3.4. Olivine norites

The rock class contains one sample (OY27039) from drill hole YLIVIESKA-19 (depth 75 m). The rock is plagioclase-pyroxene-olivine mesocumulate composed mostly of cumulus orthopyroxene, plagioclase and olivine (Fig. 28). Clinopyroxene and chromite cumulus grains are present in small amounts. The grain size of the subhedral pyroxene crystals varies from 0.3 to 3 mm. Small-scale replacement of most of the pyroxene grains by serpentine minerals and chlorite has taken place. The diameter of subhedral plagioclase grains ranges from 0.3 to 6 mm. Plagioclase is mostly fresh. Locally,

pyroxene grains form poikilitic crystals enclosing plagioclase grains (Fig. 29). Roundish olivine grains constitute approximately 15 vol% of the minerals. They are all highly serpentinized, having serpentine rims.

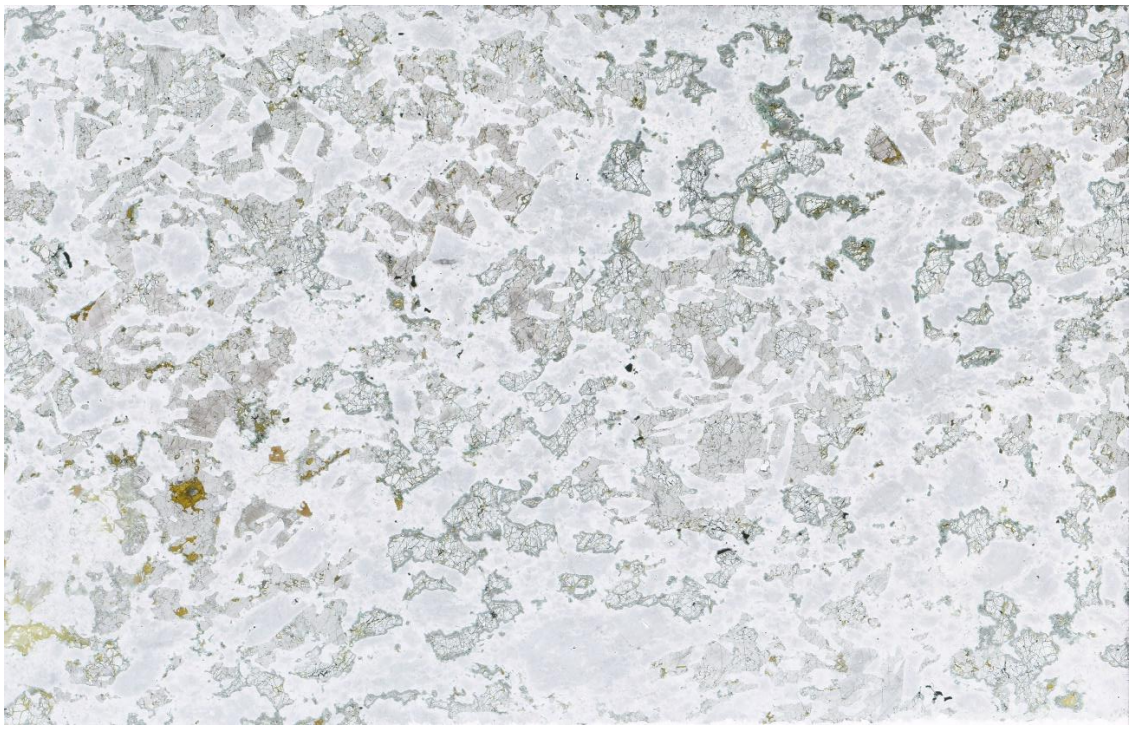

Figure 28. Scanned thin section image of plagioclase-pyroxene-olivine mesocumulate. Thin section 0Y27039. Figure height 2 cm. (PPL).

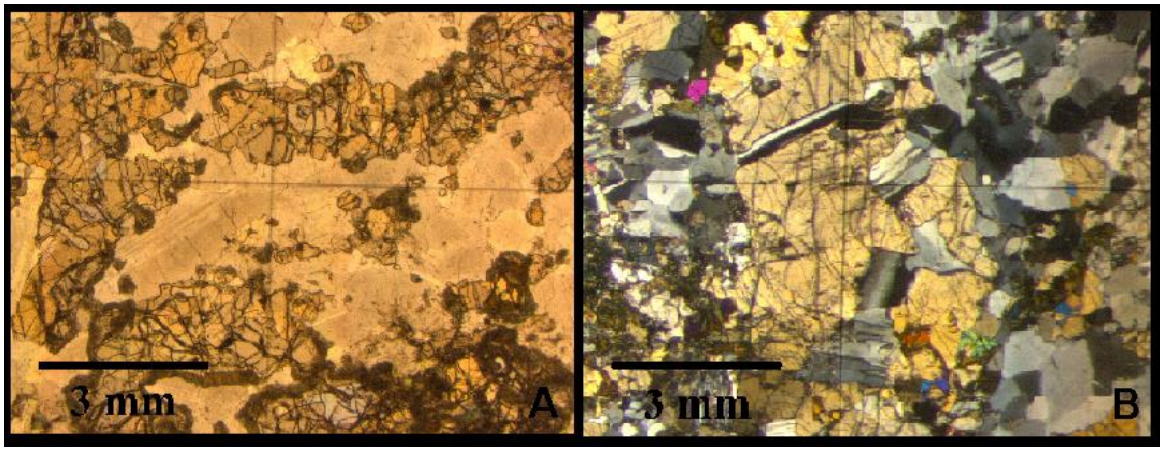

Figure 29. Photomicrographs of textural characteristics of olivine norite. A) Plagioclase-pyroxene-olivine mesocumulate. The olivine grains have thick serpentine rims. Thin section OY27039 (PPL). B) Plagioclase crystals enclosed by a poikilitic pyroxene grain. Thin section OY27039 (XPL).

Interstitial hornblende and ore minerals are present as minor phases. Additional accessory and alteration minerals include serpentine, chlorite, apatite, and talc. Thick serpentine-chlorite-rich vein constitutes one corner of thin section OY27039, altering all minerals around it. Chlorite is present also in the serpentinized areas. Talc occurs as a narrow vein in one edge of the thin section.

The ore minerals make up to 2.5 vol% of the minerals, comprising pyrrhotite, pentlandite, chalcopyrite, bornite, digenite, magnetite, and chromite. They are mostly as blebs in olivine and pyroxene grains, but some are present as interstitial disseminated blebs. However, in some grains, there is a small sulfide-filled embayment at the grain margin, so it is also possible that the appearance of sulfides as inclusions might result from a section through such an embayment. Replacement of chalcopyrite by bornite and digenite occurs in small amounts.

7. MINERAL CHEMISTRY

7.1. Olivine compositions

The samples used for mineral analysis include three olivine gabbronorite samples (OYXXXX1, OY27027 and OY27037), one olivine norite sample (OY27039), and one lherzolite sample (OY27038). Three to 10 points were analyzed from each thin section. In general, olivine is present in the samples only in small amounts and it is often largerly serpentinized, limiting the total number of analyses. Selected olivine compositions and calculated fosterite contents of different rock types are listed in Table 3. All analytical data are available in Appendix 2.

Table 3. Chemical compositions of selected olivine grains (wt%).

Sample ID	OY27038	OY27038	OYXXXX1	OY27037	OY27039
Rock type	Metalhertzolite	Metalhertzolite	Olivine gabbronorite	Olivine gabbronorite	Olivine norite
SiO2	38.3	38.3	39.1	37.8	37.5
FeO	25.62	26.91	19.10	26.429	26.25
MnO	0.35	0.38	0.27	0.26	0.33
MgO	36.98	36.02	40.22	35.00	35.82
NiO	0.12	0.11	0.12	0.08	0.06
TiO2	0.02	0.01	0.02	0.33	0.01
Total	101.5	101.8	99.8	99.9	100.0
Fo	71.7	70.2	78.0	70.0	70.6

In lherzolite, the fosterite content of olivine varies from 70.5 to 72.0 mol%, whereas in olivine gabbronorite, it fluctuates from 68.8 to 78.2 mol% and in olivine norites, from 70.8 to 71.7 mol%. Olivine in gabbronorites contains 0.00-0.12 wt% NiO, in lherzolites 0.06-0.17 wt% and in olivine norites 0.00-0.07 wt%. Nickel shows a weak positive correlation with fosterite, as shown in Fig. 30. The CaO content ranges from 0.00 to 0.04 wt% in all samples. In olivine gabbronorites, the MnO content fluctuates from 0.25 to 0.43 wt%, whereas in lherzolites, it varies from 0.35 to 0.38 wt% and in olivine norites, from 0.27 to 0.36 wt%. Manganese shows a negative correlation with fosterite (Fig. 31).

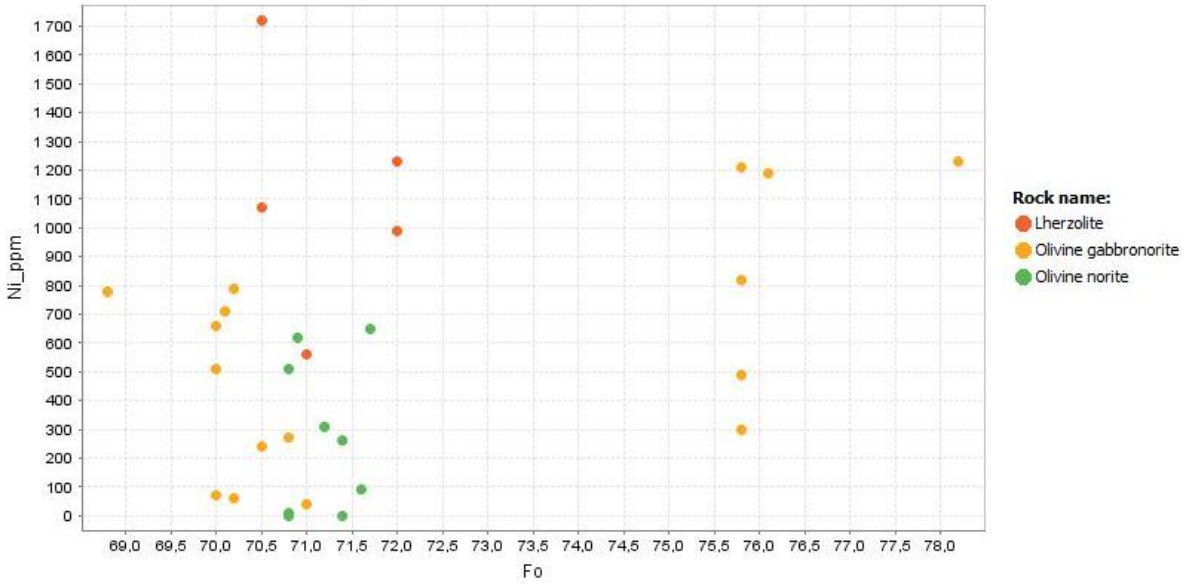

Figure 30. Fo vs. Ni plot for analyzed olivine grains.

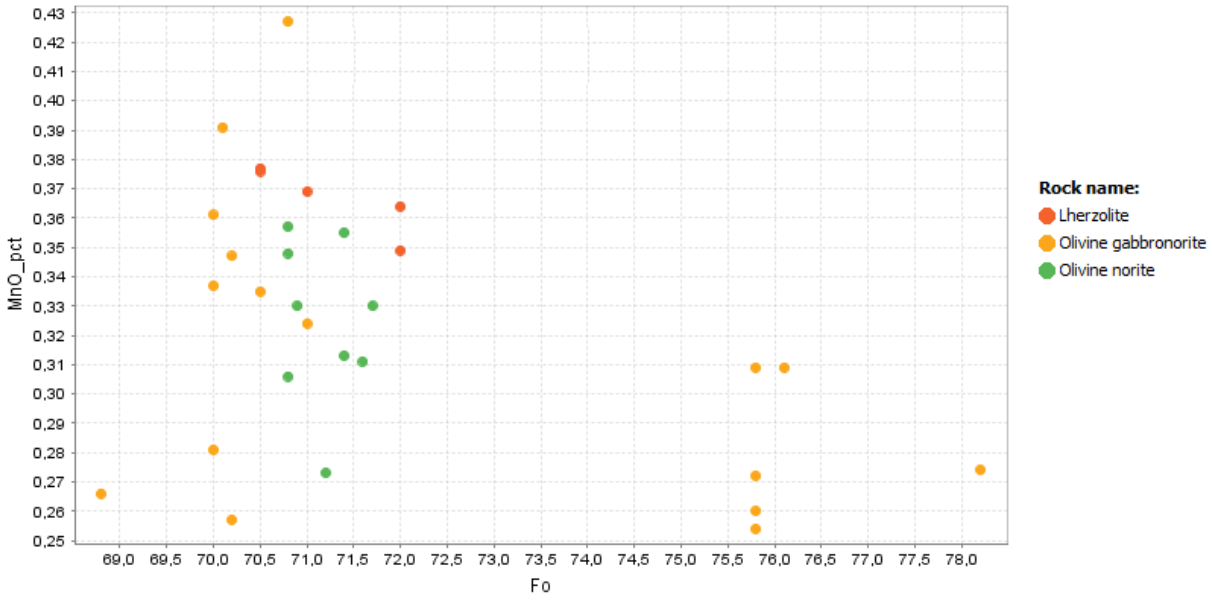

Figure 31. Fo vs. MnO plot for analyzed olivine grains.

7.2. Pyroxene compositions

The analyzed samples include hornblende pyroxenite (OY27036), websterites (OY27041, OY27042, OY27044 and OY27048), lherzolite (OY27038), olivine gabbronorite (OYXXXX1), gabbronorite (OY27031) and gabbro (OY27040). Generally, 5 to 10 points were analyzed from each thin section.

Selected pyroxene compositions from different rock types are listed in Tables 4 and 5. All analytical data are available in Appendix 3. A Ca-Mg-Fe diagram for the pyroxene grains is presented in Fig. 32. The analyzed pyroxene grains in the gabbro, websterites and hornblende pyroxenite plot all in the enstantite field and those in the olivine gabbronorites, gabbronorites and lherzolite are also mostly enstantite in composition, but also augite grains were among the analyzed crystals.

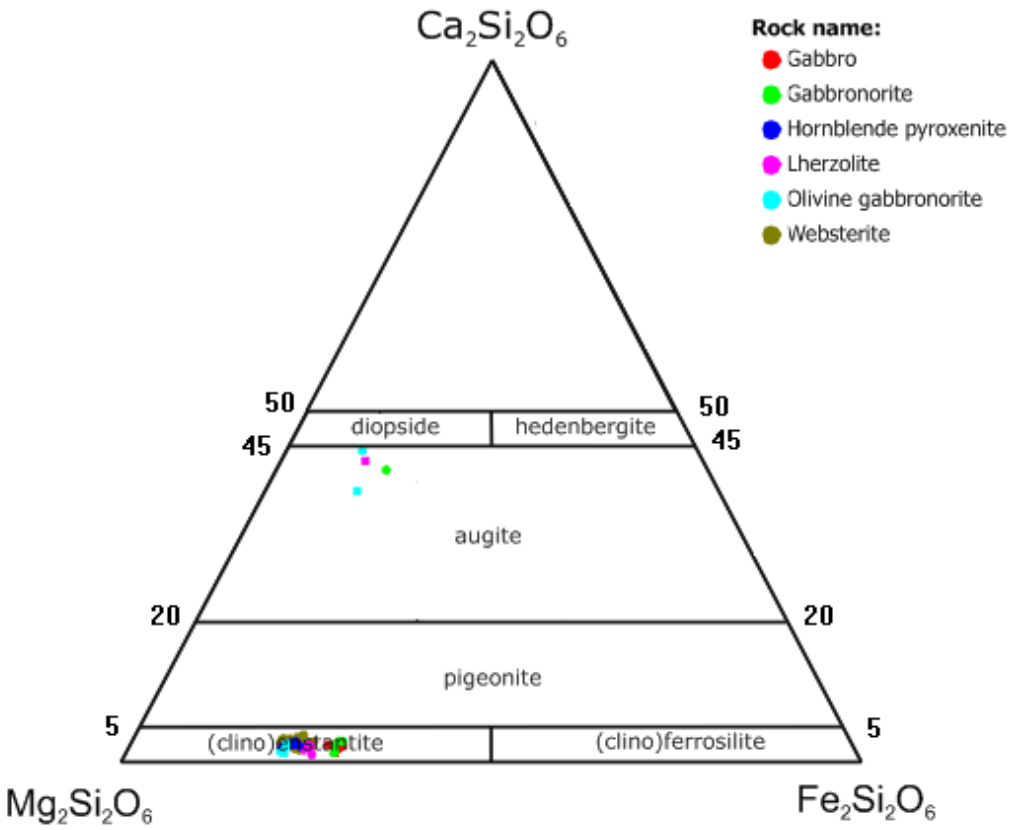

Figure 32. Ca-Mg-Fe ternary diagram for analyzed pyroxene grains (after Morimoto and Kitamura, 1983).

Table 3. Chemical compositions of selected enstantite grains (wt%).

Sample ID	OY27038	OY27036	OY27044	OYXXXX1	OY27031	OY27040
Rock type	Lherzolite	Hornblende pyroxenite	Websterite	Olivine gabbronorite	Gabbro norite	Gabbro
SiO_2	54.6	54.6	53.5	54.0	53.0	53.2
TiO_2	0.17	0.24	0.35	0.450	0.34	0.31
Cr_2O_3	0.04	0.32	0.18	0.20	0.06	0.11
Al_2O_3	1.78	1.74	2.06	1.94	1.85	1.67
FeO	15.80	14.14	14.67	13.81	17.94	18.24
MnO	0.30	0.25	0.33	0.29	0.43	0.34
MgO	26.72	27.67	27.32	28.42	25.44	25.19
CaO	1.19	1.27	1.48	1.33	0.92	1.03
Na_2O	<0.01	<0.01	0.01	<0.01	<0.01	0.01
NiO	0.03	0.03	<0.01	0.04	0.11	<0.01
Total	100.59	100.25	99.90	100.52	100.06	100.07
Mg#	75	78	77	79	72	71

Table 4. Chemical compositions of selected augite grains (wt%).

Thin section ID	OY27038	OYXXXX1	OY27031
Rock type	Metalherzolite	Olivine gabbronorite	Gabbronorite
SiO_2	51.4	51.2	51.5
TiO_2	0.94	0.81	1.03
Cr_2O_3	0.51	0.56	0.23
Al_2O_3	3.69	3.22	3.31
FeO	7.07	7.75	9.15
MnO	0.14	0.21	0.27
MgO	15.79	16.94	14.92
CaO	20.67	18.62	19.90
Na_2O	0.25	0.46	0.55
NiO	0.05	0.12	0.04
Total	100.50	99.90	100.94
Mg#	80	80	74

The Mg# [(molar 100 x Mg/(Mg + Fe_{tot})] in pyroxenes varies from 71 to 81. Pyroxenes in gabbros and gabbronorites show the lowest Mg# values whereas the highest values are present in the pyroxenites, olivine gabbronorite and lherzolite. The analyzed pyroxene grains are all Ni poor as the NiO content lies between 0 and 0.13 wt% (Fig. 33). The MnO content in pyroxenes ranges from 0.2 to 0.48 wt% and the Cr_2O_3 content varies from 0.03 to 0.68 wt%. Manganese shows a negative correlation with Mg# in pyroxenes, as shown in Fig. 34, whereas Cr_2O_3 shows positive correlation with Mg# (Fig. 35).

Augites have low Al_2O_3 content varying from 3.3 to 3.7 wt%. The analyzed orthopyroxene grains have lower Al_2O_3 content (1.39-2.11 wt%) than that of augite grains. The TiO_2 content of augites ranges from 0.81 to 1.03 wt% whereas orthopyroxenes contain 0.14-0.65 wt% of TiO_2.

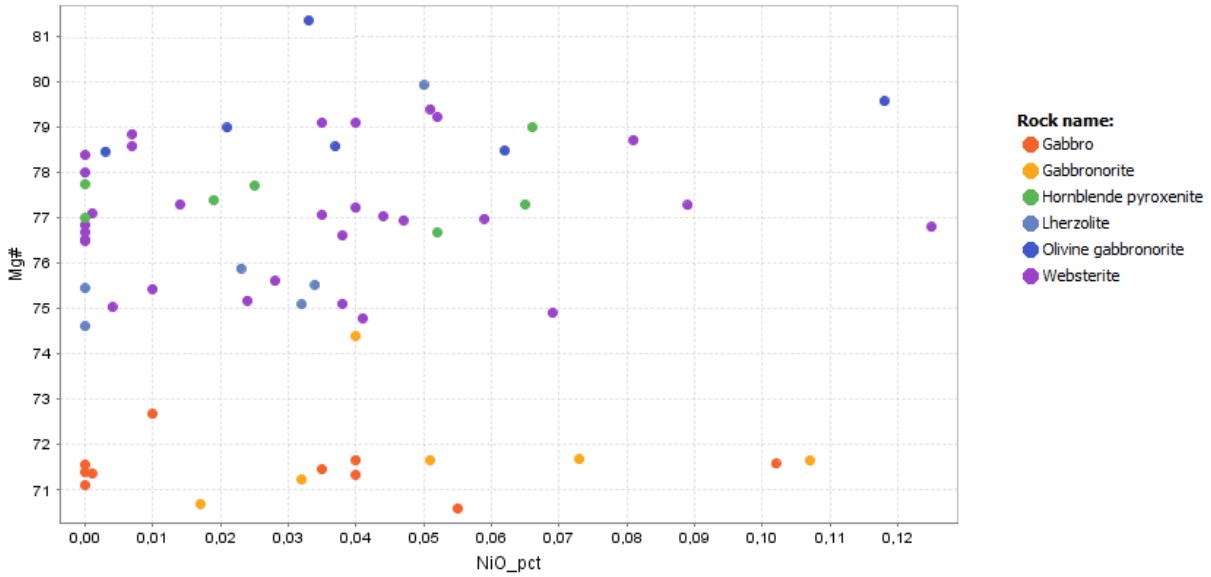

Figure 33. Mg# vs. NiO plot for analyzed pyroxene grains.

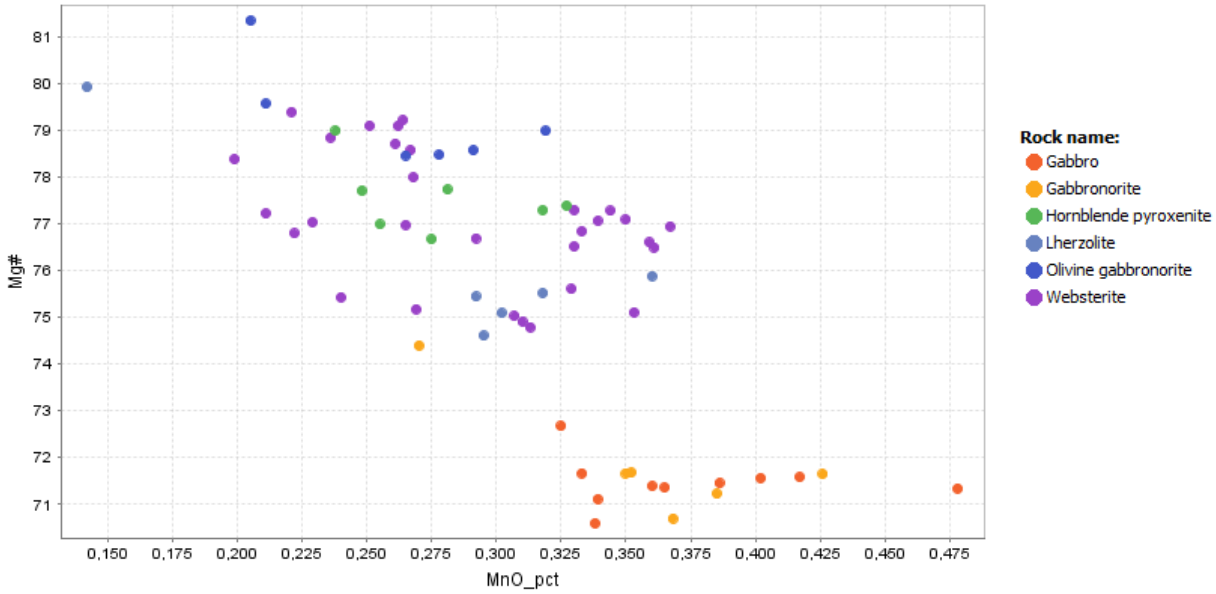

Figure 34. Mg# vs. MnO plot for analyzed pyroxene grains.

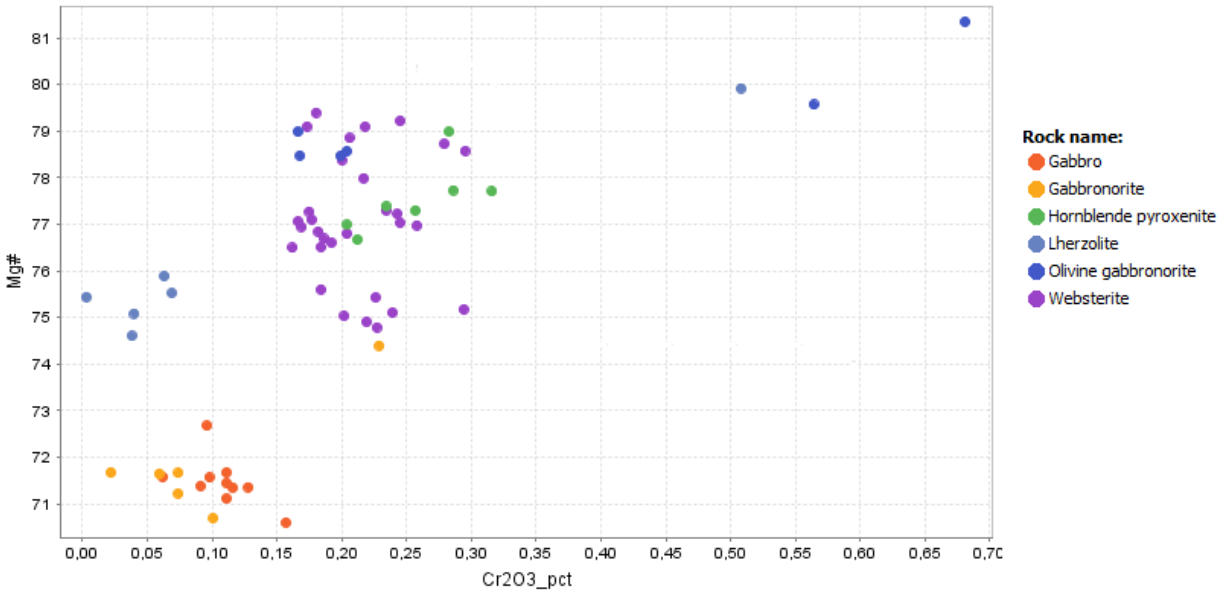

Figure 35. Mg# vs. Cr_2O_3 plot for analyzed pyroxene grains.

7.3. Plagioclase compositions

The analyzed samples included websterites (OY27041, OY27044 and OY27048), gabbro (OY27040), gabbronorite (OY27031) and olivine gabbronorite (OYXXXX1). The selected grains are cumulus minerals in the gabbroic rocks and intercumulus crystals in the websterites. Generally, 5 to 10 points were analyzed from each thin section. Selected plagioclase compositions of different rock types are listed in Table 6. All analytical data are available in Appendix 4.

The analyzed plagioclase grains in the gabbros are all bytownite in composition, varying from $An_{78}Ab_{22}$ to $An_{71}Ab_{29}$. The gabbronorites contain labradorite with a compositional range from $An_{68}Ab_{31}$ to $An_{61}Ab_{38}$ and the olivine gabbros bytownite with $An_{83}Ab_{17}$-$An_{78}Ab_{22}$. In the websterites, plagioclase analyses yielded roughly equal amounts of bytownite and labradorite, with the compositions of the former varying from $An_{81}Ab_{18}$ to $An_{70}Ab_{29}$ and those of the latter from $An_{69}Ab_{30}$ to $An_{65}Ab_{35}$.

Table 6. Chemical compositions and calculated anorthite contents of selected plagioclase grains (wt%).

Sample ID	OY27040	OY27031	OYXXXX1	OY27048	OY27048
Rock type	Gabbro	Gabbronorite	Olivine gabbronorite	Websterite	Websterite
SiO_2	50.4	53.1	49.3	50.9	51.3
Al_2O_3	31.82	29.70	32.47	31.31	31.16
FeO	0.27	0.38	0.10	0.16	0.20
CaO	14.82	12.15	15.67	14.19	13.86
Na_2O	2.67	4.25	2.41	3.14	3.30
K2O	0.10	0.21	0.024	0.10	0.03
SrO	0.06	<0.01	<0.01	<0.01	<0.01
TiO_2	<0.01	0.07	0.06	0.05	0.03
MgO	<0.01	0.13	0.01	0.14	0.01
NiO	<0.01	<0.01	0.02	<0.01	0.05
Total	**100.17**	**100.07**	**100.06**	**100.08**	**99.98**
An	74.9	60.5	78.1	71.0	69.8
Ab	24.5	38.3	21.7	28.4	30.0
Or	0.6	1.2	0.1	0.6	0.2

8. DISCUSSION

8.1. Comparison to other Kotalahti Belt intrusions

The Kotalahti-type intrusions typically consist of olivine cumulates, pyroxene cumulates and plagioclase-bearing cumulates (Makkonen et al., 2017). The studied rocks of the Ylivieska intrusion do not differ from those in other Kotalahti intrusions, being composed of olivine-pyroxene orthocumulates, pyroxene orthocumulates, plagioclase-pyroxene and pyroxene-plagioclase adcumulates, plagioclase-pyroxene mesocumulates as well as plagioclase-pyroxene-olivine meso- and adcumulates. Magmatic interstitial amphibole, phlogopite and plagioclase, which are typical for the Kotalahti-type intrusions (Makkonen, 1996; Peltonen, 2005; Lamberg, 2005), are also present in the studied intrusion.

Orthopyroxene is dominant over clinopyroxene in all rock units of the study area except in lherzolites and gabbros. Abundant orthopyroxene may indicate a high ore potential of the intrusion because, contamination of the magma by mica gneiss may result in the high amount of orthopyroxene. Mineralized intrusions of the Kotalahti belt are typically rich in orthopyroxene and barren ones rich in clinopyroxene (Makkonen et al., 2008).

Sulfides are most abundant in websterites, forming matrix ore in the study area. In the previous studies by Sipilä (1984) and Kontoniemi and Mäkinen (2001) the best mineralized intersection is observed in a metapyroxenite and the second best in plagioclase-bearing lherzolites. However, the study material contains only one peridotite sample where a minor amount of sulfides occurs as blebs between pyroxene and olivine grains. This sample does not include intercumulus plagioclase as previously observed mineralized plagioclase peridotites. To make more comprehensive and reliable comparison between the peridotitic and pyroxenitic units, more representative samples would be needed from the peridotitic units.

According to the results and previous studies, the Ylivieska intrusion differs from majority of the intrusions of the Kotalahti Belt with respect to the position of mineralized rocks, as the massive and matrix sulfides of the mineralized intrusions are usually located

in the peridotite units at the basal part of the intrusion and mineralizations in the pyroxenitic units are rare (Makkonen et al., 2008). However, there are some intrusions in the Kotalahti Nickel Belt that contain matrix sulfides in pyroxenites as well. e.g., the Rytky deposit (Mäkinen and Makkonen, 2004).

In addition to ultramafic rocks, sulfides are also present as dissemination in hornblende pyroxenites, gabbros, gabbronorites, olivine gabbronorites and olivine norites. Disseminations in gabbroic rocks are typical for Kotalahti-type intrusions (Makkonen et al., 2008). The most common ore minerals in the intrusion are pyrrhotite, chalcopyrite, and pentlandite, as in the majority of the other Kotalahti type intrusions (Makkonen et al., 2017).

8.2 Mineral chemistry constraints on petrogenesis

The lherzolites are composed of cumulus olivine, clinopyroxene and orthopyroxene. Olivine is also present as a cumulus phase in olivine gabbronorites and olivine norites together with cumulus plagioclase, augite, and orthopyroxene. In websterites and gabbronorites the cumulus olivine is present only locally in very small amounts. Olivine is absent in hornblende pyroxenites and gabbros. The amount of olivine analyses in this study is limited and does not include equal number of samples from each rock unit, which may have effects on the results. To confirm the results and to assess whether there is similar variation in all different rock units, more data would be needed. Therefore, the results should be viewed with caution.

According to Gaetani et al. (1993), De Bari and Coleman (1989) and Pichavant and MacDonald (2007), olivine is the dominant phase in cumulates in primitive arc environments, forming the first liquidus phase together with spinel and clinopyroxene. The composition of olivine can be used as an indicator of the processes that have affected the intrusion, including the potential sulfide saturation of the magma during its emplacement and subsequent crystallization (Li et al., 2007). The composition of the olivine is controlled by the parental magma composition, fractional crystallization, reaction with interstitial liquid, and hydrothermal alteration.

Tha analyzed olivine grains in lherzolites, olivine gabbronorites and olivine norites have all CaO contents (<0.01-0.04 wt%) that are lower than those of typical subduction-related magmas (0.15-0.25 wt%, Sigurdson et al., 1993; Smith and Leeman, 2005). Many researches have used the low CaO content (< 0.1 wt%) of olivine as a characteristic feature for the mantle-derived olivine based on the work by Simkin and Smith (1970). However, Li et al. (2012) presents that the Ca content of olivine is not controlled by the depth of crystallization or the temperature of sub-solidus equilibration but rather by the parental magma composition and that primitive olivine with a low Ca content can also crystallize from mantle-derived magmas at shallow depths. In addition to the studied intrusion there are some Alaskan-type complexes that are known to contain olivine with a low Ca content (e.g., Himmelberg and Loney, 1995; Batanova et al., 2005; Krause et al., 2007).

The forsterite content changes between the samples from 68.8 mol% to 78.2 mol%, varying most in the olivine gabbronorites. The nickel content of olivine varies between the rock types, being highest in lherzolites and lowest in olivine norites. It fluctuates from 0 to 1720 ppm. Some olivine grains in the lherzolite sample host sulfide globules. Within one analyzed olivine grain, the Fo content seems to decrease and Ni content to increase towards the sulfide globule. However, to confirm this phenomenon and to make wider conclusions, more analyses would be needed from olivine grains with sulfide globules.

Similarly anomalously high Ni contents of olivine (6910 ppm) to those reported by Kontoniemi and Mäkinen (2001) from the Ylivieska intrusion were not observed. This can be explained by the amount of sulfides in the samples. In the previous studies, the highest Ni contents of olivine were detected from samples that are not mineralized and when sulfides are present, the Ni content decreases to one third as more Ni tend to participate into sulfide melt. All analyzed samples in this study are mineralized, which may explain the lower Ni contents in olivine. The analyzed Fo and Ni ranges are comparable to the olivine composition recorded earlier for Kotalahti intrusions (Mäkinen, 1987). The MnO concentrations of the analyzed olivine crystals show clear negative correlation with the fosterite content (Fig. 27) whereas NiO shows weak positive correlation with the fosterite content (Fig. 26). These trends are consistent with progressive fractionation.

The pyroxenites of the Ylivieska intrusion are all pyroxene orthocumulates with cumulus orthopyroxene and augite. Cumulus chromite is present in very small amounts in some samples. In addition to peridotites and pyroxenites, augite and ortopyroxene are also present as cumulus phases in gabbroic rocks. Clinopyroxene is one of the first liquidus phases in cumulates of primitive arc environments (Gaetani et al., 1993). The number of analyzed clinopyroxene analyses is very limited in this study, which may effect the results.

All analyzed clinopyroxenes are augite in composition with low Al_2O_3 (3.3-3.7 wt%). Their Mg# ranges from 74 in gabbronorite to 81 in olivine gabbronorite. The TiO_2 content of clinopyroxenes increase with decreasing Mg#, which may reflect a crystallization trend in hydrous subduction-related arc magmas (Conrad and Kay, 1984; De Bari and Coleman, 1989; Loucks, 1990). The Cr_2O_3 concentrations of the analyzed clinopyroxenes show positive correlation with Mg#. This trend is consistent with progressive fractionation as Cr is highly compatible element and decreases in concentration with increasing differentiation (Müntener et al., 2001).

Clino- and orthopyroxenes that crystallize from hydrous arc magmas under high pressure conditions are typically enriched in Al, if there are no Al-phases precipitating (Elthon et al., 1982; Müntener et al., 2001; De Bari and Coleman 1989). According to Bender et al. (1978), an increasing degree of crystallization also increases the concentration of Al_2O_3 and FeO in pyroxenes unless major Al bearing phases (plagioclase, garnet, amphibole) crystallized (Müntener et al., 2001). The analyzed clinopyroxene grains in this study did not show any increase in Al_2O_3 with increasing differentiation. However, hornblende and plagioclase are present in large amounts in all analyzed samples, which might contribute to the low Al_2O_3 content of the clinopyroxene. Also in the earlier studies by Kontoniemi and Mäkinen (2001), plagioclase was observed as an intercumulus mineral in the beginning of the differentiation of the plagioclase peridotites. Early plagioclase fractionation might have obstructed the increase in Al in pyroxenes with increasing differentiation.

Orthopyroxene grains are magnesium rich and their Al_2O_3 content (1.39-2.11 wt%) is lower than that of the coexisting clinopyroxene grains. Mg# of the orthopyroxene varies from 71 to 80. The lowest Mg# values are observed in gabbros and gabbronorites whereas the highest values are present in the pyroxenites, olivine gabbronorite and lherzolite. In

general, Mg# of orthopyroxene decreases systematically with the MnO concentration through the ultramafic cumulates to the gabbroic rocks (Fig. 30) whereas the Cr_2O_3 content of the orthopyroxene systematically decreases with increasing differentiation (Fig. 31). These trends are consistent with the model of progressive fractionation (Müntener et al., 2001).

When the magma becomes depleted in MgO and enriched in SiO_2, its composition moves towards more evolved basaltic andesite to andesitic composition where orthopyroxene is stabilized as the liquidus phase after clinopyroxene (Pichavant and Macdonald, 2007). Cumulus orthopyroxene is more abundant compared with cumulus augite in all rock units of the study area except in lherzolites and gabbros. Also pyroxenites and gabbroic rocks have very low olivine contents in general. The abundance of orthopyroxene and the absence of olivine could be explained by the formation of the orthopyroxene by peritetic reactions between olivine and residual melt (Dessimoz et al., 2012; Müntener et al., 2001; Straub et al., 2008). This would result in a high Ni concentration in the resulting orthopyroxene as crystallization of olivine would reduce the MgO and Ni content of the magma and increase all the other components not incorporated into olivine. The observed nickel contents of the orthopyroxene in this study are mostly lower than 0.1 wt% and therefore do not show any significant enrichment. However, there are one analyzed orthopyroxene grain that contain 0.13wt% NiO. Orthopyroxene grains of the intrusion have also yielded high Ni contents in previous studies, reaching 0.21 wt% (Kontoniemi and Mäkinen, 2001), which may support the theory. Orthopyroxene in websterites also has higher MgO content than in lherzolites. However, it is also possible that an excess orthopyroxene may have formed by assimilation of silica (Ripley and Li, 2013). The latter is typical for the mineralized intrusions of the Kotalahti Belt (Makkonen et al., 2008).

The measured nickel content of the orthopyroxenes varies from below the detection limit to 1180 ppm. The range corresponds mostly to the orthopyroxene compositions recorded earlier for the intrusion intrusions (Kontoniemi and Mäkinen, 2001), even though some lower values were also observed. In the previous studies, which involved mostly non-mineralized samples, the nickel content of orthopyroxene fluctuated from 650 ppm to 2100 ppm. The difference in the ranges may be explained by the larger amount of sulfides present in the samples of this study. The observed ranges are similar with the orthopyroxene compositions of the other Kotalahti-type intrusion (Mäkinen, 1987).

Cumulus plagioclase appears as a new cumulus phase in addition to olivine and pyroxenes in gabbroic rocks. Plagioclase is also present in very small amounts in the intercumulus space of pyroxenites. The rare occurence of plagioclase in the ultramafic cumulates may be explained by a high total pressure and partial water pressure that restrain plagioclase fractionation in arc environments, leading to an enrichment of Al in the residual melt (Müntener et al., 2001; Dessimoz et al., 2012; Pichavant and Macdonald, 2007). The analyzed plagioclase grains are all intermediate to calcic in composition varying from An_{78} to An_{71}. However, in arc-cumulates, plagioclase is usually very An-rich in composition (De Bari and Coleman, 1989; Dessimoz et al., 2012).

8.3. Implications for Ni sulfide exploration potential

Lherzolites of the study area contain less than 0.5 vol.% ore minerals. Sulfides are present in lherzolites as as dissemination in the intercumulus space and rarely as small globules in olivine and pyroxene grains. Sulfide globules are also present locally in pyroxene grains of websterites and hornblende pyroxenites as well as in pyroxene and olivine grains of some the gabbroic rocks. The presence of sulfides as spherical globules in olivine and pyroxene grain indicates that the magma was saturated by sulfide melt, at least locally, during the crystallization of olivine and pyroxenes (Roedder, 2018). However, in some grains, there is a small sulfide-filled embayment at the grain margin, so it is also possible that the appearance of sulfides as inclusions might result from a section through such an embayment. To confirm the existence of sulfide inclusions, a 3D tomography study of the host grains would be needed. Also more lherzolite samples would be needed to make wider and more reliable conclusions.

The appearance of sulfide globules in mafic silicates in lherzolites and pyroxenites suggests that silicate-sulfide liquid immisicibility occurred early during the differentiation. The early immiscibility increases the possibilities for the formation of massive and matrix sulfides as there are fewer crystals in the magma, permitting the gravitative settling and concentration of the globules of relatively dense sulfide melt more efficiently (Roedder, 2018). If the immiscibility occurred later during fractional

crystallization, the formation of massive and matrix sulfides would not be possible due to crystal-rich mush.

Sulfides are most abundant in websterites where they constitute 15-45 vol% of all the minerals. The majority of them occur as a net-textured and patchy net-textured framework. Hornblende pyroxenites, gabbros, gabbronorites, and olivine norites contain 0.5-6 vol% of ore minerals that occur mostly as irregular dissemination in the intercumulus space.

Mineral geochemistry can be used to evaluate the ore potential of the studied intrusion by analyzing the Mg# and Ni, Cr, Cu content of early crystallizing minerals including olivine, orthopyroxene, and spinel (e.g. Häkli, 1971; Makkonen, 1996; Lamberg, 2005). Olivine grains analyzed from the Sydänneva area in this study contained 0-1720 ppm nickel and 68.8-72.0 mol% Fo. In previous studies of Kontoniemi and Mäkinen (2001), olivine is reported to contain up to 6910 ppm Ni and 81.7 mol% Fo. The Ni contents of orthopyroxene grains of the study area fluctuate from 0 to 1300 ppm. In previous studies, orthopyroxene has yielded higher Ni contents, reaching 2100 ppm (Kontoniemi and Mäkinen, 2001).

The Ni mineralization potential of the Ylivieska intrusion can be assessed using Mg# versus Ni plot (Fig. 26). According to Makkonen et al. (2008; 2017), the most prominent intrusions show a steep trend from high Fo (80> mol%) and Ni (>1500 ppm) contents toward low Ni contents (<500ppm), suggesting that sulfide segregation occurred within the intrusion. If only nickel-depleted olivine is present, it indicates that fractionation may have taken place before the final emplacement into the current magma chamber. The combined compositional data of olivine and orthopyroxene from this study and the study of Kontoniemi and Mäkinen (2001) display a steep trend in the Ni and Fo contents, indicating that sulfide segregation may have taken place within the intrusion. However, more compositional data are needed from different peridotite and gabbroic units of the intrusion to confirm the results and to make wider conclusions.

On the basis of the petrography, websterites seem to be the most potential for Ni-Cu mineralization. Sulfide saturation has probably occurred early during the evolution of the intrusion, as indicated by the ore mineral textures and the wide compositional range of olivine and pyroxene.

9. CONCLUSIONS

The rocks of the Sydänneva area in the Ylivieska intrusion are classified as lherzolites, hornblende pyroxenites, websterites, gabbros, gabbronorites, olivine gabbronorites and olivine norites, and using the cumulate terminology, they are olivine-pyroxene orthocumulates, pyroxene orthocumulates, plagioclase-pyroxene and pyroxene-plagioclase adcumulates, plagioclase-pyroxene mesocumulates as well as plagioclase-pyroxene-olivine meso- and adcumulates. Magmatic interstitial amphibole, phlogopite and plagioclase are common. Orthopyroxene is dominant over clinopyroxene in all rock units of the study area except in lherzolites and gabbros, which may increase the ore potential of the intrusion, due to the contamination of the magma by mica gneiss.

The studied intrusion shows similarities to other known Ni-Cu mineralized Kotalahti-type intrusions with respect to the cumulate and ore mineral assemblages and the presence of disseminated sulfides in the gabbroic rocks. Massive and matrix sulfides mainly occur in the pyroxenite unit, differing from the majority of the intrusions of the Kotalahti Belt, in which sulfides mainly occur in olivine-rich cumulates. However, there are some intrusions in the Kotalahti Belt that resemble the studied intrusion in terms of the location of mineralization, e.g., the Rytky intrusion.

The analyzed olivine grains contain less CaO than those of typical subduction-related magmas. The Fo and Ni ranges are comparable with the olivine compositional data recorded earlier for Kotalahti Belt intrusions. The MnO concentrations of the analyzed olivine crystals show a clear negative correlation with the fosterite content whereas NiO shows a weak positive correlation with the fosterite content. These trends are consistent with progressive crystal fractionation.

All analyzed clinopyroxenes are augite in composition. Their TiO_2 content increases with decreasing Mg#, which may reflect a crystallization trend in hydrous subduction-related arc magmas. The Cr_2O_3 concentrations of the analyzed clinopyroxenes show positive correlation with Mg#, being consistent with progressive fractionation. The analyzed clinopyroxene grains do not show any increase in Al_2O_3 with increasing differentiation,

differing from typical clinopyroxenes that crystallize from hydrous arc magmas under high-pressure conditions. However, hornblende and plagioclase are present in large amounts in all analyzed samples, which might contribute to the low Al_2O_3 content of clinopyroxene. Also the occurrence of plagioclase as an intercumulus mineral in the beginning of differentiation of plagioclase peridotites might have obstructed the increase in Al in pyroxenes with increasing differentiation.

Mg# of orthopyroxene decreases systematically with the MnO concentration through the ultramafic cumulates to the gabbroic rocks whereas the Cr_2O_3 content of orthopyroxene systematically decreases with increasing differentiation, being consistent with the model of progressive fractionation. The measured nickel contents correspond mostly to the orthopyroxene compositions recorded earlier for the intrusion and are similar with the orthopyroxene compositions of the other Kotalahti-type intrusions.

Abundant orthopyroxene in the studied rocks could be explained by the formation of orthopyroxene by peritetic reactions between olivine and residual melt or by assimilation of silica. However, the potential contamination event and its effects require more studies.

The most common ore minerals in the intrusion are pyrrhotite, chalcopyrite, and pentlandite. Sulfides are most abundant in websterites, forming matrix ore. Sulfides are also present as dissemination in lherzolites, hornblende pyroxenites, gabbros, gabbronorites, olivine gabbronorites, and olivine norites. On the basis of the petrography, websterites seem to be most potential for Ni-Cu mineralization. Sulfide saturation has probably occurred early during the evolution of the magma, as indicated by the ore mineral textures and the wide compositional range of olivine and pyroxene, indicating a high ore potential of the intrusion.

10. ACKNOWLEDGEMENTS

First, I would like to thank Timo Mäki from Pyhäsalmi Mine Oy for providing the sample and background material and giving me the opportunity to work on the thesis subject. I would also like to thank my supervisors Shenghong Yang and Eero Hanski from the University of Oulu for their guidance and corrections, which were invaluable and highly appreciated, enchancing the end result of this thesis. Shenghong and Eero are also thanked for financial support in mineral chemistry studies. I am also grateful for Tapio Halkoaho from GTK for providing background material and comments on thesis, which are valued highly.

Furthermore, I would also like to give my gratitude to Leena Palmu and Marko Moilanen from the Center for Material Analysis for their collaboration and guidance with the microprobe analyses.

To my family and friends, thanks for your endless support and encouragement.

11. REFERENCES

Ashwal, L.D. 1993. Anorthosites. Springer-Verlag, Berlin, 422 pp.

Barnes, S.J., Makovicky, E., Rose-Hansen, J. and Karup-Moller, S. 1997. Partition coefficients for Ni, Cu, Pd, Pt, Rh, and Ir between monosulfide solid solution and sulfide liquid and the formation of compositionally zoned Ni – Cu sulfide bodies by fractional crystallization of sulfide liquid. Canadian Journal of Earth Sciences 34, 366–374

Barnes, S.J., Makkonen, H.V., Dowling, S.E., Hill, R.E.T. and Peltonen, P. 2009. The 1.88 Ga Kotalahti and Vammala nickel belts, Finland: geochemistry of the mafic andultramafic metavolcanic rocks. Bulletin of the Geological Society of Finland 81, 103-141.

Barnes, S.J. and Lightfoot, P. 2005. Formation of magmatic nickel sulfide ore deposits and processes affecting the Cu and PGE contents. Economic Geology, 100th Anniversary Volume, Littleton, CO, Society of Economic Geologists, Inc., p. 179–214.

Batanova, V.G., Pertsev A.N., Kamenetsky V.S., Ariskin A.A., Mochalov A.G. and Sobolev A.V. 2005. Crustal evolution of island-arc ultramafic magma: Galmoenan pyroxenite–dunite plutonic complex, Koryak highland (Far East Russia). Journal of Petrology 46, 1345–1366.

Bender, J.F., Hodges, F.N. and Bence, A.E. 1978. Petrogenesis of basalts from the project FAMOUS area: experimental study from 0 to 15 kbars. Earth and Planetary Science Letters 41, 277–302.

Boudreau, A.E. and McBirney, A.R. 1997. The Skaergaard Layered Series. Part III. Non-dynamic layering. Journal of Petrology 38, 1003–1020.

Boyd, R. and Mathieson, C.O. 1979. The nickel mineralisation of the Råna mafic intrusion, Nordland, Norway. Canadian Mineralogist 17, 287–298.

Boyd, R., Barnes, S.-J. and Grönlie, A. 1988. Noble metal geochemistry of some Ni-Cu deposits in the Sveconorwegian and Caledonian orogens in Norway. In: Prichard, H.M., Potts, P.J., Bowles, J.F.W. and Cribb, S.J. (Eds.) Geo-Platinum 87. Elsevier, London, p. 144–158.

Campbell, I.H. and Naldrett, A.J. 1979. The influence of silicate: Sulfide ratios on the geochemistry of magmatic sulfides. Economic Geology 74, 1503–1506.

Cawthorn, R.G., Barnes, S.J., Ballhaus, C. and Malitch, K.N. 2005. Platinum group element, chromium, and vanadium deposits in mafic and ultramafic rocks. In: Hedenquist, J.W. et al. (Eds) Economic Geology, 100th Anniversary Volume, Littleton, CO, Society of Economic Geologists, Inc., p. 215-250.

Conrad, W.K. and Kay, R.W. 1984. Ultramafic and mafic inclusions from Adak Island—crystallization history, and implications for the nature of primary magmas and crustal evolution in the Aleutian arc. Journal of Petrology 25, 88–125.

Cox, D. and Singer, D. 1986. Mineral Deposit Models. U.S. Geological Survey, Bulletin 1693, 379 p.

Dare, S.A.S, Barnes, S.J., Prichard, H.M and Fisher, P.C. 2014. Mineralogy and Geochemistry of Cu-Rich Ores from the McCreedy East Ni-Cu-PGE Deposit (Sudbury, Canada): Implications for the Behavior of Platinum Group and Chalcophile Elements at the End of Crystallization of a Sulfide Liquid. Economic Geology 109, 343–366.

DeBari, S.M. and Coleman, R.G. 1989. Examination of the deep levels of an island arc: Evidence from the Tonsina ultramafic-mafic assemblage, Tonsina, Alaska. Journal of Geophysical Research: Solid Earth 94, 4373-4391.

Dessimoz, M., Müntener, O. and Ulmer, P. 2012. A case for hornblende dominated fractionation of arc magmas: the Chelan Complex (Washington Cascades). Contributions to Mineralogy and Petrology 163, 567-589.

Bedrock of Finland – DigiKP. Digital map database [Electronic resource]. Espoo: Geological Survey of Finland [referred 10 September 2019], Version 2.2., available at: https://gtkdata.gtk.fi/Kalliopera/index.html

Elthon, D., Casey, J.F. and Komor, S. 1982. Mineral chemistry of ultramafic cumulates from the North Arm Mountain Massif of the Bay of Islands ophiolite: Evidence for highpressure crystal fractionation of oceanic basalts. Journal of Geophysical Research: Solid Earth 87, 8717-8734.

Gaetani, G.A., Grove, T.L. and Bryan, W.B. 1993. The influence of water on the petrogenesis of subduction related igneous rocks. Nature 365, 332–334.

Grove, T.L. 2000. Origin of magmas. In: Sigurdsson, H. (Ed.) Encyclopedia of Volcanoes. Academic Press, San Diego, p. 133–147.

Heaman, L.M., Machado, N., Krogh, T.E. and Weber, W. 1986. Precise U-Pb zircon ages for the Molson dyke swarm and the Fox River sill: constraints for Early Proterozoic crustal evolution in northeastern Manitoba, Canada. Contributions to Mineralogy and Petrology 94, 82–89.

Himmelberg G.R. and Loney R.A. 1995. Characteristics and petrogenesis of Alaskan-type ultramafic-mafic intrusions, southeastern Alaska. USGS Professional Paper 1564, 1–47.

Hoatson, D.M. and Blake, D.H. 2000. Geology and economic potential of the Palaeoproterozoic layered mafic–ultramafic intrusions in the east Kimberley, Western Australia. Australian Geological Survey Organisation, Bulletin 246, 476 p.

Hulbert, L.J., Hamilton, M.A., Horan, M.F. and Scoates, R.F.J. 2005. U-Pb zircon and Re-Os isotope geochronology of mineralized ultramafic intrusions and associated nickel ores from the Thompson nickel belt, Manitoba, Canada. Economic Geology 100, 29-41.

Hunter, R.H. 1996. Texture development in cumulate rocks. In: Cawthorn, R.G. (Ed.) Layered intrusions. Elsevier Science B.V., Amsterdam, p. 103–145.

Häkli, T.A. 1971. Silicate nickel and its application to the exploration of nickel ores. Bulletin of the Geological Society of Finland 43, 247-263.

Häkli, T.A., Vormisto, K. and Hanninen, E., 1979. Vammala, a nickel deposit in layered ultramafite, southwest Finland. Economic Geology 74, 1166–1182.

Irvine, T.N. 1974. Petrology of the Duke Island ultramafic complexes, south-eastern Alaska. Geological Society of America Memoir 138, 240 p.

Irvine, T.N. 1982. Terminology for layered intrusions. Journal of Petrology 23, 127–162.

Isohanni, M., Ohenoja, V. and Papunen, H. 1985. Geology and nickel-copper ores of the Nivala area. In Papunen, H. and Gorbunov, G.J. (Eds.) Nickel-Copper deposits of the Baltic Shield and Scandinavian Caledonides. Geological Survey of Finland, Bulletin 333, 211-228.

Jerram, D.A., Cheadle, M.J. and Philpotts, A.R. 2003. Quantifying the building blocks of igneous rocks: are clustered crystal frameworks the foundation? Journal of Petrology 44, 2033–2051.

Kalliomäki, H., Torvela, T., Moreau, J. and Kähkönen, Y. 2014. Relationships between basin architecture, basin closure, and occurrence of sulphide-bearing schists: an example from Tampere Schist Belt, Finland. Journal of the Geological Society of London 171, 659-671.

Kontoniemi, O. and Mäkinen, J. 2001. Ylivieskan perkkiön peridotiitin ja sen ympäristön petrologinen ja geokemiallinen luonne. Geological Survey of Finland, Archive Report M19/2431/2001/1/10, 17 p.

Korsman, K., Koistinen, T., Kohonen, J., Wennerström, M., Ekdahl, E., Honkamo, M., Idman, H. and Pekkala, Y. (Eds.) 1997. Suomen kallioperäkartta - Bedrock map of Finland 1: 1000000. Geological Survey of Finland.

Krause, J., Brügmann, G.E., Pushkarev, E.V. 2007. Accessory and rock forming minerals monitoring the evolution of zoned mafic–ultramafic complexes in the Central Ural Mountains. Lithos 95, 19–42.

Kullerud, G., Yund, R.A. and Moh, G.H. 1969. Phase relations in the Cu-Fe-S, Cu-Ni-S, and Fe-Ni-S systems. Economic Geology Monograph 4, 323–343.

Kähkönen, Y. 2005. Svecofennian supracrustal rocks. In: Lehtinen, M., Nurmi, P.A. and Rämö, O.T. (Eds.) Pre-cambrian Geology of Finland — Key to the Evolution of the Fennoscandian Shield. Elsevier, Amsterdam, p. 343–406.

Lahtinen, R., Huhma, H., Lahaye, Y, Kousa, J. and Luukas, J. 2015. Archean–Proterozoic collision boundary in central Fennoscandia: Revisited. Precambrian Research 261, 127-165.

Lahtinen, R., Korja, A. and Nironen, M. 2005. Paleoproterozoic tectonic evolution. In: Lehtinen, M., Nurmi, P.A. and Rämö, O.T. (Eds.) Precambrian Geology of Finland – Key to the Evolution of the Fennoscandian Shield. Elsevier B.V., Amsterdam, p. 481–532.

Laine, E.-L., Luukas, J. Mäki, T., Kousa, J., Ruotsalainen, A., Suppala, I., Imana, M., Heinonen, S. and Häkkinen, T. 2015. The Vihanti–Pyhäsalmi area. In: Weihed, P. (Ed.)

3D, 4D and Predictive Modelling of Major Mineral Belts in Europe. Spinger, Berlin-Heidelberg, p. 123-144.

Lamberg, P. 2005. From genetic concepts to practice – lithogeochemical identification of Ni-Cu mineralised intrusions and localisation of the ore. Geological Survey of Finland, Bulletin 402, 264 p.

Latypov, R. 2015. Basal reversals in mafic sills and layered intrusions. In: Charlier, B., Namur, O., Latypov, R. and Tegner, C. (Eds.) Layered Intrusions. Springer, Dordrecht, p. 259-293.

Lebrun, E., Árting, T.B., Kolb, J., Fiorentini, M., Kokfelt, T., Johannesen, A.B., Maas, R., Thebaud, N., Martin, L.A.J. and Murphy, R.C. 2018. Genesis of the Paleoproterozoic Ammassalik Intrusive Complex, south-east Greenland. Precambrian Research 315, 19–44.

Li, C., Naldrett, A.J., Coats, C.J.A. and Johannessen, P. 1992. Platinum, palladium, gold, copper-rich stringers at the Strathcona Mine, Sudbury; their enrichment by fractionation of a sulfide liquid. Economic Geology 87, 1584–1598.

Li, C., Naldrett, A.J. and Ripley, E.M. 2007. Controls on the Fo and Ni contents of olivine in sulfide-bearing mafic/ultramafic intrusions: Principles, modeling, and examples from Voisey's Bay. Earth Science Frontiers, 14, 177–183.

Li, C., Thakurta, J. and Ripley, E.M. 2012. Low-Ca contents and kink-banded textures are not unique to mantle olivine: evidence from the Duke Island Complex, Alaska. Mineralogy and Petrology 104, 147-153.

Loucks, R.R. 1990. Discrimination of ophiolitic from nonophiolitic ultramafic–mafic allochthons in orogenic belts by the Al/Ti ratio in clinopyroxene. Geology 18, 346–349.

Lundqvist, T. and Autio, S. (Eds.) 2000. Description to the Bedrock Map of Central Fennoskandia (Mid-Norden). Geological Survey of Finland, Special Paper 28, 176 p.

Luukas, J., Kousa, J., Nironen, M. and Vuollo, J. 2017. Major stratigraphic units in the bedrock of Finland, and an approach to tectonostratigraphic division. In: Nironen, M. (Ed.) Bedrock of Finland at the Scale 1:1 000 000 - Major Stratigraphic Units, Metamorphism and Tectonic Evolution. Geological Survey of Finland, Special Paper 60, 9–40.

Maier, W.D. 2015. Geology and petrogenesis of magmatic Ni-Cu-PGE-Cr-V deposits: An introduction and overview. In: Maier, W.D., Lahtinen, R. and O'Brien, H. (Eds.) Mineral Deposits of Finland. Elsevier, Amsterdam, p. 73–92.

Makkonen, H. 1996. 1.9 Ga tholeiitic magmatism and related Ni-Cu deposition in the Juva area, SE Finland. Geological Survey of Finland, Bulletin 386, 101 p.

Makkonen, H.V. 2015. Nickel deposits of the 1.88 Ga Kotalahti and Vammala belt. In: Maier, W.D., O'Brien, H., Lahtinen, R. (Eds.) Mineral Deposits of Finland. Elsevier, Amsterdam, p. 253–290.

Makkonen, H.V. and Halkoaho, T. 2007. Whole rock analytical data (XRF, REE, PGE) for several Svecofennian (1.9 Ga) and Archaean (2.8 Ga) nickel deposits in eastern Finland. Geological Survey of Finland, Archive Report, M19/3241/2007/32, 49 p.

Makkonen, H.V., Mäkinen, J. and Kontoniemi, O., 2008. Geochemical discrimination between barren and mineralized intrusions in the Svecofennian (1.9 Ga) Kotalahti Nickel Belt, Finland. Ore Geology Reviews 33, 101–114.

Makkonen, H.V, Halkoaho, T., Konnunaho, J., Rasilainen, K., Kontinen, A. and Eilu P. 2017. Ni-(Cu-PGE) deposits in Finland – Geology and exploration potential. Ore Geology Reviews 90, 667–696.

Makkonen, H. and Huhma, H. 2007. Sm-Nd data for mafic-ultramafic intrusions in the Svecofennian (1.88 Ga) Kotalahti nickel belt, Finland – implications for crustal contamination at the Archean/Proterozoic boundary. Bulletin of the Geological Society of Finland 79, 175-201.

Makkonen, H.V., Mäkinen, J. and Kontoniemi, O. 2008. Geochemical discrimination between barren and mineralized intrusions in the Svecofennian (1.9 Ga) Kotalahti Nickel Belt, Finland. Ore Geology Reviews 33, 101–114.

Manor, M.J., Scoates, J.S., Nixon, G.T. and Ames, D.E. 2016. The Giant Mascot Ni-Cu-PGE Deposit, British Columbia: mineralized conduits in a convergent margin tectonic setting. Economic Geology 111, 57–87.

Mavrogenes, J.A. and O'Neill, H.S. 1999. The relative effects of pressure, temperature and oxygen fugacity on the solubility of sulfide in mafic magmas. Geochimica et Cosmochimica Acta 63, 1173–1180.

McBirney, A.R. and Nicolas, A. 1997. The skaergaard layered series. Part II. Magmatic flow and dynamic layering. Journal of Petrology 38, 569–580.

Morimoto, N. and Kitamura, M. 1983. Q-J diagram for classification of pyroxenes. Journal of the Japanese Association of Mineralogist, Petrologist and Economic Geologist. 78, 141.

Morse, S.A. 1986. Convection in aid of adcumulus growth. Journal of Petrology 27, 1183–1214.

Müntener, O., Kelemen, P.B. and Grove, T.L. 2001. The role of H2O during crystallization of primitive arc magmas under uppermost mantle conditions and genesis of igneous pyroxenites: an experimental study. Contributions to Mineralogy and Petrology 141, 643–658.

Mäki, T., Imana, O., Kousa, J. and Luukas, J. 2015. The Vihanti-Pyhäsalmi VMS Belt. In: Maier, W.D, Lahtinen, R. and O'Brien, H. (Eds.) Mineral Deposits of Finland. Elsevier, Amsderdam, p. 507-530.

Mäkinen, J. 1987. Geochemical characteristics of Svecokarelidic mafic-ultramafic intrusions associated with Ni-Cu occurrences in Finland. Geological Survey of Finland, Bulletin 342, 109 p.

Mäkinen, J. and Makkonen, H.V. 2004. Petrology and structure of the Palaeoproterozoic (1.9 Ga) Rytky nickel sulphide deposit, Central Finland: a comparison with the Kotalahti nickel deposit. Mineralium Deposita 39, 405-421.

Naldrett, A.J. 1989. Magmatic Sulfide Deposits. Clarendon Press, Oxford Univ. Press, Oxford, 186 p.

Naldrett, A.J. 1997. Key factors in the genesis of Noril'sk, Sudbury, Jinchuan, Voisey's Bay and other world-class Ni-Cu-PGE deposits: implications for exploration. Australian Journal of Earth Sciences 44, 283–315.

Naldrett, A.J. 2004. Magmatic Sulfide Deposits: Geology, Geochemistry and Exploration, 1st Ed. Springer, Berlin, 728 p.

Naldrett, A. J. 2010. Secular variation of magmatic sulfide deposits and their source magmas. Economic Geology 105, 669–688.

Naldrett, A.J. 2011. Fundamentals of magmatic sulfide deposits. Review. Economic Geology 17, 1–50.

Namur, O., Abily, B., Boudreay, A.E., Blanchette, F., Bush, J.W.M., Ceuleneer G, Charlier, B., Don-aldson, C.H., Duchesne, J.-C., Higgins, M.D., Morata, D., Nielsen, T.F.D., O'Driscoll, B. and Pang, K.N. 2015. Igneous layering in basaltic magma chambers. In: Charlier, B., Namur, O., Latypov, R. and Tegner, C. (Eds.) Layered Intrusions. Springer, London, p. 75–152

Naslund, H.R. and McBirney, A.R. 1996. Mechanisms of formation of igneous layering. In: Cawthorn, R.G. (Ed.) Layered Intrusions. Elsevier, Amsterdam, p. 1–43.

Nironen, M. 1997. The Svecofennian Orogen: a tectonic model. Precambrian Research, 86, 21–44.

Nironen, M. 2005. Proterozoic orogenic granitoid rocks. In: Lehtinen, M., Nurmi, P.A. and Rämö, O.T. (Eds.) Precambrian Geology of Finland – Key to the Evolution of the Fennoscandian Shield. Elsevier B.V., Amsterdam, p. 443-480.

Nironen, M. 2017. Bedrock of Finland at the scale 1: 1 000 000 – Major stratigraphic units, metamorphism and tectonic evolution. Geological Survey of Finland, Special Paper 60, 128 p.

Pajunen, M., Airo, M-L., Elminen, T., Mänttäri, I., Niemelä, R., Vaarma, M., Wasenius, P. and Wennerström, M. 2008. Tectonic evolution of the Svecofennian crust in southern Finland. In: Pajunen, M. (Ed.) Tectonic Evolution of the Svecofennian Crust in Finland – a Basis for Characterizing Bedrock Technical Properties. Geological Survey of Finland, Special Paper 47, 15-160.

Papunen, H. 1986. Platinum-group elements in Svecokarelian nickel-copper deposits, Finland. Economic Geology 81, 1236-1241.

Papunen, H. 1989. Platinum-group elements in metamorphosed Ni-Cu deposits in Finland. In: Magmatic Sulphides - The Zimbabwe Volume. The Institutuion of Mining and Metallurgy, London, p. 165-176.

Papunen, H. 2003. Ni-Cu sulfide deposits in mafic-ultramafic orogenic intrusions. Examples from the Svecofennian areas, Finland. In: Eliopolous, D.G., et al. (Eds.) Mineral Exploration and Sustainable Development. Millpress, Rotterdam, p. 551-554.

Peltonen, P. 1995. Magma-country rock interaction and the genesis of Ni-Cu deposits in the Vammala nickel belt, SW Finland. Mineralogy and Petrology 52, 1-24.

Peltonen, P. 2005. Svecofennian mafic-ultramafic intrusions. In: Lehtinen, M., Nurmi, RA. and Rämö, O.T. (Eds.) Precambrian Geology of Finland - Key to the Evolution of the Fennoscandian Shield. Elsevier B.V., Amsterdam, p. 407-442.

Pesonen, L. and Stigzelius, E. 1972. On petrophysical and paleomagnetic investifations of the gabbros of the Pohjanmaa region, Middle-West Finland. Geological Survey of Finland, Bulletin 260, 5-13.

Pichavant, M. and Macdonald, R. 2007. Crystallization of primitive basaltic magmas at crustal pressures and genesis of the calc-alkaline igneous suite: experimental evidence from St Vincent, Lesser Antilles arc. Contributions to Mineralogy and Petrology 154, 535–558.

Piña, R., Romeo, I., Ortega, L., Lunar, R., Capote, R., Gervilla, F., Tejero, R. and Quesada, C. 2010. Origin and emplacement of the Aguablancamagmatic Ni-Cu-(PGE) sulphide deposit, SW Iberia: A multidisciplinary approach. Bulletin of the Geological Society of America 122, 915–925.

Puustinen, K., Saltikoff, B. and Tontti, M. 1995. Distribution and metallogenictypes of nickel deposits in Finland. Geological Survey of Finland, Report of Investigation 132, 38 p.

Rasilainen, K., Eilu, P., Äikäs, O., Halkoaho, T., Heino, T., Iljina, M., Juopperi, H., Kontinen, A., Kärkkäinen, N., Makkonen, H., Manninen, T., Pietikäinen, K., Räsänen, J., Tiainen, M., Tontti, M. and Törmänen, T. 2012. Quantitative mineral resource assessment of nickel, copper and cobalt in undiscovered Ni-Cu depos-its in Finland. Geological Survey of Finland, Report of Investigation 194, 514 p.

Ripley, E. and Li, C. 2013. Sulfide saturation in mafic magmas: is external sulfur required for magmatic Ni–Cu–(PGE) ore genesis? Economic Geology 108, 45–58.

Roedder, E. 2018. Fluid inclusions. De Gruyter, Berlin, Boston, 652p.

Salli, I. 1955. Kallioperäkarttojen selitys, Pre-Quaternary rocks, sheet 2431, Ylivieska. Geological map of Finland 1:100 000, Geological Survey of Finland, 33p.

Scoates J. and Wall C. 2015. Geochronology of layered intrusions. In: Charlier B., Namur O., Latypov, R. and Tegner, C. (Eds.) Layered Intrusions. Springer Geology. Springer, Dordrecht, p. 3-74.

Sigurdsson, I.A., Kamenetsky, V.S., Crawford, A.J., Eggins, S.M. and Zlobin, S.K. 1993. Primitive island arc and oceanic lavas from the Hunter ridge- Hunter fracture zone. Evidence from glass, olivine and spinel compositions. Mineralogy and Petrology 47, 149-169.

Simkin, T. and Smith, J.V. 1970. Minor-element distribution in olivine. Journal of Geology 78, 304–325.

Simonen, A. 1980. The Precambrian in Finland. Geological Survey of Finland, Bulletin 304, 58 p.

Smith, D.R. and Leeman, W.P. 2005. Chromian spinel-olivine phase chemistry and the origin of primitive basalt of the southern Washington Cascades. Journal of Volcanology and Geothermal Research 140, 49-66.

Sipilä, E. 1976. Raportti Geologisen tutkimuslaitoksen malmitutkimuksista Ylivieskan gabroalueella 1973-1975. Geological Survey of Finland, Unpublished Report M19/2431/-76/1/10, 12 p.

Sipilä, E. 1984. Raportti Ylivieskan gabromassiivin malmietsinnällisesti kiinnostavasta suur-ja syvärakennetutkimuksesta ja ultraemäksisen osan tarkastuskairauksesta. Geological Survey of Finland, Unpublished Report M 19/2431/84/1/10, 22 p.

Straub, S.M., LaGatta, A.B., Martin-Del Pozzo, A.L. and Langmuir, C.H. 2008. Evidence from high-Ni olivines for a hybridized peridotite/pyroxenite source for orogenic andesites from the central Mexican Volcanic Belt. Geochemistry, Geophysics, Geosystems 9.

Streckeisen, A.L. 1974. Classification and nomenclature of igneous rocks. Geologische Rundschau 63, 773-786.

Thakurta, J., Ripley, E.M. and Li C. 2008. Geochemical constraints on the origin of sulfide mineralization in the Duke Island Complex, southeastern Alaska, Geochemistry, Geophysics, Geosystems 9, Q07003.

Thompson, J.F.H. and Naldrett, A.J. 1984. Sulfide-silicate reactions as a guide to Ni-Cu-Co mineralization in central Maine (USA). In: Buchanan, D.L. and Jones M.J. (Eds.)

Sulfide Deposits in Mafic and Ultramafic Rocks. Institution of Mining and Metallurgy. London, Special Publication, p. 103-113.

Turek, A., Woodhead, J. and Zwanzig, H.V. 2000. U-Pb age of the gabbro and otherplutons at Lynn Lake (part of NTS 64C). In: Report of Activities 2000, ManitobaIndustry, Trade and Mines. Manitoba Geological Survey, p. 97–104.

Vaarma, M. and Kähkönen, Y. 1994. Geochemistry of the Paleoproterozoic metavolcanic rocks at Evijärvi, western Finland. Geological Survey of Finland, Special Paper 19, 47-59.

Wager, L.R. and Brown, G.M. 1967. Layered Igneous Rocks. Oliver & Boyd, Edinburgh, 588 p.

Weihed, P., Bergman, J. and Bergström, U., 1992. Metallogeny and tectonic evolution ofthe Early Proterozoic Skellefte district, northern Sweden. Precambrian Research 58, 143–167.

Weihed, P. and Mäki, T. 1997. Volcanic hosted massive sulphide an gold deposits in the Skellefte District, Sweden and Western Finland. Excursion guidebook A2. 4th Biennal SGA Meeting, August 11-13, 1997, Turku, Finland, 81 p.

Winter, J.D. 2001. An Introduction to Igneous and Metamorphic Petrology. Prentice Hall, Upper Saddle River, NJ, 697 p.

APPENDICES

1. **Petrographical observation sheets.**
2. **Olivine electron microprobe results.**
3. **Pyroxene electron microprobe results.**
4. **Plagioclase electron microprobe results.**

APPENDIX 1. Petrographical observation sheets.

Thin section ID	Rock name	Hole ID/ Depth	Location
OY27038	Lherzolite	Ylivieska-19/7,5m	Sydänneva

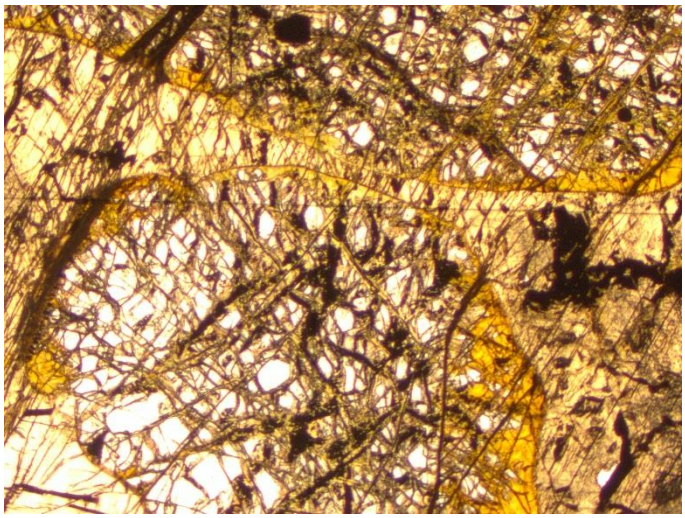

Figure 1: *Serpentine minerals replacing coarse grained olivine grains in OY27038. (1,25x magnification with PPL)*

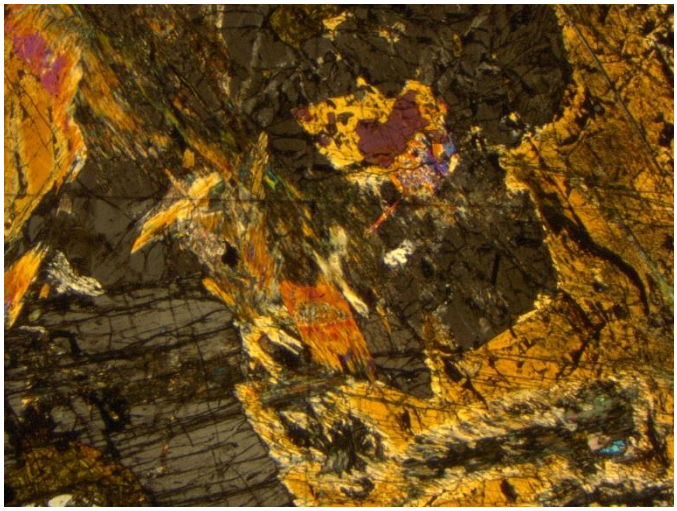

Figure 2: *Most of the pyroxene grains have altered into actinolite (1,25x magnification with XPL)*

Main minerals:	olivine, augite, orthopyroxene, serpentine, hornblende, actinolite, chlorite
Accessory minerals:	talc, titanite
Ore/opaque minerals:	pyrrhotite, bornite, chalcopyrite, pentlandite, digenite
Texture:	olivine orthocumulate
Mineral alteration:	serpentinization, amphibolization
Rock/hydrothermal alteration:	-
EPMA analyses:	Six pyroxene grains and five olivine grains were analysed.

Description:	The olivine grains are the most abundant minerals constituting 70% of the all minerals. They occur as subhedral cumulus crystal and they have all altered to serpentine minerals. The diameter of olivine grains varies from 3mm to 9mm. Cumulus phases also incorporate augite and orthopyroxene. The alteration of pyroxene minerals to secondary amphiboles is common. The intercumulus material is mostly composed of hornblende. Chlorite and serpentine minerals are present in the altered parts. Talc and titanite are present in small amounts. The ore minerals occur as blebs in olivine and pyroxene grains constituting 0,25% of the all minerals. Chalcopyrite is often altered to bornite and digenite.

Thin section ID	Rock name	Hole ID/ Depth	Location
OY27022	Websterite	M52-2431-95-426/ 27m	Sydänneva

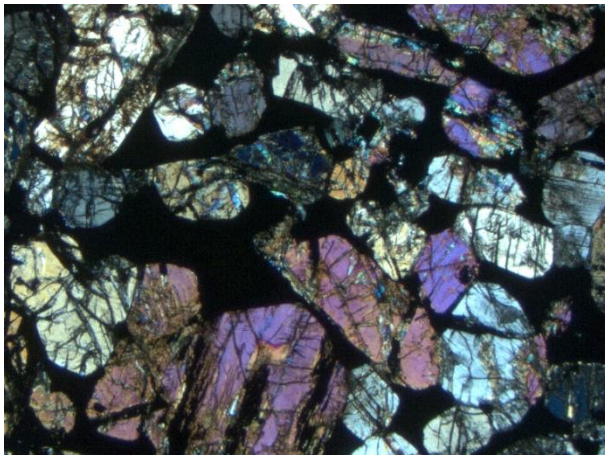

Figure 1: *Subhedral pyroxene cumulus grains in net-textured ore mineral matrix. (1,25x magnification with XPL)*

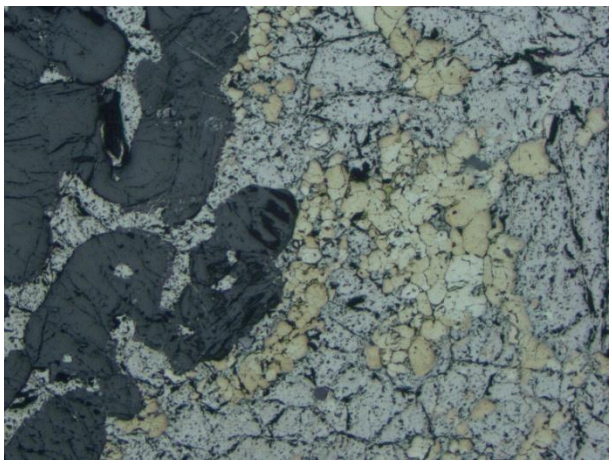

Figure 2: *The matrix is mainly composed of pyrrhotite, chalcopyrite and pentlandite (2,5x magnification with reflective light).*

Main minerals:	orthopyroxene, augite
Accessory minerals:	titanite, actinolite, hornblende, chlorite, talc, serpentine
Ore/opaque minerals:	pyrrhotite, chalcopyrite, pentlandite, ilmenite, magnetite, chromite, mackinawite, cubanite, digenite, bornite
Texture:	pyroxene orthocumulate
Mineral alteration:	uralitization
Rock/hydrothermal alteration:	-
EPMA analyses:	-
Description:	The diameter of the subhedral pyroxene cumulus grains varies from 0,5mm to 4 mm. The pyroxenes have locally altered to actinolites. Titanite is abundant in one corner of the OY27022.

The ore minerals form net textured matrix of the rock, constituting 45% of the all minerals. Pyrrhotite, chalcopyrite and pentlandite are most abundant occurring in the intercumulus space as net-textured framework and as blebs in the pyroxene grains. Chalcopyrite often form veins within the pyrrhotite. The chalcopyrite grains have occasionally cubanite lamellaes and have altered to bornite and digenite.

Ilmenite, magnetite and chromite grains appear locally within the pyrrhotite or as blebs in the pyroxene grains.

Thin section ID	Rock name	Hole ID/ Depth	Location
OY27024	Websterite	M52-2431-95-426/ 28,6m	Sydänneva

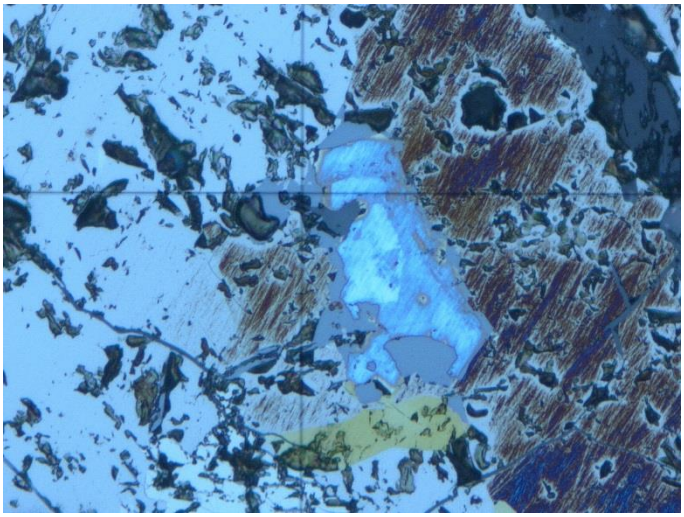

Figure 1: *Magnetite, bornite, digenite and chalcopyrite within the pyrrhotite. The bornite has been partially replaced by digenite (20x magnification with reflected light).*

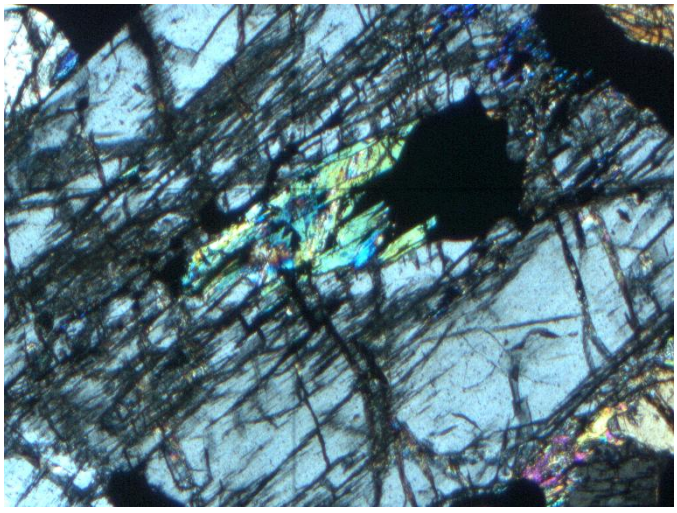

Figure 2: *Actinolite is typical alteration product of clinopyroxene in the OY27024. (10x magnification with XPL)*

Main minerals:	orthopyroxene, augite
Accessory minerals:	actinolite, titanite, chlorite, talc, hornblende
Ore/opaque minerals:	pyrrhotite, pentlandite, chalcopyrite, bornite, digenite, magnetite, ilmenite
Texture:	pyroxene orthocumulate
Mineral alteration:	uralitization
Rock/hydrothermal alteration:	-
EPMA analyses:	-
Description:	The diameter of the subhedral pyroxene cumulus grains varies from 0.25 mm to 9 mm. Augites have frequently altered to actinolite. Chlorite and titanite occur locally within the pyroxene grains.

	The ore minerals form net textured matrix of the rock, constituting 25% of the all minerals. Pyrrhotite, chalcopyrite and pentlandite are the most abundant. Pentlandite occur as a feather like pattern in the pyrrhotite. Ilmenite and magnetite appear every here and there. Alteration of chalcopyrite to bornite an digenite is present in small amounts.

Thin section ID	Rock name	Hole ID/ Depth	Location
OY27041	Websterite	Ylivieska-3/123,4m	Sydänneva

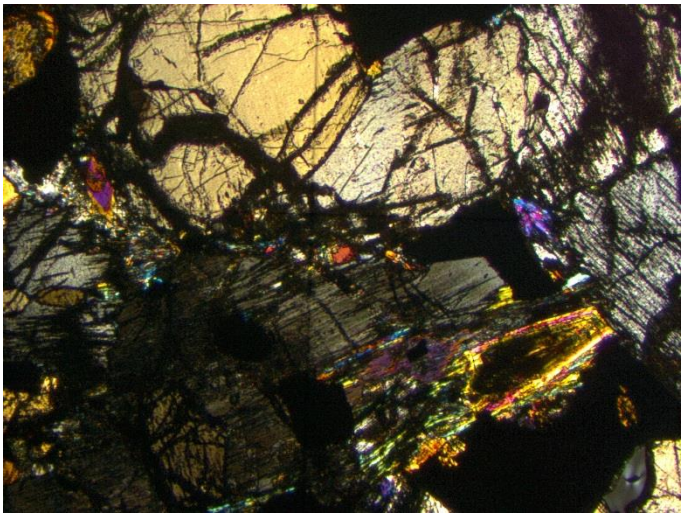

Figure 1: *Alteration of pyroxene grains to secondary amphiboles and serpentine minerals in OY27041. (5x magnification with XPL)*

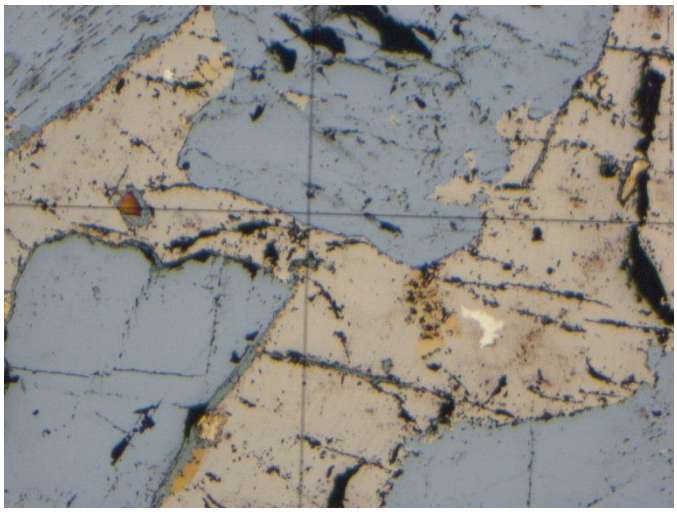

Figure 2: *Ore minerals in the matrix and within the pyroxene grain. (10x magnification with reflective light)*

Main minerals:	orthopyroxene, augite
Accessory minerals:	actinolite, serpentine, chlorite, talc, plagioclase, biotite
Ore/opaque minerals:	pyrrhotite, chalcopyrite pentlandite, violarite, bornite, digenite, magnetite, ilmenite, chromite
Texture:	medium-grained, pyroxene orthocumulate
Mineral alteration:	uralitization, serpentinization
Rock/hydrothermal alteration:	-
EPMA analyses:	Five plagioclase and ten pyroxene grains were analyzed.
Description:	The pyroxene cumulus grains are subhedral and their diameter varies from 1 to 6 mm. Accessory and ore minerals are present in the intercumulus space. The pyroxenes have altered to secondary amphiboles and serpentine minerals. Chlorite,

and talc appear in the altered parts. Alteration rims on the edges of the pyroxene grains are common. Intercumulus plagioclase occur in two areas within the thin section. The plagioclase is bytownite in composition. Intercumulus phases also include biotite.

Ore minerals occur mostly in the intercumulus space constituting 15% of the all minerals. Small amounts of ore minerals are located within the cracks of the pyroxene grains. Pyrrhotite, chalcopyrite, bornite and violarite are the most abundant ore minerals. Pentlandite, ilmenite, chromite and magnetite occur locally within the pyrrhotite.

The ore minerals are altered to a high degree and there are many replacement textures visible. Chalcopyrite is frequently altered to bornite and digenite whereas pyrrhotite and pentlandite have altered to violarite.

Thin section ID	Rock name	Hole ID/ Depth	Location
OY27042	Websterite	Ylivieska-3/126.25m	Sydänneva

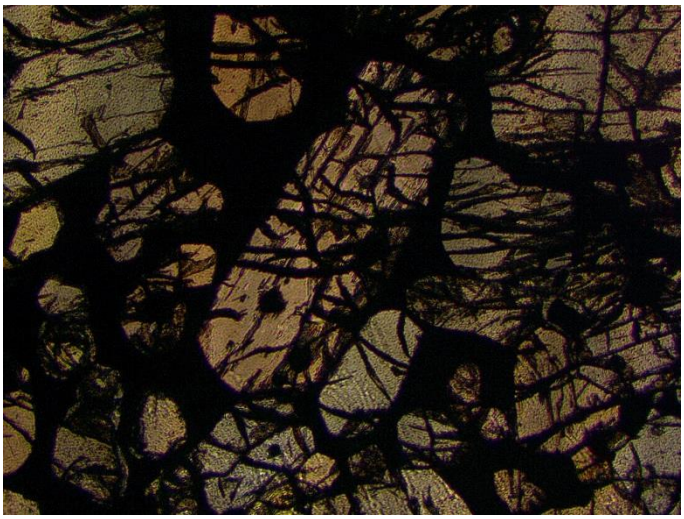

Figure 1: *Size of the pyroxene cumulus grains varies from fine to medium.*

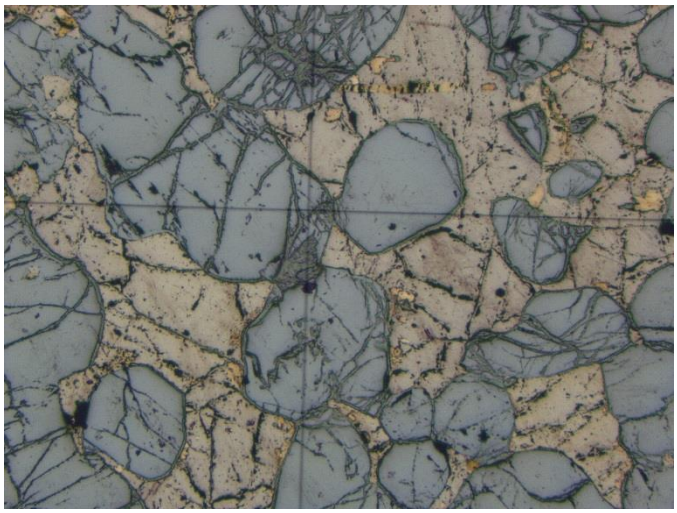

Figure 2: *The ore minerals form net textured matrix for the rock in the OY27042.*

Main minerals:	orthopyroxene, augite
Accessory minerals:	talc, serpentine, chlorite, biotite, hornblende
Ore/opaque minerals:	pyrrhotite, chalcopyrite, cubanite, pentlandite, violarite, magnetite
Texture:	pyroxene orthocumulate
Mineral alteration:	serpentinization
Rock/hydrothermal alteration:	-
EPMA analyses:	Five pyroxene grains were analyzed.
Description:	The pyroxene cumulus grains are mostly subhedral and their diameter varies from 0,4mm to 6 mm. The pyroxenes have altered to serpentinite minerals. Chlorite and talc are common in the altered parts. Sometimes the

pyroxene grains have alteration rims that are composed of serpentine minerals or talc. Talc also forms veins in the matrix. Intercumulus phases consist of ore minerals, biotite and hornblende.

The ore minerals constitute 40% of the all minerals forming net textured matrix for the rock. Some pyroxene grains have small ore mineral blebs in the cracks. Pyrrhotite, chalcopyrite and violarite and pentlandite are most abundant ore minerals. Alteration of chalcopyrite to bornite and pentlandite to violarite occurs every here and there. The cubanite lamellae's in the chalcopyrite grains are common. Magnetite is observed in small amounts.

Thin section ID	Rock name	Hole ID/ Depth	Location
OY27044	Websterite	Ylivieska-3/132.3m	Sydänneva

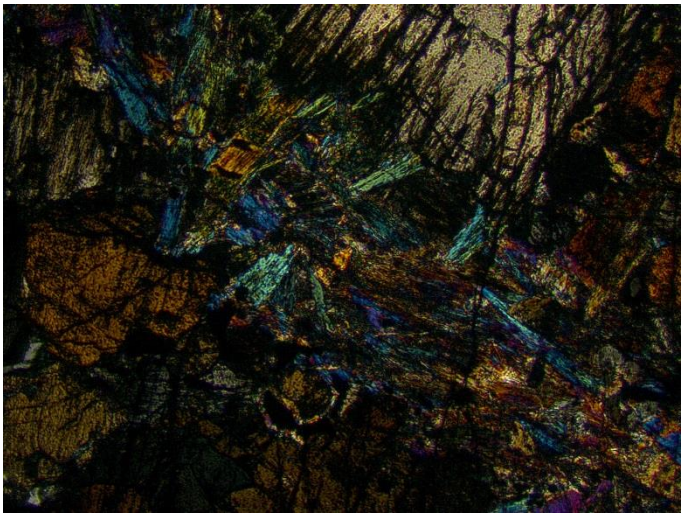

Figure 1: *Actinolite rich vein intersecting the websterite (1,25x magnification with XPL).*

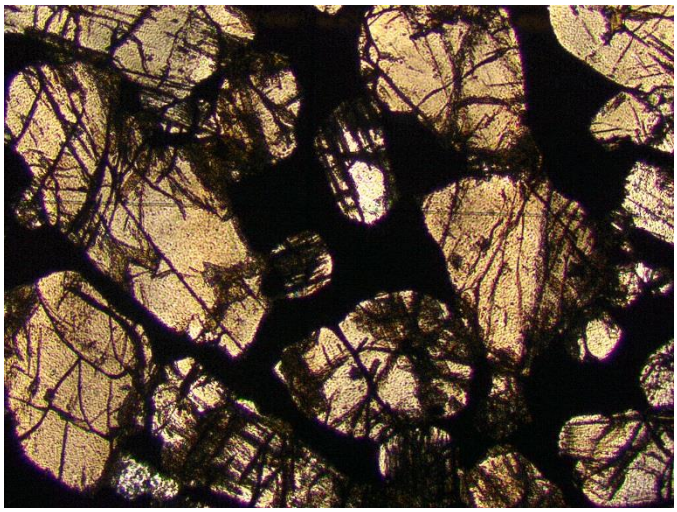

Figure 2: *Most of the OY27044 is composed of subhedral pyroxene cumulus grains that are within the ore mineral matrix (1,25x magnification with PPL).*

Main minerals:	orthopyroxene, augite
Accessory minerals:	serpentine, actinolite, chlorite, talc, biotite, plagioclase, titanite
Ore/opaque minerals:	pyrrhotite, chalcopyrite, bornite, pentlandite, violarite, cubanite, ilmenite
Texture:	pyroxene orthocumulate
Mineral alteration:	serpentinisation, uralitization
Rock/hydrothermal alteration:	-
EPMA analyses:	Nine pyroxene and six plagioclase grains were analysed.
Description:	A vein rich of secondary amphiboles, mostly actinolite, crosses the thin section in one side of the thin section. The pyroxene grains around the vein have altered and are mostly subhedral. In the other parts the pyroxene grains are euhedral

and less altered. Augite and orthopyroxene are the cumulus phases. The diameter of the pyroxene grains varies from 0,5mm to 4,5 mm. The pyroxenes have commonly altered to serpentine minerals. Serpentines occur usually within the cracks of the pyroxene grains and as alteration rims in the edges of the grains. The talc is present in the altered parts as well as a rim on the pyroxene grains. Chlorite is also common in the altered parts.

Intercumulus material consists mainly of opaque minerals. Biotite, titanite and plagioclase are also present as intercumulus phases in smaller amounts. The plagioclase is labradorite in composition.

The ore minerals are mostly within the non-altered part of the thin section forming net textured matrix for the pyroxene grains. The ore minerals constitute 30% of the all minerals. Majority of the ore minerals are pyrrhotite, but bornite, violarite and chalcopyrite and pentlandite are also abundant. Cubanite lamellae's are present in some of the chalcopyrite grains. Ilmenite occur every here and there within the pyrrhotite.

Thin section ID	Rock name	Hole ID/ Depth	Location
OY27045	Websterite	Ylivieska-3/132.3m	Sydänneva

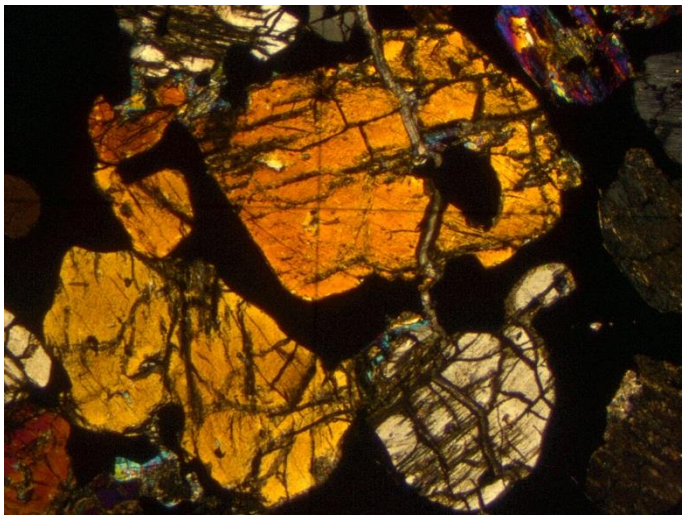

Figure 1: *Talc vein crossing the subhedral pyroxene cumulus grains (1,25x magnification with XPL).*

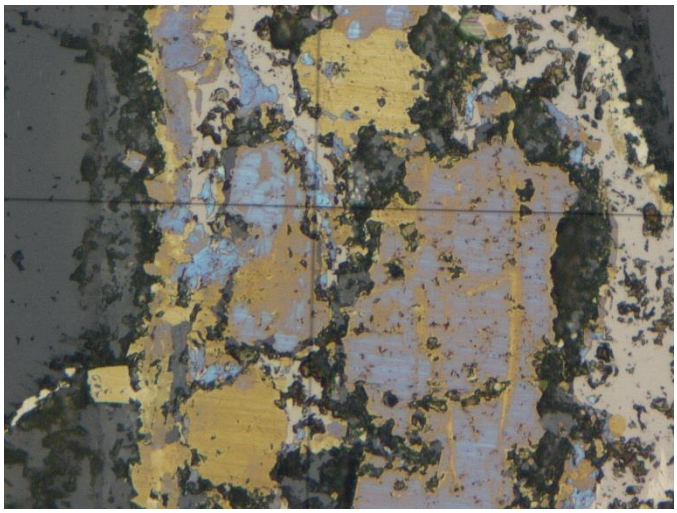

Figure 2: *Replacement of the chalcopyrite by bornite and digenite (x20 magnification with reflected light).*

Main minerals:	orthopyroxene, clinopyroxene
Accessory minerals:	actinolite, talc, hornblende, apatite, biotite
Ore/opaque minerals:	pyrrhotite, chalcopyrite, bornite, digenite, cubanite, pentlandite, magnetite, chromite
Texture:	pyroxene orthocumulate
Mineral alteration:	amphibolization
Rock/hydrothermal alteration:	-
EPMA analyses:	-
Description:	The diameter of subhedral pyroxene cumulus grains varies from 0,5mm to 4mm. Alteration rims on the edges of the grains are very abundant consisting of talc and actinolite. Actinolite occurs in the cracks of the pyroxene grains as well. In

addition to actinolite, the cracks contain locally some hornblende, talc and biotite. Intercumulus phases comprise of biotite, hornblende and ore minerals.

The ore minerals form net-textured matrix for the rock making up to 40% of the all minerals. The main ore minerals are pyrrhotite, chalcopyrite and pentlandite, but also magnetite and chromite appear locally. Chalcopyrite grains may incorporate cubanite lamellaes and they are usually placed in the edges of the pyrrhotite. The replacement of the chalcopyrite by bornite and digenite has taken place in several points. Pentlandite occur as flame-like texture within the pyrrhotite and in the edges of the pyrrhotite.

Thin section ID	Rock name	Hole ID/ Depth	Location
OY27047	Websterite	Ylivieska-4/66,7m	Sydänneva

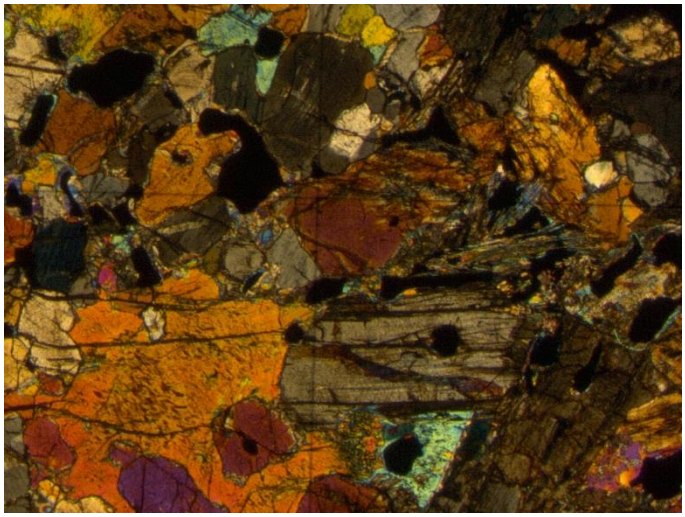

Figure 1: *Alteration of the pyroxenes to secondary amphiboles is common in OY27047. (1,25x magnification with XPL)*

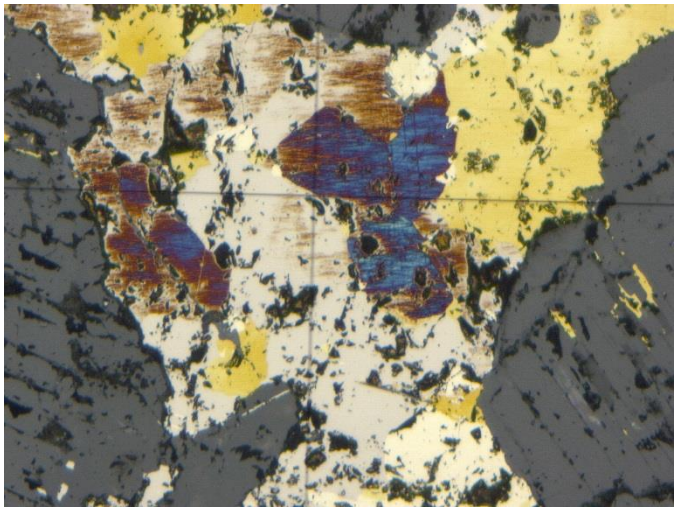

Figure 2: *Bornite, chalcopyrite and pentlandite within the pyrrhotite (20x magnification with reflected light).*

Main minerals:	orthopyroxene, augite
Accessory minerals:	actinolite, talc, hornblende, titanite
Ore/opaque minerals:	pyrrhotite, pentlandite, chalcopyrite, violarite, bornite, digenite, cubanite, chromite, magnetite
Texture:	pyroxene orthocumulate
Mineral alteration:	amphibolization
Rock/hydrothermal alteration:	-
EPMA analyses:	-
Description:	The pyroxene cumulus grains have commonly altered to actinolite. Talc veins intersect the thin section and pyroxene grains in multiple places. Talc also occur as alteration rims on the edges of the pyroxene grains. Titanite is present in small

amounts locally. Intercumulus phases comprise of hornblende, titanite and ore minerals.

The ore minerals constitute 15% of the all minerals forming net-textured matrix. Pyrrhotite, chalcopyrite and pentlandite are most abundant ore minerals. Pentlandite occur as a flame like pattern and as separate grains within the pyrrhotite. The chalcopyrite is often altered to bornite and to digenite. Cubanite lamellaes are present in some of the chalcopyrite grains. Chromite is mostly located in the edges of the chalcopyrite grains.

Thin section ID	Rock name	Hole ID/ Depth	Location
OY27048	Websterite	Ylivieska-4/71,2m	Sydänneva

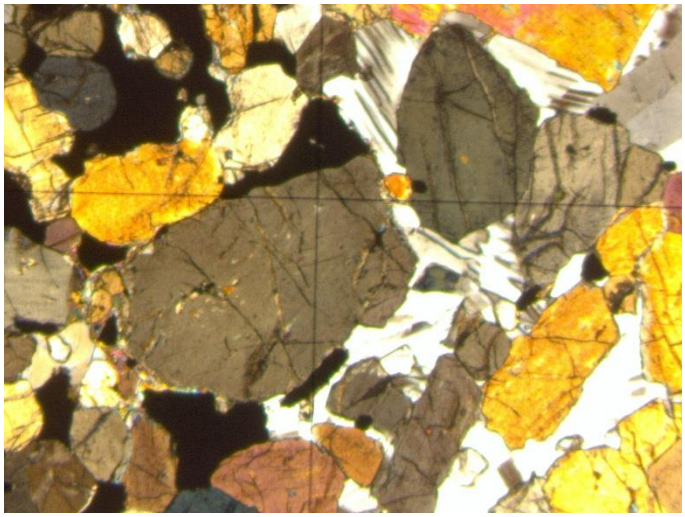

Figure 1: *The pyroxene cumulus grain with plagioclase and ore minerals as intercumulus phases (1,25x magnification with XPL).*

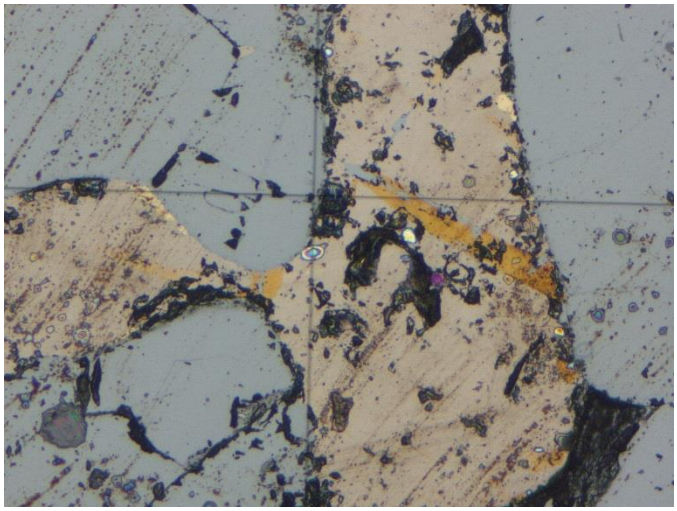

Figure 2: *Bornite, ilmenite and pentlandite within the pyrrhotite (20x magnification with reflected light.*

Main minerals:	orthopyroxene, augite
Accessory minerals:	plagioclase, biotite, titanite, actinolite, hornblende, talc
Ore/opaque minerals:	pyrrhotite, chalcopyrite, pentlandite, bornite, ilmenite, magnetite
Texture:	pyroxene orthocumulate
Mineral alteration:	amphibolization
Rock/hydrothermal alteration:	-
EPMA analyses:	Ten plagioclase grains and pyroxene grains were analyzed.
Description:	The diameter of the subhedral pyroxene cumulus grains varies largely from 8 mm to 0,4 mm. Intercumulus phases comprise of plagioclase, biotite, titanite, hornblende and ore minerals. In the parts where the ore minerals are present in

the interstitials the plagioclase isn't and vice versa. The plagioclase is labradorite in composition.

Alteration of the pyroxenes to secondary amphiboles is present every here and there. Talc occurs as alteration rim on the edges of the pyroxene grains.

The ore minerals occur as disseminated in intercumulus and as blebs at the pyroxene grains constituting 5% of the all minerals. Pyrrhotite, bornite and pentlandite are most abundant. The replacement textures of the chalcopyrite by bornite are present in many parts.

Thin section ID	Rock name	Hole ID/ Depth	Location
OY27049	Websterite	Ylivieska-4/73m	Sydänneva

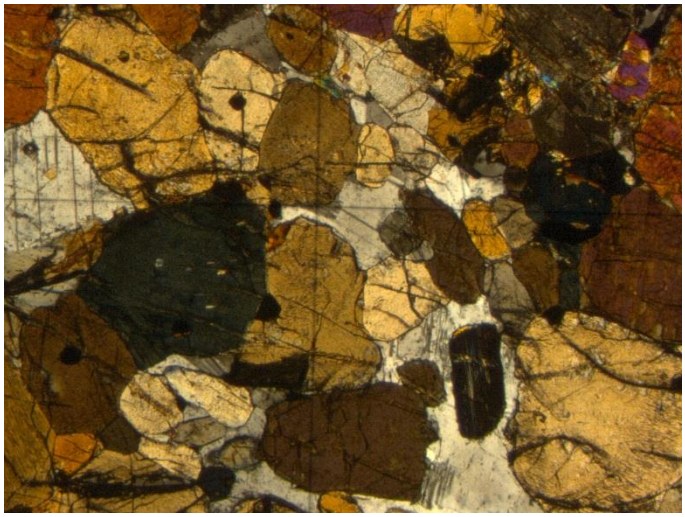

Figure 1: *The plagioclase is the most common mineral in the intercumulus space of the OY27049. (1,25x magnification with XPL)*

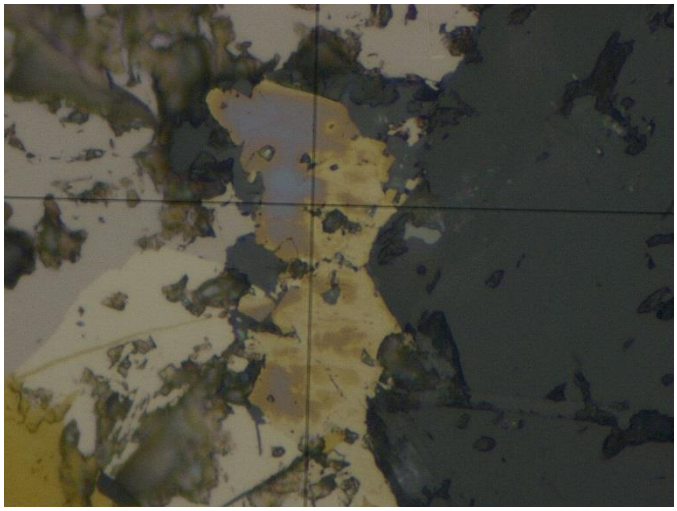

Figure 2: *Pentlandite, chromite and chalcopyrite grains within the pyrrhotite. The chalcopyrite has altered first to bornite and then to digenite. (50x magnification with reflected light)*

Main minerals:	orthopyroxene, augite
Accessory minerals:	plagioclase, hornblende, actinolite, apatite, biotite
Ore/opaque minerals:	pyrrhotite, chalcopyrite, pentlandite, bornite, digenite, ilmenite, chromite, cubanite
Texture:	pyroxene orthocumulate
Mineral alteration:	amphibolization
Rock/hydrothermal alteration:	-
EPMA analyses:	-
Description:	The diameter of the subhedral pyroxene cumulus grains varies from 4,5mm to 0,3mm. The orthopyroxenes are dominant. Pyroxenes have locally altered to actinolite. Intercumulus phases are mostly plagioclase and ore minerals, but also

hornblende and biotite are present in small amounts. Alteration of the pyroxenes to secondary amphiboles takes place locally.

The ore minerals occur as dissemination in the intercumulus space and as blebls at pyroxene grains constituting 2,5% of the all minerals. Pyrrhotite, chalcopyrite and pentlandite are most abundant. The replacement textures of the chalcopyrite by bornite and digenite are present in some parts. There are also cubanite lamellaes in some of the chalcopyrite grains.

Thin section ID	Rock name	Hole ID/ Depth	Location
OY27030	Websterite	Ylivieska-12/50,5m	Sydänneva

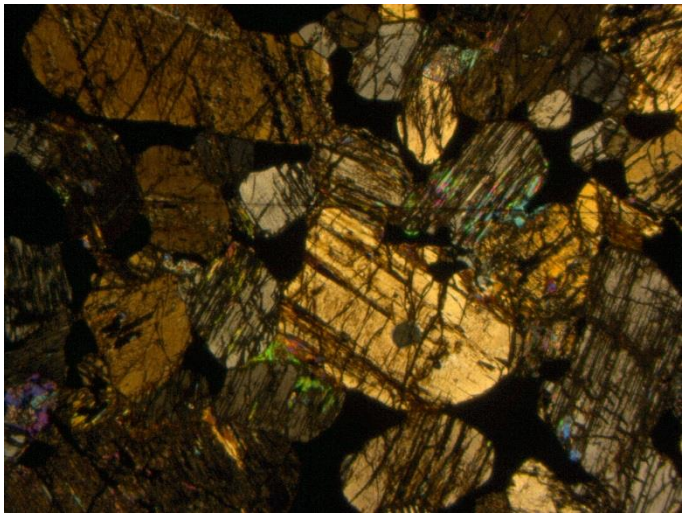

Figure 1: *The alteration of pyroxenes into secondary amphiboles is common in OY27030. (1,25x magnification with XPL)*

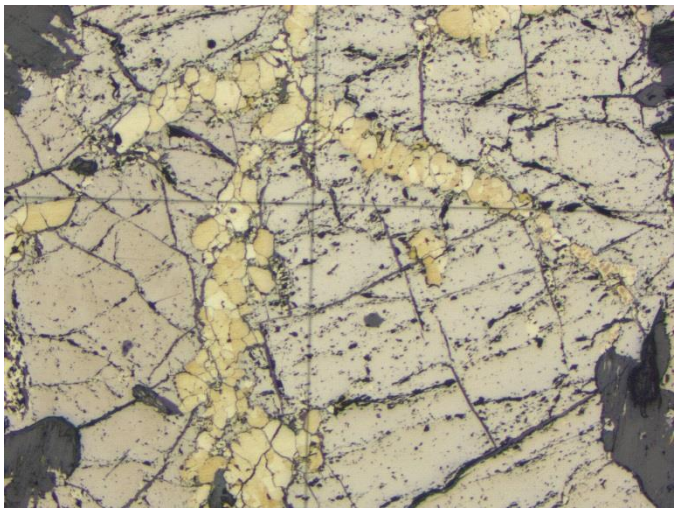

Figure 2: *Chalcopyrite and pentlandite are present as granular veinlets within the pyrrhotite. (1,25x magnification with reflected light)*

Main minerals:	orthopyroxene, augite
Accessory minerals:	actinolite, hornblende, talc, chlorite
Ore/opaque minerals:	pyrrhotite, pentlandite, bornite, ilmenite, chromite, magnetite, cubanite
Texture:	pyroxene orthocumulate
Mineral alteration:	uralitization
Rock/hydrothermal alteration:	-
EPMA analyses:	-
Description:	The pyroxene cumulus grains are subhedral and their diameter varies from 0,4mm to 4mm. The orthopyroxenes are dominant. The alteration of pyroxenes to secondary amphiboles is common. Actinolite is the most abundant alteration product occurring in the intercumulus or as a

alteration rim on the edges of the pyroxene grains. Hornblende occurs in small amounts as an intercumulus phase. Talc occurs as veins crossing the thin section and as rims on the edges of the pyroxene grains. The chlorite is present in some of the altered parts.

The ore minerals form net-textured matrix, constituting 38% of the all minerals. Pyrrhotite, pentlandite and chalcopyrite are the main ore minerals, but also ilmenite and chromite appear locally. The chalcopyrite and pentlandite occur as granular veinlets and as separate patches within the pyrrhotite. In some parts the pentlandite is present as exsolution lamellaes and flames within the pyrrhotite. Alteration of chalcopyrite to bornite and digenite takes place locally. Some chalcopyrite grains contain cubanite lamellaes.

Thin section ID	Rock name	Hole ID/ Depth	Location
OY27035	Websterite	Ylivieska-19/29,5m	Sydänneva

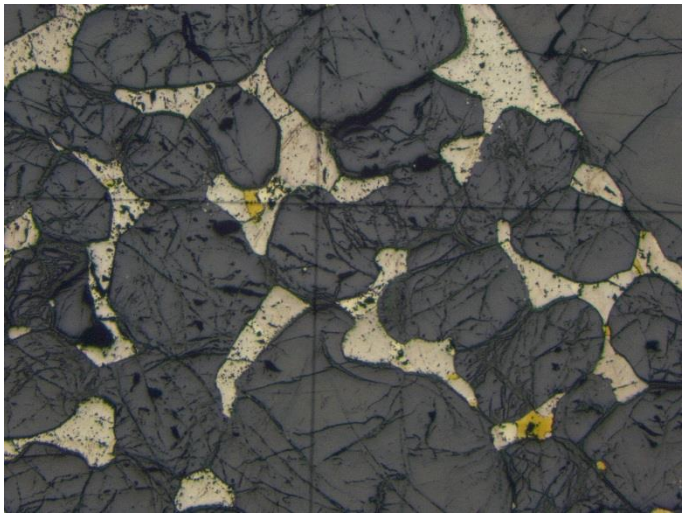

Figure 1: *The ore minerals form net-textured matrix for pyroxene cumulus grains in various parts of the OY27035. (1,25x magnification with reflected light).*

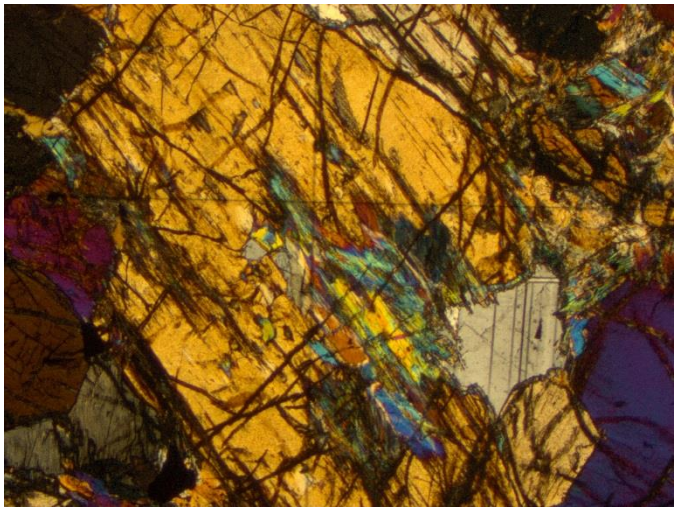

Figure 2: *Actinolite and calcite replacing orthopyroxene. (1,25x magnification with XPL).*

Main minerals:	orthopyroxene, augite
Accessory minerals:	calcite, hornblende, actinolite, tremolite, chlorite, talc, phlogopite, titanite, serpentine
Ore/opaque minerals:	pyrrhotite, pentlandite, chalcopyrite, bornite, digenite, chromite
Texture:	pyroxene orthocumulate
Mineral alteration:	amphibolization, uralitization
Rock/hydrothermal alteration:	-
EPMA analyses:	-
Description:	The pyroxenes are mainly orthopyroxenes, but also augites occur locally. The pyroxene grains are present as subhedral cumuus grains. The diameter of pyroxene grains varies from 0,4mm to 9mm. Intercumulus phases comprise of hornbende, phlogopite, titanite and ore minerals.

Replacement of pyroxenes by actinolite, tremolite and calcite takes occasionally place. Talc and chlorite are present in small amounts in the altered parts. Narrow titanite and serpentine veins crosses thin section in the part where the ore minerals are abundant in the intercumulus space.

The ore minerals occur as a net-textured matrix and as blebs at pyroxene grains. They make up to 18% of the all minerals. Pyrrhotite, pentlandite and chalcopyrite are most abundant ore minerals. Pentlandite occur as granular veinlets as well as exsolution lamellaes within the pyrrhotite. The chalcopyrite occur as separate grains in the edges of the pyrrhotite grains. Replacement of chalcopyrite by bornite and digenite has taken place in small amounts.

Thin section ID	Rock name	Hole ID/ Depth	Location
OY27040	Gabbro	Ylivieska-3/117,2m	Sydänneva

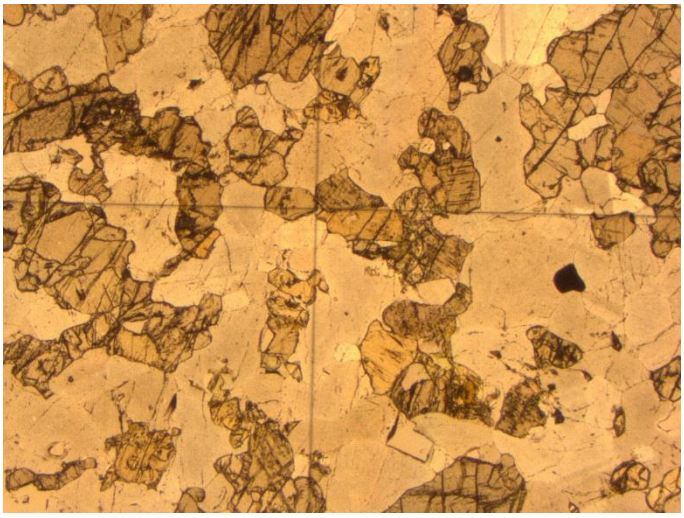

Figure 1: *Plagioclase-pyroxene adcumulate. (1,25x magnification with PPL)*

Figure 2: *Hornblende as a rim around pyroxene grain. (5x magnification with PPL)*

Main minerals:	plagioclase, augite, orthopyroxene
Accessory minerals:	hornblende, apatite, biotite, chlorite
Ore/opaque minerals:	pyrrhotite, pentlandite, chalcopyrite, bornite, magnetite, chromite
Texture:	plagioclase-pyroxene adcumulate
Mineral alteration:	amphibolization
Rock/hydrothermal alteration:	-
EPMA analyses:	Eight plagioclase and ten pyroxene grains were analysed.
Description:	The grain size of minerals varies from fine-to medium grained. The diameter of cumulus plagioclase fluctuates from 0,2mm to 2mm whereas the diameter of pyroxene cumulus grains ranges from 0,15mm to 2,6mm. The

plagioclases are bytownite in composition. Majority of pyroxenes are clinopyroxenes, even though orthopyroxenes are present in small amounts. Intercumulus phases comprise of biotite and hornblende.

The ore minerals occur as blebs at the pyroxene grains and as dissemination in the intercumulus space. They make up to 1.5% of the all minerals. Pyrrhotite, pentlandite, bornite and chalcopyrite are most abundant ore minerals. Chalcopyrite is often replaced by bornite.

Thin section ID	Rock name	Hole ID/ Depth	Location
OY27043	Gabbro	Ylivieska-3/131m	Sydänneva

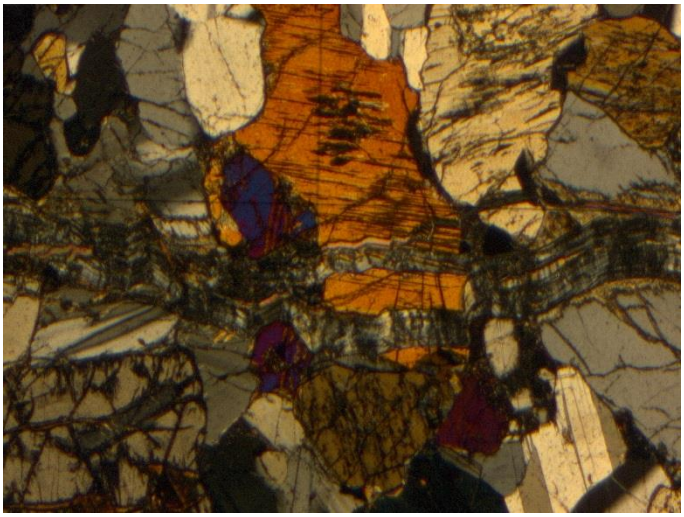

Figure 1: *Serpentine vein crossing the thin section OY27043. (2,25x magnification with XPL)*

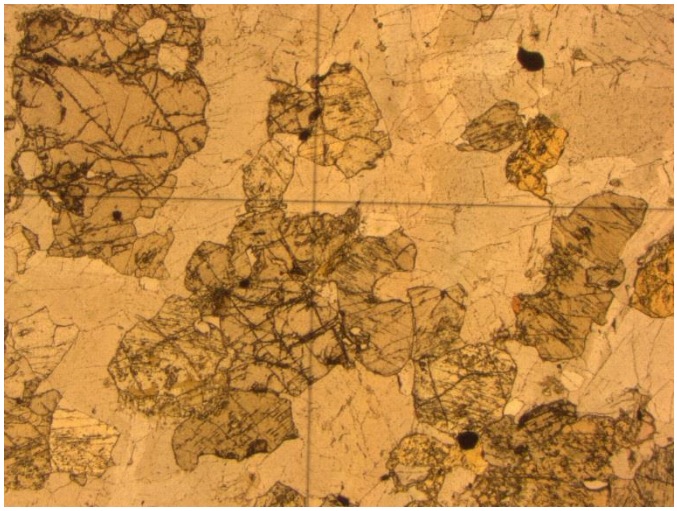

Figure 2: *The grain size of pyroxene and plagioclase cumulus grains varies from fine to medium grained. (1.25x magnification with PPL)*

Main minerals:	plagioclase, augite
Accessory minerals:	hornblende, serpentine, biotite, chlorite, talc, titanite
Ore/opaque minerals:	pyrrhotite, chalcopyrite, cubanite, pentlandite, ilmenite, bornite, digenite
Texture:	plagioclase-pyroxene adcumulate
Mineral alteration:	amphibolization, serpentinization
Rock/hydrothermal alteration:	-
EPMA analyses:	-
Description:	Rock is mostly composed of cumulus plagioclase and pyroxene. The pyroxenes are all augite and their diameter varies from 0,25mm to 2,4mm. Pyroxene are present locally as poikilitic crystals enclosing plagioclase grains. The diameter of the

subhedral plagioclase grains fluctuates from 0,25mm to 2,6mm.

Intercumulus consist of biotite, hornblende, titanite and opaque minerals. Augites are frequently partially replaced by serpentine. A group of serpentine veins crosses the thin section from the middle. The veins also contain minor amounts of talc.

The ore minerals occur as dissemination in intercumulus space as well as blebs at pyroxene grains. They make up to 2.5% of the all minerals. Pyrrhotite, chalcopyrite and pentlandite are most abundant ore minerals. Replacement of chalcopyrite by bornite and digenite takes place in small amounts.

Thin section ID	Rock name	Hole ID/ Depth	Location
OY27028	Gabbro	Ylivieska-12/37,1m	Sydänneva

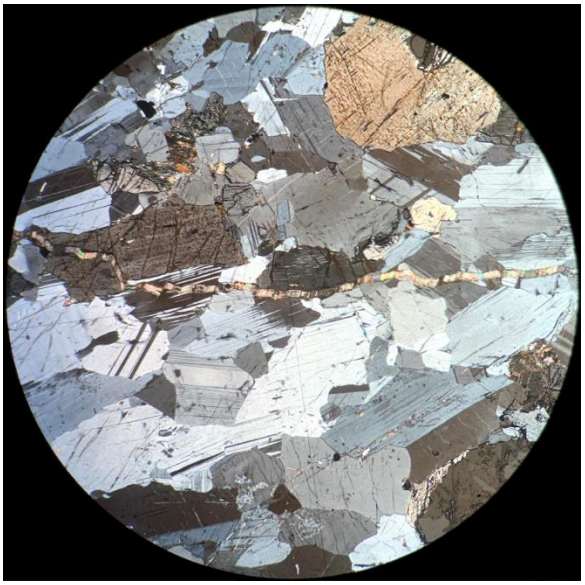

Figure 1: *Talc vein crossing plagioclase-pyroxene adcumulate (4x magnification with XPL).*

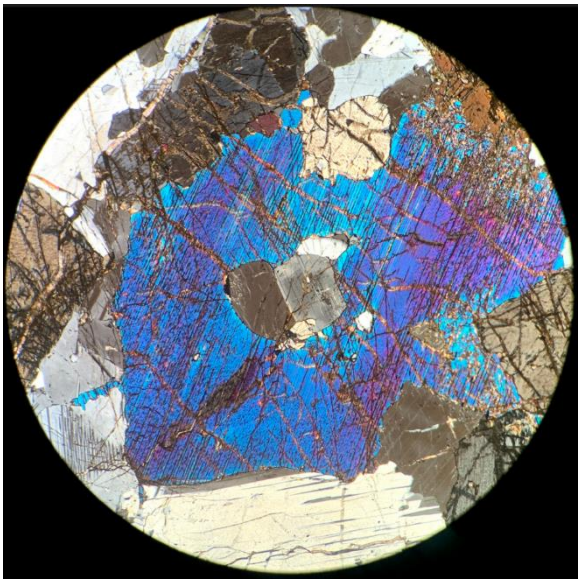

Figure 2: *Poikilitic clinopyroxene crystal enclosing plagioclase grains (4x magnification with XPL).*

Main minerals:	plagioclase, augite
Accessory minerals:	serpentine, hornblende, chlorite, talc, actinolite-tremolite
Ore/opaque minerals:	magnetite, chromite, pyrrhotite, chalcopyrite, pentlandite
Texture:	plagioclase-pyroxene adcumulate
Mineral alteration:	serpentinization, amphibolization
Rock/hydrothermal alteration:	-
EPMA analyses:	-
Description:	The grain size of cumulus plagioclase and cumulus pyroxene varies greatly from fine-to medium grained being mostly

medium grained. The diameter of pyroxene grains ranges from 0,3mm to 7mm and the diameter of plagioclase grains fluctuates from 0,2mm to 4,3mm. Plagioclase grains are partially or completely enclosed by poikilitic pyroxene crystals every here and there. Hornblende is present in small amounts as intercumulus phase.

The replacement of pyroxenes by serpentine minerals and secondary amphiboles have taken place in some parts. Talc and serpentine veins crosses the thin section in several areas.

The ore minerals occur as irregular dissemination constituting 1% of the all minerals. Magnetite, pyrrhotite, chalcopyrite and pentlandite are the most common opaque minerals.

Thin section ID	Rock name	Hole ID/ Depth	Location
OY27046	Gabbronorite	Ylivieska-3/137,5m	Sydänneva

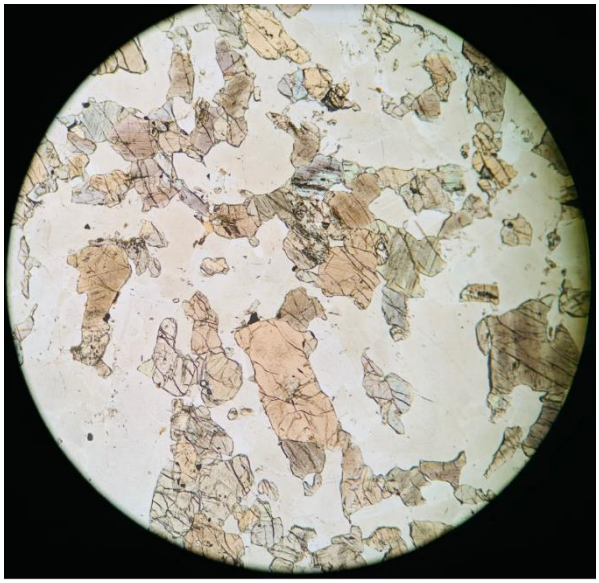

Figure 1: *Plagioclase-pyroxene adcumulate (4x magnification with PPL).*

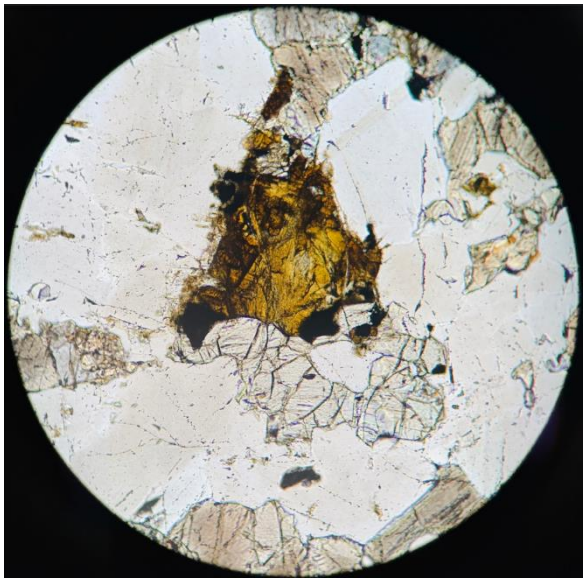

Figure 2: *Pyroxene grain that is replaced by serpentine (4x magnification with PPL).*

Main minerals:	orthopyroxene, augite, plagioclase
Accessory minerals:	serpentine, hornblende, titanite, biotite, apatite, talc
Ore/opaque minerals:	pyrrhotite, pentlandite, chalcopyrite, magnetite, ilmenite, bornite, digenite, chromite
Texture:	plagioclase-pyroxene adcumulate
Mineral alteration:	serpentinization
Rock/hydrothermal alteration:	-
EPMA analyses:	-

Description:

The grain size of the plagioclase and pyroxene cumulus grains varies from fine-to medium grained fluctuating from 0,1mm to 3mm. Pyroxene grains have been locally replaced by serpentine minerals. Intercumulus phases consist of hornblende, titanite and biotite. Minor amount of talc is present in association with serpentine.

Majority of the ore minerals occur as irregular dissemination in the intercumulus space though some are present as blebs on the pyroxene grains. The ore minerals make up to 3% of the all minerals. Pyrrhotite, pentlandite, chalcopyrite and magnetite are the most abundant opaque minerals. There are ilmenite lamellaes in some of the magnetite grains. Alteration of chalcopyrite to bornite and digenite has locally taken place.

Thin section ID	Rock name	Hole ID/ Depth	Location
OY27029	Gabbronorite	Ylivieska-12/41,1m	Sydänneva

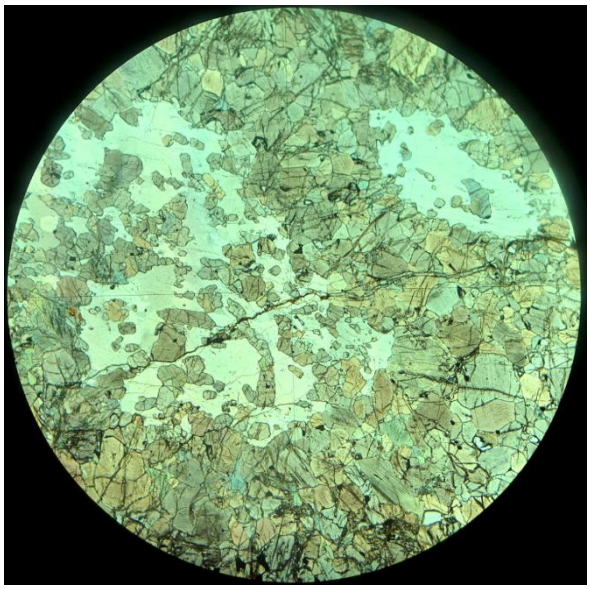

Figure 1: *Pyroxenite-plagioclase adcumulate (2,5x magnification with PPL).*

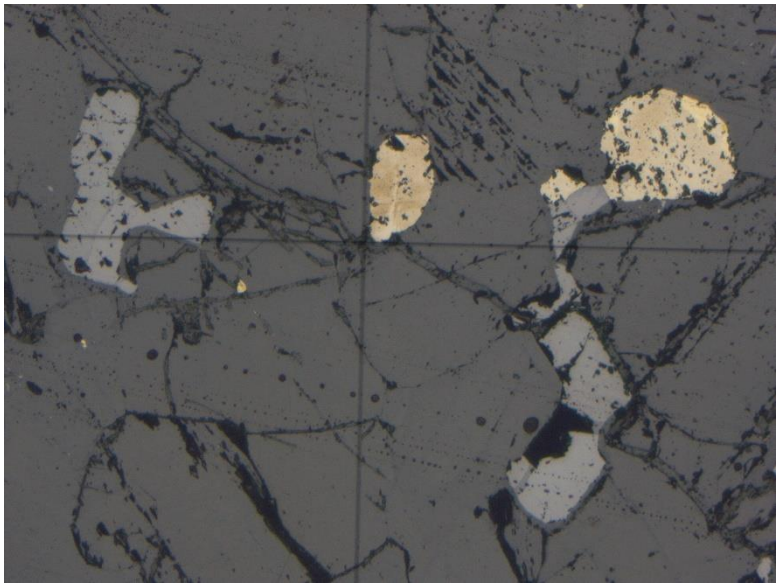

Figure 2: *Magnetite, ilmenite, pyrrhotite, bornite and chalcopyrite in the interstitial of subhedral pyroxene cumulus grains (10x magnification with reflective light).*

Main minerals:	augite, orthopyroxene, plagioclase
Accessory minerals:	actinolite, hornblende, titanite
Ore/opaque minerals:	pyrrhotite, magnetite, chalcopyrite, pentlandite, bornite, ilmenite, digenite
Texture:	pyroxenite-plagioclase adcumulate
Mineral alteration:	amphibolization
Rock/hydrothermal alteration:	-

EPMA analyses:	-
Description:	The diameter of the subhedral pyroxene cumulus grains varies from 0,2mm to 2,3mm. Cumulus plagioclase constitute 25% of the all minerals. The diameter of the subhedral plagioclase grains ranges from 0,2mm to 3,5mm. Titanite, hornblende and ore minerals are present as intercumulus phases. Narrow titanite vein crosses the thin section from the middle. Small-scale alteration of pyroxenes to secondary amphiboles takes place occasionally. The ore minerals occur mostly as blebs at pyroxene grains. In pyroxene rich parts the ore minerals are present in the intercumulus space. Opaques make up to 5% of the all minerals. Magnetite, pyrrhotite and chalcopyrite are the most abundant. Pentlandite is present as exsolution lamellaes in pyrrhotite. Replacement of

	chalcopyrite by bornite and digenite takes place locally.

Thin section ID	Rock name	Hole ID/ Depth	Location
OY27031	Gabbronorite	Ylivieska-12/53,5m	Sydänneva

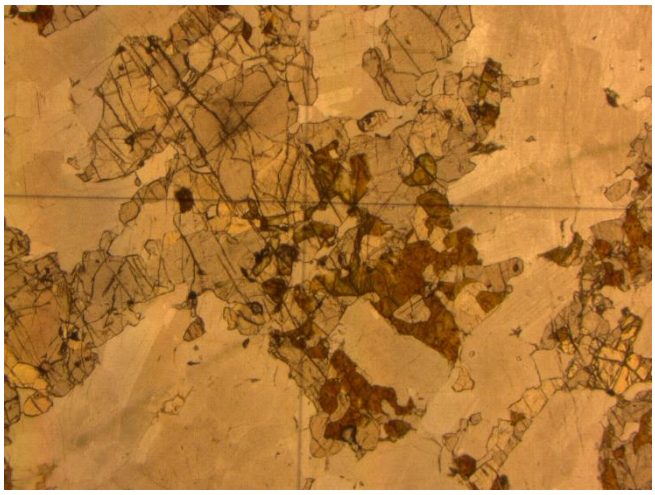

Figure 1: *Serpentine minerals partially replacing pyroxene grains in thin section OY27031 (1,5x magnification with PPL).*

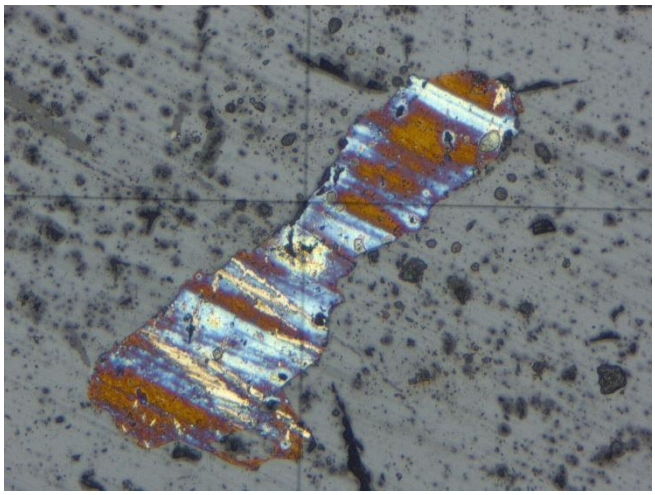

Figure 2: *Bornite and digenite replacing chalcopyrite grain (10x magnification with reflective light).*

Main minerals:	plagioclase, augite, orthopyroxene
Accessory minerals:	serpentine, phlogopite, titanite, chlorite, talc, actinolite
Ore/opaque minerals:	pentlandite, bornite, chromite, magnetite, ilmenite, digenite, pyrrhotite, chalcopyrite
Texture:	plagioclase-pyroxene mesocumulate

Mineral alteration:	serpentinization
Rock/hydrothermal alteration:	-
EPMA analyses:	Seven Plagioclase and six Pyroxene grains were analyzed.
Description:	Rock is mostly composed of cumulus plagioclase and cumulus pyroxenes. The diameter of subhedral pyroxene grains varies from 0,1mm to 7mm. Majority of them are medium grained. Pyroxenes are frequently replaced by serpentine minerals. Small-scale replacement of pyroxenes by actinolite takes place locally. Some clinopyroxenes form poikilitic crystals enclosing plagioclase grains. Plagioclases are present as subhedral grains. Their diameter ranges from 0,15mm to 3,5mm. Intercumulus phases comprise phlogopite, titanite and opaque minerals. Talc, chlorite and micas are mostly located in the altered parts. The ore minerals occur as irregular dissemination making up to 2% of the all minerals. Magnetite, chromite, pyrrhotite

	and bornite are the most abundant ore minerals. Almost all chalcopyrite grains have been replaced by bornite and digenite.

Thin section ID	Rock name	Hole ID/ Depth	Location
OY27033	Olivinegabbronorite	Ylivieska-19/115,8m	Sydänneva

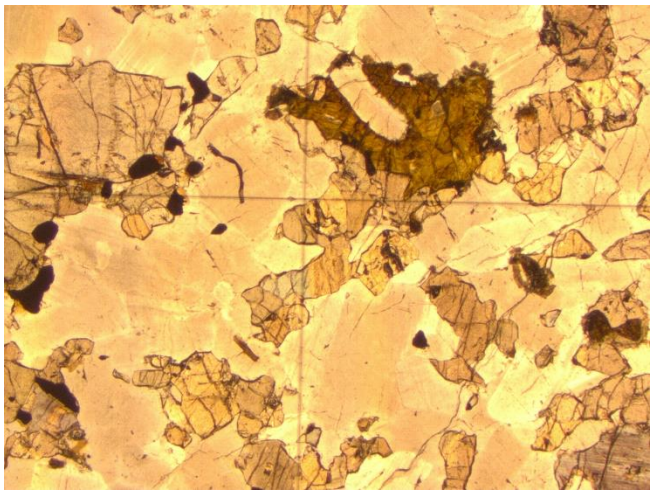

Figure 1: *Plagioclase-pyroxene adcumulate. Pyroxene grain in the middle is partially replaced by serpentine (1,5x magnification with PPL).*

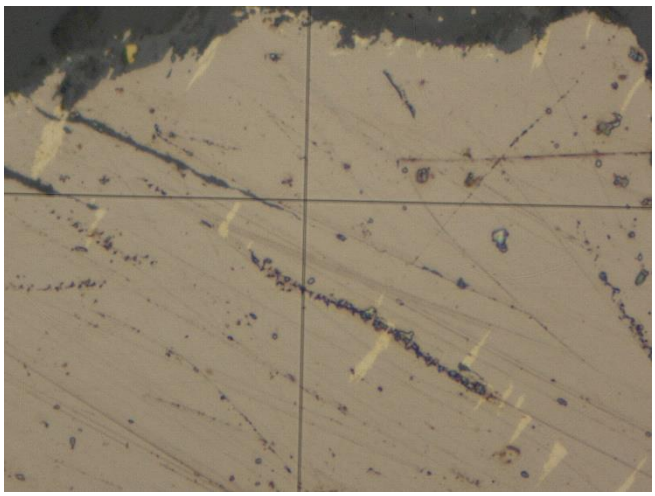

Figure 2: *Exsolution lamellas and flames of pentlandite in pyrrhotite (50x magnification with reflected light).*

Main minerals:	orthopyroxene, augite, plagioclase
Accessory minerals:	olivine, serpentine, hornblende, biotite
Ore/opaque minerals:	pyrrhotite, pentlandite, chalcopyrite, magnetite
Texture:	plagioclase-pyroxene adcumulate with accessory olivine
Mineral alteration:	serpentinization, amphibolization
Rock/hydrothermal alteration:	-
EPMA analyses:	-
Description:	Rock is mostly composed of cumulus plagioclase and cumulus pyroxenes. The grain size of the

subhedral pyroxene grains varies from 0,15mm to 4mm. The diameter of subhedral plagioclase grains varies from 0,1mm to 3mm. Roundish cumulus olivine grains exist in small amounts in one edge of the thin section. The grains are highly serpentinized.

Serpentine minerals partially replace pyroxene grains locally. Intercumulus phases comprise of hornblende, biotite and ore minerals. The ore minerals make up to 6% of the all minerals and occur mostly as irregular dissemination on the cracks and edges of the pyroxene grains. Pentlandite is mostly present as exsolution lamellaes and flames within the pyrrhotite. Chalcopyrite is typically located on the edges of the pyrrhotite grains.

Thin section ID	Rock name	Hole ID/ Depth	Location
OY27027	Olivinegabbronorite	Ylivieska-12/23m	Sydänneva

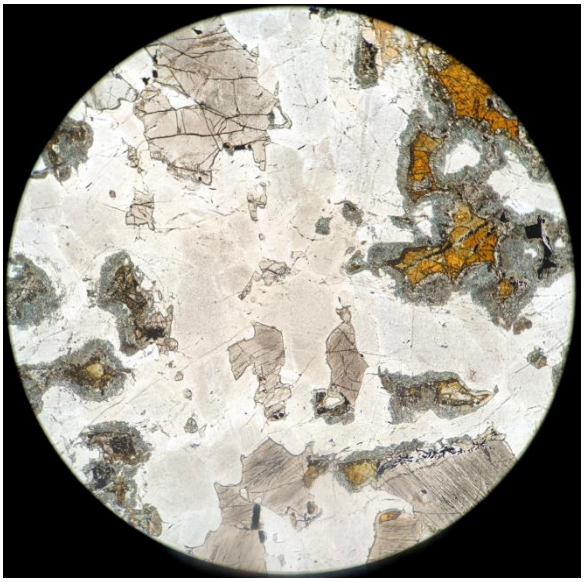

Figure 1: *Roundish cumulus olivine with subhedral plagioclase and pyroxene cumulus grains (4x magnification with PPL).*

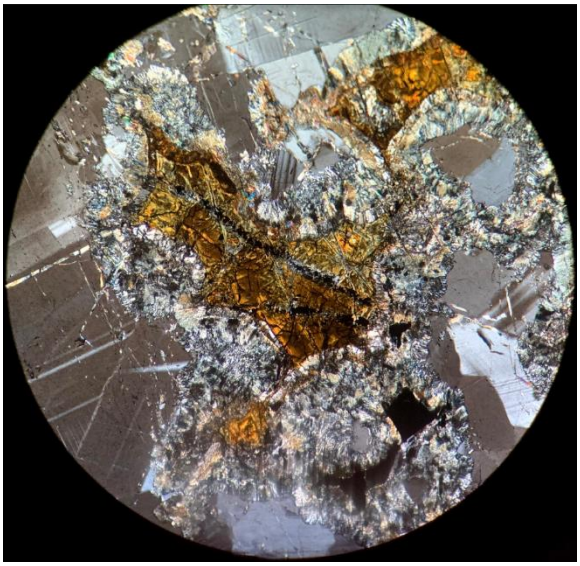

Figure 2: *Completely serpentinized olivine crystal (10x magnification with XPL).*

Main minerals:	plagioclase, orthopyroxene, augite, olivine
Accessory minerals:	serpentine, uralite, hornblende, chlorite, phlogopite
Ore/opaque minerals:	magnetite, ilmenite, pentlandite, chromite, chalcopyrite, pyrrhotite, bornite, digenite
Texture:	plagioclase-pyroxene-olivine orthocumulate
Mineral alteration:	serpentinization, uralitization
Rock/hydrothermal alteration:	-
EPMA analyses:	-

Description:

Rock is mostly composed of cumulus plagioclase, pyroxenes and olivine. The plagioclases occur as subhedral grains and their diameter varies from 0,2mm to 2mm. The pyroxene grains are mostly clinopyroxenes and their diameter ranges from 0,4mm to 4mm. The augites form locally poikilitic crystals enclosing plagioclase crystals in. Almost all olivine grains are roundish and are mostly replaced by serpentine minerals.

Intercumulus phases comprise phlogopite, hornblende and ore minerals. The alteration of pyroxenes by secondary amphiboles and serpentine minerals has taken place in several areas, especially near the serpentine veins.

4mm thick Serpentine and Uralite vein intersects the thin section from the middle. In addition multiple narrow serpentine veins cross the thin section from several directions.

	The ore minerals are disseminated and majority of them are in the serpentinized areas. They make up to 5% of the all minerals. Magnetite and is locally replacing the olivine grains and occasionally replaces the grain completely. Opaque minerals are also present in the cracks and edges of pyroxene grains as well as in the intercumulus space. Magnetite, ilmenite, pentlandite, pyrrhotite and chalcopyrite are the most abundant ore minerals. Alteration of chalcopyrite to bornite and digenite takes place locally.

Thin section ID	Rock name	Hole ID/ Depth	Location
OY27037	Olivinegabbronorite	Ylivieska-19/47,7m	Sydänneva

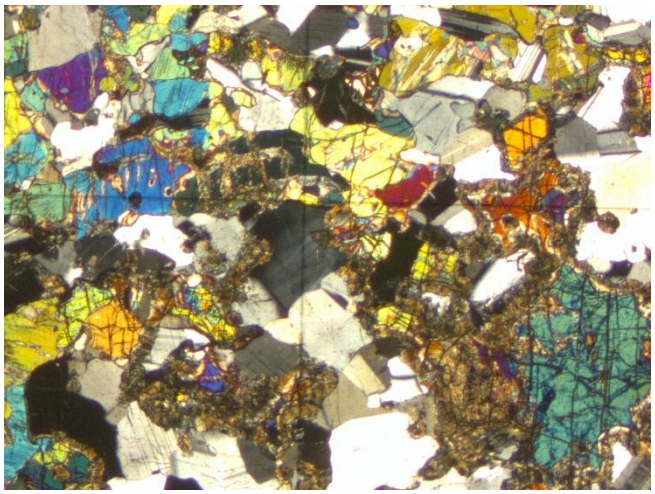

Figure 1: *The roundish olivine grains in the olivine gabbronorite are all partly replaced by serpentine minerals (1,5x magnification with XPL).*

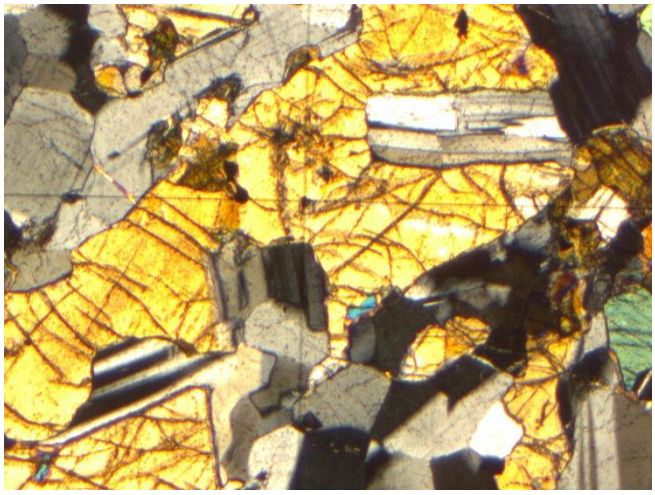

Figure 2: *Subpoikilitic pyroxene grain enclosing several plagioclase grains in (2,5x magnification with XPL).*

Main minerals:	olivine, augite, orthopyroxene
Accessory minerals:	serpentine, chlorite, phlogopite, hornblende, uralite
Ore/opaque minerals:	pyrrhotite, chalcopyrite, magnetite, pentlandite
Texture:	plagioclase-pyroxene-olivine mesocumulate
Mineral alteration:	serpentinization, uralitization
Rock/hydrothermal alteration:	-
EPMA analyses:	-
Description:	Rock is mostly composed of cumulus plagioclase, pyroxenes and olivine. The grain size of the subhedral pyroxene and plagioclase crystals varies from

fine- to medium grained. Roundish olivine grains are mostly medium grained, and they contain thick alteration rims composed of serpentine minerals. Pyroxene grains have altered locally to secondary amphiboles and serpentine minerals. Some clinopyroxenes form poikilitic crystals enclosing in plagioclase grains. Intercumulus phases comprise hornblende and phlogopite.

The ore minerals occur as irregular dissemination in the cracks of pyroxene grains and in the intercumulus space. Ore minerals, especially magnetite, also replace olivine grains. Pyrrhotite, magnetite and chalcopyrite are the most abundant ore minerals.

Thin section ID	Rock name	Hole ID/ Depth	Location
OYXXXX1	Olivine gabbronorite	Ylivieska-19/100,9m	Sydänneva

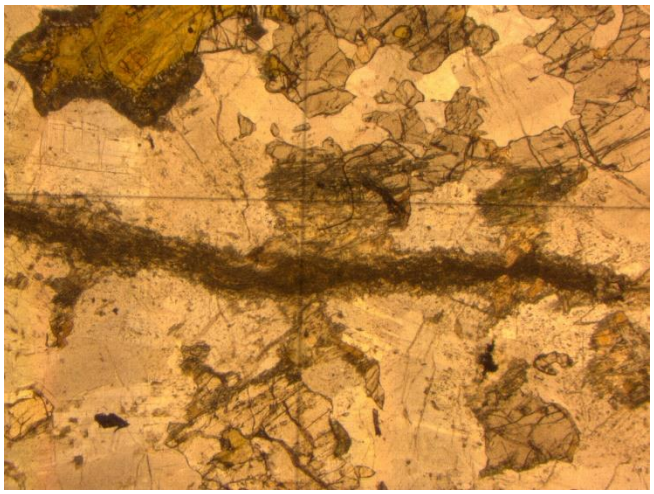

Figure 1: *Thick serpentine-actinolite vein crosses the OYXXXX1 from the middle (1,5x magnification with PPL).*

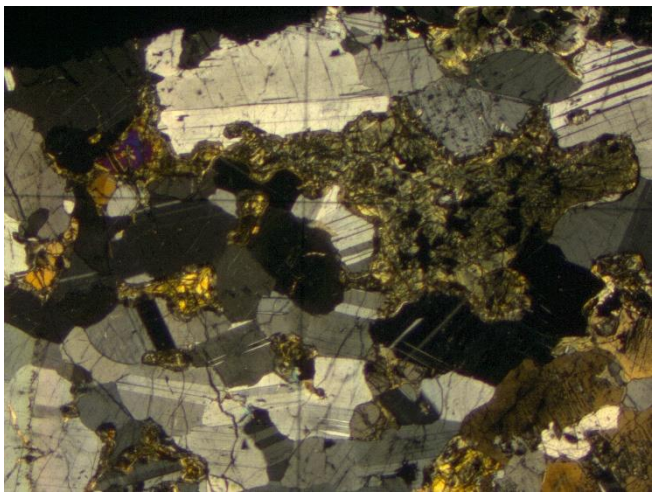

Figure 2: *Roundish olivine pseudomorphs (2,5x magnification with XPL).*

Main minerals:	orthopyroxene, olivine, augite
Accessory minerals:	serpentine, actinolite, talc, hornblende, chlorite
Ore/opaque minerals:	pyrrhotite, chalcopyrite, pentlandite, bornite, magnetite
Texture:	plagioclase-pyroxene-olivine orthocumulate
Mineral alteration:	serpentinisation, uralitization
Rock/hydrothermal alteration:	-
EPMA analyses:	Seven plagioclase, six pyroxene and six olivine grains were analysed.
Description:	Rock is mostly composed of cumulus plagioclase, cumulus pyroxenes and cumulus olivine.

The grain size of the subhedral pyroxene varies from 0,3mm to 3,5mm. The olivines occur as roundish grains and are highly serpentinized. Some grains have been totally replaced by serpentine. Plagioclase occurs as subhedral crystals and is locally enclosed by subpoikilitic to poikilitic pyroxene grains. Hornblende is present as intercumulus phase.

Alteration of pyroxenes to secondary amphibole and serpentine minerals is present locally. Thick serpentine-actinolite-tremolite crosses the thin section from the middle and altering the minerals around it. Smaller serpentine veins cross the thin section from various locations. Chlorite is present in the altered areas.

Ore minerals make up to 0.5% of the all minerals and they mainly occur as irregular dissemination in the cracks of the olivine and pyroxene grains.

Thin section ID	Rock name	Hole ID/ Depth	Location
OY27039	Olivine norite	Ylivieska-19/75m	Sydänneva

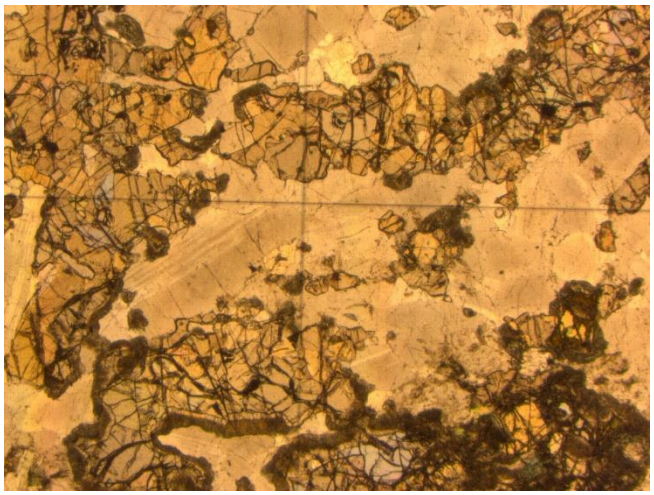

Figure 1: *Plagioclase-pyroxene-olivine mesocumulate. The olivine grains are encircled by thick serpentine rims (1,5x magnification with PPL).*

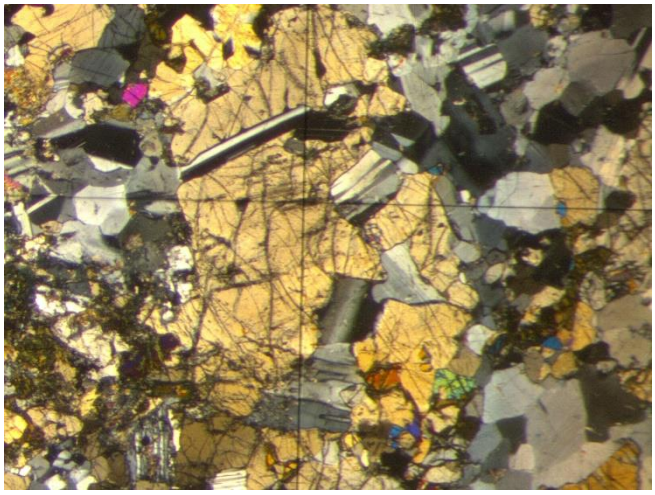

Figure 2: *Subpoikilitic pyroxene crystal enclosing plagioclase grains (1,5x magnification with XPL).*

Main minerals:	orthopyroxene, olivine, plagioclase
Accessory minerals:	clinopyroxene, serpentine, chlorite, apatite, hornblende, talc
Ore/opaque minerals:	pyrrhotite, pentlandite, chalcopyrite, bornite, digenite, magnetite, chromite
Texture:	Plagioclase-pyroxene-olivine mesocumulate
Mineral alteration:	serpentinization
Rock/hydrothermal alteration:	-
EPMA analyses:	-

Description:

Rock is mostly composed of cumulus plagioclase, orthopyroxene and olivine. The grain size of the subhedral pyroxene varies from 0,3mm to 3mm. The pyroxenes are mostly orthopyroxene. Clinopyroxenes occur in small amounts. Small scale replacement of the pyroxenes by serpentine and chlorite takes place in most of the grains.

The diameter of subhedral plagioclase grains ranges from 0,3mm to 6mm. Plagioclase are enclosed by subpoikilitic and poikilitic pyroxene grains locally. Roundish olivine grains constitute 15% of the all minerals. They are all highly serpentinized and encircled by serpentine rims. Hornblende is present as intercumulus phase.

Thick serpentine-chlorite rich vein constitutes one corner of the thin section altering all minerals around it. Chlorite is also present in the serpentinized areas. Talc

occurs as a narrow vein in one edge of the thin section.

The ore minerals make up to 2.5% of the all minerals and are mostly located as blebs at olivine and pyroxene grains. Magnetite is the most abundant and it frequently replaces olivine and pyroxene grains. Replacement of the chalcopyrite by bornite and digenite occurs in small amounts.

APPENDIX 2. Olivine electron microprobe results.

	No.	1	2	3	4	5	6	7
		OY27038	OY27038	OY27038	OY27038	OY27038	OYXXXX1	OYXXXX1
SiO2	wt%	38.4	38.3	38.2	38.3	38.4	38.9	39.1
TiO2	wt%	0.01	0.02	0.00	0.01	0.02	0.01	0.02
Al2O3	wt%	0.00	0.02	0.00	0.00	0.00	0.11	0.00
Cr2O3	wt%	0.00	0.00	0.04	0.01	0.02	0.03	0.00
FeO	wt%	25.75	25.62	26.97	26.91	26.28	22.00	22.48
MnO	wt%	0.36	0.34	0.38	0.38	0.37	0.31	0.25
MgO	wt%	37.16	36.98	36.11	36.02	36.17	39.32	39.48
CaO	wt%	0.01	0.00	0.03	0.02	0.01	0.04	0.02
Na2O	wt%	0.00	0.01	0.00	0.00	0.05	0.04	0.04
K2O	wt%	0.00	0.00	0.01	0.03	0.03	0.01	0.00
NiO	wt%	0.10	0.12	0.17	0.11	0.06	0.12	0.12
Total	wt%	101.8	101.5	101.9	101.8	101.4	100.8	101.4
Te	wt%	0.40	0.38	0.42	0.42	0.41	0.34	0.28
Fo	wt%	71.7	71.7	70.2	70.2	70.6	75.8	75.6
Fa	wt%	27.9	27.9	29.4	29.4	28.8	23.8	24.1
Ca-Ol	wt%	0.01	0.00	0.03	0.03	0.01	0.06	0.02

	No.	8	9	10	11	12	13	14
		OYXXXX1	OYXXXX1	OYXXXX1	OYXXXX1	OY27027	OY27027	OY27027
SiO2	wt%	39.1	39.1	40.2	39.1	48.1	46.6	48.1
TiO2	wt%	0.02	0.00	0.00	0.00	0.00	0.00	0.00
Al2O3	wt%	0.00	0.17	0.02	0.00	4.58	4.23	2.86
Cr2O3	wt%	0.00	0.02	0.02	0.00	0.00	0.00	0.00
FeO	wt%	20.00	22.21	21.12	22.46	20.58	21.53	20.39
MnO	wt%	0.27	0.27	0.26	0.31	0.13	0.28	0.18
MgO	wt%	40.22	39.11	37.09	39.51	12.48	9.87	13.32
CaO	wt%	0.00	0.02	0.00	0.00	1.26	1.16	0.86
Na2O	wt%	0.00	0.00	0.00	0.01	0.02	0.04	0.05
K2O	wt%	0.01	0.02	0.01	0.00	0.04	0.03	0.02
NiO	wt%	0.12	0.05	0.03	0.08	0.00	0.00	0.02
Total	wt%	99.8	101.0	98.8	101.4	87.2	83.8	85.8
Te	wt%	0.30	0.30	0.30	0.34	0.29	0.69	0.39
Fo	wt%	78.0	75.6	75.6	75.6	49.9	43.0	52.3
Fa	wt%	21.8	24.8	24.1	24.9	46.2	52.7	44.9
Ca-Ol	wt%	0.00	0.03	0.00	0.00	3.6	3.6	2.4

	No.	15	16	17	18	19	20	21
		OY27037	OY27037	OY27037	OY27037	OY27037	OY27037	OY27037
SiO2	wt%	37.4	37.5	37.5	37.4	37.0	37.3	37.4
TiO2	wt%	0.00	0.04	0.01	0.00	0.03	0.08	0.02
Al2O3	wt%	0.00	0.00	0.00	0.00	0.00	0.00	0.00
Cr2O3	wt%	0.00	0.00	0.00	0.01	0.00	0.00	0.00
FeO	wt%	26.42	26.73	26.41	26.42	25.85	25.35	26.55
MnO	wt%	0.35	0.28	0.39	0.36	0.43	0.32	0.34
MgO	wt%	34.88	34.97	34.81	34.58	35.26	35.07	34.80
CaO	wt%	0.00	0.00	0.00	0.00	0.01	0.01	0.00
Na2O	wt%	0.01	0.03	0.00	0.03	0.00	0.03	0.00
K2O	wt%	0.01	0.00	0.00	0.01	0.01	0.02	0.00
NiO	wt%	0.01	0.07	0.07	0.05	0.03	0.00	0.01
Total	wt%	99.1	99.6	99.2	98.9	98.7	98.2	99.1
Te	wt%	0.40	0.32	0.45	0.41	0.49	0.37	0.38
Fo	wt%	69.9	69.8	69.8	69.7	70.5	70.9	69.8
Fa	wt%	29.9	29.9	29.7	29.9	29.0	28.8	29.9
Ca-Ol	wt%	0.00	0.00	0.00	0.00	0.01	0.01	0.00

	No.	22	23	24	25	26	27	28
		OY27037	OY27037	OY27037	OY27039	OY27039	OY27039	OY27039
SiO2	wt%	37.7	37.8	37.1	37.6	37.5	37.5	37.5
TiO2	wt%	0.00	0.33	0.00	0.00	0.03	0.00	0.00
Al2O3	wt%	0.00	0.00	0.02	0.00	0.00	0.01	0.00
Cr2O3	wt%	0.00	0.01	0.00	0.00	0.03	0.02	0.00
FeO	wt%	26.17	26.43	27.54	26.26	25.76	25.35	26.26
MnO	wt%	0.34	0.26	0.27	0.35	0.31	0.33	0.36
MgO	wt%	35.17	35.00	34.10	35.81	36.04	36.09	35.72
CaO	wt%	0.00	0.00	0.00	0.00	0.00	0.00	0.00
Na2O	wt%	0.01	0.00	0.00	0.02	0.00	0.07	0.00
K2O	wt%	0.00	0.00	0.00	0.00	0.02	0.02	0.00
NiO	wt%	0.02	0.08	0.08	0.05	0.03	0.07	0.00
Total	wt%	99.5	99.9	99.2	100.1	99.7	99.4	99.8
Te	wt%	0.38	0.29	0.30	0.39	0.35	0.37	0.40
Fo	wt%	70.3	70.0	68.6	70.6	71.1	71.5	70.5
Fa	wt%	29.3	29.7	31.1	29.0	28.5	28.2	29.1
Ca-Ol	wt%	0.00	0.00	0.00	0.00	0.00	0.00	0.00

	No.	29	30	31	32	33
		OY27039	OY27039	OY27039	OY27039	OY27039
SiO2	wt%	37.9	37.8	37.9	37.5	37.9
TiO2	wt%	0.00	0.00	0.02	0.01	0.00
Al2O3	wt%	0.00	0.01	0.00	0.03	0.00
Cr2O3	wt%	0.00	0.02	0.01	0.00	0.02
FeO	wt%	26.43	25.67	25.91	26.25	26.02
MnO	wt%	0.31	0.31	0.36	0.33	0.27
MgO	wt%	35.90	36.25	36.23	35.82	36.03
CaO	wt%	0.00	0.00	0.00	0.01	0.00
Na2O	wt%	0.00	0.01	0.00	0.01	0.00
K2O	wt%	0.00	0.00	0.01	0.00	0.01
NiO	wt%	0.00	0.01	0.00	0.06	0.03
Total	wt%	100.6	100.0	100.4	100.0	100.3
Te	wt%	0.34	0.35	0.40	0.37	0.31
Fo	wt%	70.5	71.3	71.1	70.6	71.0
Fa	wt%	29.1	28.3	28.5	29.0	28.8
Ca-Ol	wt%	0.00	0.00	0.00	0.01	0.00

APPENDIX 3. Pyroxene electron microprobe results.

	No.	1	2	3	4	5	6	7
		OY27040	OY27040	OY27040	OY27040	OY27040	OY27040	OY27040
SiO2	wt%	53.6	54.0	54.0	53.0	54.2	53.9	54.0
TiO2	wt%	0.30	0.26	0.30	0.37	0.32	0.33	0.31
Al2O3	wt%	1.66	1.52	1.53	1.67	1.57	1.75	1.68
FeO	wt%	18.09	18.49	18.16	18.17	17.96	18.50	17.98
CaO	wt%	1.34	0.67	0.95	1.18	0.87	1.13	1.11
Na2O	wt%	0.00	0.00	0.00	0.12	0.04	0.12	0.21
K2O	wt%	0.02	0.02	0.01	0.04	0.00	0.00	0.00
MgO	wt%	25.57	25.97	25.38	25.41	25.37	24.92	25.53
MnO	wt%	0.42	0.39	0.48	0.37	0.40	0.34	0.33
Cr2O3	wt%	0.06	0.11	0.12	0.13	0.10	0.160	0.11
BaO	wt%	0.04	0.06	0.01	0.04	0.01	0.00	0.02
NiO	wt%	0.10	0.04	0.04	0.00	0.00	0.06	0.04
Total	wt%	101.20	101.51	100.96	100.49	100.87	101.16	101.37

	No.	8	9	10	11	12	13	14
		OY27040	OY27040	OY27040	OY27041	OY27041	OY27041	OY27041
SiO2	wt%	53.5	53.2	53.8	55.5	55.2	54.6	54.5
TiO2	wt%	0.29	0.31	0.23	0.30	0.20	0.28	0.26
Al2O3	wt%	1.68	1.67	1.60	1.63	1.44	1.70	1.72
FeO	wt%	18.07	18.24	17.01	13.70	13.18	13.40	13.49
CaO	wt%	0.93	1.03	1.24	1.67	1.63	1.62	1.71
Na2O	wt%	0.08	0.01	0.00	0.03	0.04	0.05	0.08
K2O	wt%	0.00	0.00	0.01	0.03	0.04	0.01	0.01
MgO	wt%	25.31	25.19	25.34	27.89	27.99	28.66	28.65
MnO	wt%	0.36	0.34	0.33	0.20	0.25	0.26	0.26
Cr2O3	wt%	0.09	0.11	0.10	0.20	0.21	0.25	0.17
BaO	wt%	0.00	0.00	0.03	0.03	0.00	0.00	0.00
NiO	wt%	0.00	0.00	0.01	0.00	0.04	0.05	0.04
Total	wt%	100.34	100.07	99.73	101.18	100.24	100.84	100.91

	No.	15	16	17	18	19	20	21
		OY27041	OY27041	OY27041	OY27041	OY27042	OY27042	OY27042
SiO2	wt%	55.0	55.4	54.6	55.0	54.3	55.1	55.0
TiO2	wt%	0.39	0.29	0.27	0.48	0.25	0.23	0.21
Al2O3	wt%	1.87	1.74	1.77	1.75	1.91	1.76	1.63
FeO	wt%	14.15	13.06	13.42	13.32	14.55	13.73	14.65
CaO	wt%	1.65	1.53	1.53	1.63	0.94	1.59	1.36
Na2O	wt%	0.06	0.03	0.00	0.05	0.00	0.00	0.20
K2O	wt%	0.00	0.00	0.01	0.03	0.02	0.01	0.06
MgO	wt%	28.15	28.24	27.85	27.88	27.40	28.26	27.49
MnO	wt%	0.27	0.22	0.26	0.24	0.23	0.27	0.27
Cr2O3	wt%	0.22	0.18	0.28	0.21	0.25	0.30	0.26
BaO	wt%	0.00	0.00	0.02	0.02	0.00	0.00	0.00
NiO	wt%	0.00	0.05	0.08	0.01	0.04	0.01	0.06
Total	wt%	101.72	100.75	100.11	100.63	99.90	101.26	101.19

	No.	22	23	24	25	26	27	28
		OY27042	OY27042	OY27044	0Y27044	0Y27044	0Y27044	0Y27044
SiO2	wt%	55.0	55.3	54.1	53.5	53.8	55.2	53.8
TiO2	wt%	0.23	0.27	0.68	0.35	0.41	0.32	0.28
Al2O3	wt%	1.63	1.53	1.80	2.06	1.65	1.70	1.46
FeO	wt%	14.56	14.42	14.91	14.67	15.14	14.68	14.73
CaO	wt%	1.45	1.27	1.10	1.48	0.89	1.28	1.37
Na2O	wt%	0.00	0.01	0.00	0.01	0.00	0.05	0.09
K2O	wt%	0.00	0.00	0.02	0.02	0.00	0.01	0.03
MgO	wt%	27.70	27.56	27.52	27.32	27.82	27.51	28.11
MnO	wt%	0.21	0.33	0.29	0.33	0.36	0.34	0.34
Cr2O3	wt%	0.24	0.23	0.19	0.18	0.19	0.17	0.18
BaO	wt%	0.03	0.02	0.00	0.00	0.03	0.00	0.00
NiO	wt%	0.04	0.01	0.00	0.00	0.04	0.05	0.09
Total	wt%	101.10	100.98	100.56	99.90	100.37	101.34	100.50

	No.	29	30	31	32	33	34	35
		0Y27044	0Y27044	0Y27044	0Y27044	OY27048	OY27048	OY27048
SiO2	wt%	54.6	54.6	54.3	54.3	54.5	53.7	53.5
TiO2	wt%	0.36	0.29	0.38	0.31	0.37	0.42	0.65
Al2O3	wt%	1.99	1.86	1.77	1.91	1.39	1.64	1.54
FeO	wt%	14.53	14.78	15.06	14.70	15.72	15.99	15.42
CaO	wt%	1.87	2.00	1.35	1.32	0.96	1.08	1.09
Na2O	wt%	0.03	0.00	0.08	0.00	0.01	0.02	0.06
K2O	wt%	0.00	0.01	0.01	0.00	0.02	0.01	0.00
MgO	wt%	27.40	27.03	27.51	27.77	27.34	27.08	26.82
MnO	wt%	0.34	0.33	0.36	0.35	0.22	0.35	0.33
Cr2O3	wt%	0.17	0.18	0.16	0.18	0.20	0.24	0.18
BaO	wt%	0.00	0.00	0.00	0.00	0.08	0.06	0.05
NiO	wt%	0.04	0.00	0.00	0.00	0.13	0.04	0.03
Total	wt%	101.34	101.06	100.95	100.80	100.89	100.59	99.73

	No.	36	37	38	39	40	41	42
		OY27048	OY27048	OY27048	OY27048	OY27048	OY27031	OY27031
SiO2	wt%	54.1	54.4	53.9	54.4	54.5	53.4	51.5
TiO2	wt%	0.64	0.29	0.62	0.29	0.36	0.27	1.03
Al2O3	wt%	1.54	1.74	1.71	1.53	1.68	1.83	3.31
FeO	wt%	15.77	15.37	15.88	16.03	16.16	18.00	9.15
CaO	wt%	1.32	1.37	1.40	1.52	0.93	0.64	19.90
Na2O	wt%	0.00	0.00	0.01	0.00	0.00	0.00	0.55
K2O	wt%	0.00	0.00	0.00	0.00	0.00	0.01	0.03
MgO	wt%	26.60	26.48	26.99	26.69	27.07	25.56	14.92
MnO	wt%	0.31	0.24	0.27	0.31	0.31	0.35	0.27
Cr2O3	wt%	0.20	0.23	0.29	0.23	0.22	0.02	0.23
BaO	wt%	0.00	0.01	0.02	0.00	0.00	0.01	0.04
NiO	wt%	0.00	0.01	0.02	0.04	0.07	0.07	0.04
Total	wt%	100.44	100.10	101.13	101.02	101.33	100.12	100.94

	No.	43	44	45	46	47	48	49
		OY27031	OY27031	OY27031	OY27031	OY27038	OY27038	OY27038
SiO2	wt%	53.2	52.5	53.7	53.0	51.4	54.9	55.1
TiO2	wt%	0.47	0.57	0.39	0.34	0.94	0.14	0.18
Al2O3	wt%	1.81	1.75	1.86	1.85	3.69	1.62	1.35
FeO	wt%	18.03	18.49	17.65	17.94	7.07	15.68	16.47
CaO	wt%	1.57	1.48	1.31	0.92	20.67	1.21	0.56
Na2O	wt%	0.00	0.07	0.00	0.00	0.25	0.00	0.07
K2O	wt%	0.00	0.00	0.00	0.01	0.00	0.01	0.02
MgO	wt%	25.04	25.03	25.05	25.44	15.79	27.16	27.16
MnO	wt%	0.39	0.37	0.35	0.43	0.14	0.32	0.30
Cr2O3	wt%	0.07	0.10	0.07	0.06	0.51	0.07	0.04
SrO	wt%	0.00	0.00	0.00	0.00	0.00	0.00	0.00
BaO	wt%	0.04	0.04	0.00	0.00	0.02	0.00	0.00
NiO	wt%	0.03	0.02	0.05	0.11	0.05	0.03	0.00
Total	wt%	100.59	100.45	100.44	100.06	100.50	101.16	101.25

	No.	50	51	52	53	54	55	56
		OY27038	OY27038	OY27038	OY27036	0Y27036	0Y27036	0Y27036
SiO2	wt%	54.5	54.8	54.2	55.1	54.7	54.6	54.2
TiO2	wt%	0.17	0.21	0.20	0.31	0.24	0.24	0.26
Al2O3	wt%	1.78	1.70	1.69	1.91	1.81	1.74	1.88
FeO	wt%	15.80	15.51	15.65	14.49	14.88	14.14	14.53
CaO	wt%	1.19	0.91	1.20	1.48	1.17	1.27	1.49
Na2O	wt%	0.00	0.00	0.00	0.03	0.00	0.00	0.00
K2O	wt%	0.00	0.01	0.00	0.00	0.00	0.01	0.01
MgO	wt%	26.72	27.40	26.98	27.84	27.44	27.67	27.76
MnO	wt%	0.30	0.36	0.29	0.33	0.28	0.25	0.32
Cr2O3	wt%	0.04	0.06	0.00	0.23	0.21	0.32	0.26
NiO	wt%	0.03	0.02	0.00	0.02	0.05	0.03	0.07
Total	wt%	100.59	100.95	100.18	101.70	100.73	100.25	100.73

	No.	57	58	59	60	61	62	63
		0Y27036	0Y27036	0Y27036	OYXXXX1	OYXXXX1	OYXXXX1	OYXXXX1
SiO2	wt%	55.2	55.0	54.6	54.5	52.1	54.8	51.2
TiO2	wt%	0.19	0.38	0.25	0.23	0.82	0.39	0.81
Al2O3	wt%	1.55	1.61	1.73	2.11	3.40	1.89	3.22
FeO	wt%	14.15	13.54	14.87	14.07	6.41	13.96	7.75
CaO	wt%	1.40	1.01	1.31	0.66	21.40	1.22	18.62
Na2O	wt%	0.11	0.07	0.03	0.00	0.46	0.00	0.46
K2O	wt%	0.02	0.00	0.01	0.00	0.01	0.01	0.02
MgO	wt%	27.73	28.58	27.91	28.80	15.70	28.55	16.94
MnO	wt%	0.28	0.24	0.26	0.28	0.21	0.27	0.21
Cr2O3	wt%	0.29	0.28	0.20	0.17	0.68	0.20	0.56
BaO	wt%	0.00	0.00	0.00	0.00	0.04	0.00	0.02
NiO	wt%	0.00	0.07	0.00	0.06	0.03	0.00	0.12
Total	wt%	100.90	100.77	101.14	100.90	101.07	101.27	99.90

	No.	64	65
		OYXXXX1	OYXXXX1
SiO2	wt%	55.1	54.0
TiO2	wt%	0.26	0.50
Al2O3	wt%	1.81	1.94
FeO	wt%	13.69	13.81
CaO	wt%	0.75	1.33
Na2O	wt%	0.00	0.00
K2O	wt%	0.02	0.00
MgO	wt%	28.88	28.42
MnO	wt%	0.32	0.29
Cr2O3	wt%	0.17	0.20
BaO	wt%	0.01	0.00
NiO	wt%	0.02	0.04
Total	wt%	101.01	100.52

APPENDIX 4. Plagioclase electron microprobe results.

	No.	1	2	3	4	5	6	7
		OY27040	OY27040	OY27040	OY27040	OY27040	OY27040	OY27040
SiO2	wt%	49.2	49.8	49.5	49.8	48.9	49.8	50.4
TiO2	wt%	0.02	0.03	0.01	0.04	0.06	0.01	0.00
Al2O3	wt%	31.98	31.97	31.92	32.14	32.00	32.41	31.82
Cr2O3	wt%	0.00	0.00	0.00	0.04	0.01	0.00	0.01
FeO	wt%	0.16	0.12	0.13	0.19	0.11	0.19	0.27
MnO	wt%	0.00	0.03	0.05	0.01	0.02	0.03	0.02
MgO	wt%	0.03	0.03	0.04	0.00	0.00	0.00	0.00
CaO	wt%	15.29	15.03	15.22	15.27	15.20	15.12	14.82
BaO	wt%	0.00	0.00	0.00	0.01	0.01	0.00	0.00
Na2O	wt%	2.39	2.62	2.63	2.76	2.74	2.98	2.67
K2O	wt%	0.06	0.07	0.07	0.07	0.08	0.11	0.10
SrO	wt%	0.00	0.00	0.00	0.00	0.00	0.01	0.06
NiO	wt%	0.01	0.00	0.00	0.02	0.01	0.00	0.00
Total	wt%	99.17	99.69	99.55	100.39	99.16	100.61	100.17
An	wt%	77.6	75.7	75.9	75.0	75.0	73.3	74.9
Ab	wt%	22.0	23.9	23.7	24.5	24.5	26.1	24.5
Or	wt%	0.4	0.4	0.4	0.4	0.5	0.6	0.6

	No.	8	9	10	11	12	13	14
		OY27040	OY27041	OY27041	OY27041	OY27041	OY27041	OY27044
SiO2	wt%	50.7	48.5	49.2	48.1	49.0	48.1	50.7
TiO2	wt%	0.00	0.02	0.01	0.02	0.03	0.02	0.02
Al2O3	wt%	30.35	32.07	32.87	32.89	32.98	33.11	31.59
Cr2O3	wt%	0.00	0.00	0.00	0.00	0.00	0.03	0.01
FeO	wt%	0.19	0.15	0.00	0.07	0.12	0.16	0.09
MnO	wt%	0.00	0.00	0.00	0.02	0.00	0.01	0.00
MgO	wt%	0.02	0.07	0.01	0.03	0.00	0.21	0.00
CaO	wt%	14.44	15.40	15.77	15.98	16.12	16.00	14.00
BaO	wt%	0.00	0.00	0.00	0.01	0.00	0.00	0.00
Na2O	wt%	3.25	2.41	2.24	2.11	2.29	2.00	2.88
K2O	wt%	0.09	0.04	0.03	0.04	0.01	0.02	0.03
SrO	wt%	0.03	0.01	0.00	0.00	0.00	0.00	0.02
NiO	wt%	0.00	0.00	0.00	0.01	0.06	0.04	0.00
Total	wt%	99.04	98.63	100.12	99.30	100.63	99.68	99.35
An	wt%	70.7	77.8	79.4	80.5	79.5	81.5	72.7
Ab	wt%	28.8	22.0	20.4	19.3	20.5	18.4	27.1
Or	wt%	0.5	0.2	0.2	0.2	0.0	0.1	0.2

	No.	15	16	17	18	19	20	21
		OY27044	OY27044	OY27044	OY27044	OY27048	OY27048	OY27048
SiO2	wt%	50.5	50.9	51.2	51.9	51.3	51.9	51.9
TiO2	wt%	0.02	0.05	0.09	0.08	0.03	0.03	0.05
Al2O3	wt%	31.49	31.14	29.97	29.66	31.16	30.15	30.89
Cr2O3	wt%	0.00	0.00	0.02	0.01	0.00	0.00	0.00
FeO	wt%	0.12	0.12	0.44	0.30	0.20	0.12	0.07
MnO	wt%	0.00	0.00	0.01	0.00	0.00	0.00	0.00
MgO	wt%	0.00	0.00	0.47	0.03	0.01	0.06	0.00
CaO	wt%	14.01	14.04	12.89	13.22	13.86	12.92	13.49
BaO	wt%	0.00	0.00	0.00	0.00	0.01	0.02	0.02
Na2O	wt%	2.95	3.22	3.57	3.89	3.30	3.72	3.42
K2O	wt%	0.05	0.05	0.08	0.08	0.03	0.06	0.03
SrO	wt%	0.06	0.00	0.00	0.00	0.00	0.00	0.00
NiO	wt%	0.00	0.00	0.00	0.00	0.05	0.02	0.00
Total	wt%	99.25	99.48	98.74	99.17	99.98	99.03	99.82
An	wt%	72.2	70.4	66.3	64.9	69.8	65.5	68.5
Ab	wt%	27.5	29.3	33.2	34.6	30.0	34.2	31.4
Or	wt%	0.3	0.3	0.5	0.5	0.2	0.3	0.2

	No.	22	23	24	25	26	27	28
		OY27048	OY27048	OY27048	OY27048	OY27048	OY27048	OY27048
SiO2	wt%	52.1	50.8	50.9	50.7	50.8	51.2	51.0
TiO2	wt%	0.03	0.04	0.05	0.05	0.06	0.04	0.03
Al2O3	wt%	30.79	31.09	31.31	31.54	31.56	31.54	31.01
Cr2O3	wt%	0.00	0.01	0.01	0.02	0.00	0.00	0.00
FeO	wt%	0.22	0.13	0.16	0.14	0.12	0.06	0.17
MnO	wt%	0.03	0.00	0.00	0.00	0.00	0.00	0.01
MgO	wt%	0.13	0.02	0.14	0.02	0.00	0.00	0.00
CaO	wt%	13.20	13.00	14.19	14.12	13.97	13.63	13.48
BaO	wt%	0.01	0.00	0.04	0.00	0.00	0.00	0.00
Na2O	wt%	3.77	3.63	3.14	3.06	3.35	3.42	3.22
K2O	wt%	0.07	0.00	0.10	0.04	0.05	0.02	0.09
NiO	wt%	0.00	0.00	0.00	0.01	0.00	0.00	0.00
Total	wt%	100.38	99.69	100.08	99.69	99.86	99.88	99.01
An	wt%	65.7	68.0	71.0	71.7	69.5	68.7	69.4
Ab	wt%	33.9	32.0	28.4	28.1	30.2	31.2	30.0
Or	wt%	0.4	0.0	0.6	0.2	0.3	0.1	0.5

	No.	29	30	31	32	33	34	35
		OY27031	OY27031	OY27031	OY27031	OY27031	OY27031	OY27031
SiO2	wt%	51.0	53.1	53.3	52.3	52.4	52.53	51.0
TiO2	wt%	0.07	0.07	0.04	0.04	0.06	0.05	0.05
Al2O3	wt%	30.97	29.70	29.96	29.21	30.56	29.68	30.69
Cr2O3	wt%	0.00	0.02	0.00	0.01	0.00	0.00	0.01
FeO	wt%	0.07	0.38	0.13	1.15	0.20	0.18	0.21
MnO	wt%	0.00	0.03	0.00	0.06	0.00	0.01	0.05
MgO	wt%	0.05	0.13	0.00	0.98	0.01	0.03	0.09
CaO	wt%	13.90	12.15	12.15	11.74	13.11	12.81	13.80
BaO	wt%	0.00	0.00	0.01	0.00	0.00	0.00	0.04
Na2O	wt%	3.56	4.25	4.11	3.66	3.87	3.66	3.26
K2O	wt%	0.11	0.21	0.12	0.09	0.12	0.16	0.13
SrO	wt%	0.00	0.00	0.00	0.00	0.00	0.01	0.00
NiO	wt%	0.02	0.00	0.01	0.00	0.00	0.00	0.00
Total	wt%	99.72	100.07	99.79	99.27	100.31	99.10	99.36
An	wt%	67.9	60.5	61.6	63.6	64.7	65.3	65.6
Ab	wt%	31.5	38.3	37.7	35.9	34.6	33.8	33.6
Or	wt%	0.6	1.2	0.7	0.6	0.7	0.9	0.8

	No.	36	37	38	39	40	41
		OY27031	OYXXXX1	OYXXXX1	OYXXXX1	OYXXXX1	OYXXXX1
SiO2	wt%	52.3	49.5	48.4	49.3	48.4	48.3
TiO2	wt%	0.00	0.00	0.05	0.06	0.04	0.03
Al2O3	wt%	30.70	32.81	32.84	32.47	32.63	32.88
Cr2O3	wt%	0.00	0.00	0.04	0.00	0.01	0.00
FeO	wt%	0.15	0.11	0.16	0.10	0.13	0.06
MnO	wt%	0.00	0.02	0.02	0.01	0.00	0.04
MgO	wt%	0.07	0.00	0.02	0.01	0.00	0.05
CaO	wt%	13.13	15.79	16.26	15.67	15.87	15.89
BaO	wt%	0.00	0.00	0.00	0.00	0.00	0.02
Na2O	wt%	3.72	2.51	1.85	2.41	2.08	2.13
K2O	wt%	0.13	0.01	0.02	0.02	0.02	0.06
NiO	wt%	0.00	0.00	0.04	0.02	0.03	0.03
Total	wt%	100.16	100.73	99.7	100.06	99.16	99.51
An	wt%	65.6	77.6	82.8	78.1	80.7	80.2
Ab	wt%	33.6	22.3	17.0	21.7	19-2	19.5
Or	wt%	0.8	0.1	0.1	0.1	0.1	0.4

	No.	42 OYXXXX1
SiO2	wt%	48.3
TiO2	wt%	0.03
Al2O3	wt%	32.95
Cr2O3	wt%	0.00
FeO	wt%	0.13
MnO	wt%	0.00
MgO	wt%	0.01
CaO	wt%	15.85
BaO	wt%	0.02
Na2O	wt%	2.09
K2O	wt%	0.05
NiO	wt%	0.03
Total	wt%	99.47
An	wt%	80.5
Ab	wt%	19.2
Or	wt%	0.3